Exploring El Niño mechanisms in climate models

Sjoukje Yvette Philip

EXPLORING EL NIÑO MECHANISMS IN CLIMATE MODELS

El Niño mechanismen in klimaatmodellen
(met een samenvatting in het Nederlands)

PROEFSCHRIFT

ter verkrijging van de graad van doctor aan de Universiteit Utrecht
op gezag van de rector magnificus, prof.dr. J.C. Stoof, ingevolge het
besluit van het college voor promoties
in het openbaar te verdedigen op
maandag 30 november 2009 des middags te 2.30 uur

door

Sjoukje Yvette Philip

geboren op 21 april 1981 te Rotterdam

Promotor: Prof. dr. B.J.J.M. van den Hurk
Co-promotor: Dr. G.J. van Oldenborgh

ABSTRACT

Increasing our understanding of the equatorial Pacific climate phenomenon El Niño – Southern Oscillation (ENSO) is important for making progress in climate prediction and establishing the effects of Global Change on ENSO. The GCMs that are used for IPCC scenarios all show ENSO-like behavior, but the resemblance to the observed ENSO varies from model to model. We wonder whether we can analyse how these differences arise. Which mechanisms are important for ENSO? Are they modelled correctly in climate models? Are models good enough to describe the asymmetry between El Niño and La Niña? Can we say something about El Niño in a future climate?

We trace the mechanisms governing El Niño in observations and in a set of 19 coupled global climate models (GCMs). To this end, we use a conceptual model that describes the relations between subsystems that play a role in ENSO using local linear regressions. The first relation describes a wind response to SST variability. The second and third relation describe the response of SST to both thermocline variability and wind stress variability. Finally, a temporal damping on SST is described. We categorize six GCMs as having the most realistic balance of the various feedback mechanisms compared to observations. In four of these models the interannual mode also resembles the observed ENSO both spatially and temporally. In the other 13 models at least one part in the feedback loop between the ocean and atmosphere behaves differently as in observations. We thus selected a subset of best models based on the mechanisms that are important to describe El Niño.

For a subset of models as defined above we make projections into a future stable, warmer climate. Although there are large changes in the mean state, the overall ENSO properties do not change much. This is due to the fact that the effects of the changes in the different ENSO relations tend to cancel. In all models, the signs of the changes in ENSO mechanisms are similar. However, the sign of the small net effect differs from model to model.

A description in terms of linear couplings leads to symmetry between El Niño and La Niña events. In general, however, El Niño is larger than La Niña. In other words, the distribution of SST anomalies in the East Pacific is positively skewed as a result of nonlinear interactions in the system. Can we use nonlinearities in our conceptual model for analysing what is the likely origin of the skewness of ENSO? What is the role of atmospheric noise in this respect?

For observations the linear couplings are extended with a new description of atmospheric noise properties and some nonlinearities in the atmospheric terms. The effect of these nonlinearities are studied with an Intermediate Complexity Model (ICM) in which the fitted couplings and noise properties are implemented, but no further tuning is carried

out. The description of atmospheric noise properties in terms of standard deviation and spatial and temporal correlation is sufficient for the excitation of ENSO in this ICM. The ENSO period and pattern of the ICM agree reasonably well with that found in observations. The skewness of SST anomalies has been evaluated after adding a nonlinearity in the response of the wind stress to SST anomalies, the state-dependence of atmospheric noise, and the positively skewed nature of atmospheric noise. The SST skewness is most affected by a nonlinearity in the response of the wind stress to SST anomalies. This is followed by the state-dependence of atmospheric noise. The skewed nature of atmospheric noise has only a minor effect on SST skewness.

GCMs tend to simulate lower atmospheric noise amplitudes than observations. Some GCMs show a nonlinear response of wind stress to SST, although weaker than in observations. These models simulate the most realistic SST skewness. Overall, both a nonlinear atmospheric response to SST and the dependence of noise on the background SST influence the El Niño/La Niña asymmetry.

Finally, we investigate the sensitivity of ENSO to uncertainties in the description of physical processes in a GCM by examining a set of GCM experiments with perturbations to key atmospheric and oceanic GCM parameters. For analyzing the runs, we use the same method as for the multi-model ensemble. The advantage of a perturbed physics ensemble is that it is not principally controlled by variations in the mean climate state. Studying only changes related to perturbed GCM parameters we conclude that feedbacks involved in the ICM response of SST to variations in wind stress and damping of SST anomalies provide the leading-order control on ENSO amplitude and spatial structure.

The method described in this thesis provides the possibility of using observations for exploring model biases in individual ENSO feedback processes in a quick and transparent way. Using this method will give better insight in GCMs and seasonal forecast models, which will help modellers improving their models. This will facilitate better seasonal forecasts and climate projections.

CONTENTS

Contents

1. EL NIÑO – SOUTHERN OSCILLATION

1.1   Introduction

'El Niño' or 'the little boy' was the name the Peruvian fishermen gave to a warm ocean current. This warm ocean current occurs near the coast of Peru every year around Christmas. As fish prefer cooler, nutrient-rich water, during the warm 'El Niño' there is much less fish near the coast. Therefore this Christmas child is an unwelcome guest for the fishermen.

Nowadays, the term El Niño is used more generally to describe periods in which the surface water in the central to eastern equatorial Pacific ocean is warmer than normal. The definition of an El Niño event is no longer restricted to the coastal zone around Peru and Equador being warmer and wetter than normal. However, also in the current definition the peak of the warm El Niño event is around Christmas.

The fluctuations in sea water temperature are not an isolated phenomenon. There is a relationship between the warm ocean water and the atmosphere, which suggests that El Niño is part of a wider phenomenon. Indeed, the fluctuations in air pressure difference over the eastern and western Pacific equatorial region (named the Southern Oscillation) are related to the fluctuations in water temperature. Together they form the so called El Niño – Southern Oscillation (ENSO).

Although the El Niño phenomenon originates from the equatorial Pacific region, its influence is more globally. ENSO affects the weather in large parts of the world. The state of the equatorial Pacific ocean is coupled to the atmosphere above it and this in turn influences the atmosphere around the globe. The SST persistence makes the state of the equatorial Pacific valuable for seasonal forecasts. To improve these seasonal forecasts it is important to understand ENSO and the evolution of El Niño events.

Many studies have been carried out to investigate El Niño, its impacts around the world and its response to climate change. Ocean and atmosphere data are collected on a regular basis since about 1988 by an array of buoys in the Pacific ocean (McPhaden et al, 1998). Studies have been carried out with models ranging from relatively simple models to advanced coupled global climate models. This has led to better understanding of the phenomenon and a better representation of ENSO in models. However, there are still a lot of open questions. This thesis treats a small selection of them.

This chapter first describes the basic characteristics of the Pacific ocean in Section 1.2, El Niño in Section 1.3 and the ENSO cycle (i.e., the evolution of an event), in Section 1.4. Section 1.5 shows a conceptual model with which ENSO can be described. Finally, the outline of the rest of this thesis is given in Section 1.6.

1.2   The Pacific Ocean – mean state

El Niño develops against the backdrop of the mean state of the equatorial Pacific Ocean. This mean state is quite an interesting system in itself. The region contains the coldest sea surface temperature (SST) of the equatorial area. At the other side of the vast ocean, it contains the warmest ocean temperatures of the world as well. Consequently, it also has the largest east-west temperature difference. Understanding of the ENSO phenomenon starts with understanding this mean state, in which wind stress, a zonal sea surface temperature gradient and the thermocline (a vertical temperature gradient in the ocean, see later) balance each other. See also Figure 1.1a.

The atmospheric circulation is characterized by two overturning circulation systems. The atmospheric equator or Intertropical Convergence Zone (ITCZ) is situated just north of the equator. This is a band where the sun warms the air most and mean temperatures are highest. The ITCZ is just north of the equator and not on the equator due mainly to the majority of land masses being situated on the northern hemisphere. Near this warm atmospheric equator the air rises, and in the subtropics it sinks. This drives a circulation directed towards the ITCZ near the surface, and reverse high in the atmosphere, in the upper troposphere. The resulting cell is called the Hadley cell.

As the earth rotates, the Coriolis force acts on the poleward and equatorward branches of this Hadley cell; moving air is deflected to the right on the Northern hemisphere and to the left on the Southern hemisphere. This results in surface winds blowing from the northeast just north of the ITCZ and from the southeast south of the ITCZ. These surface winds converge at the ITCZ, resulting in the westward blowing trade winds.

In addition to these trade winds the east-west SST gradient adds a component to these winds, forming another atmospheric convective cell, the Walker cell. Above the warm region the direction of motion is upward. In the upper troposphere an eastward flow is directed towards the cold tongue area. In the East Pacific above this area the motion is downward, and near the surface an additional westward wind component adds to the trade winds.

As part of the Walker cell, above the warm area in the West Pacific the rising warm air results in a low pressure area. Then, when air flows to the east and descends above the cold area in the East Pacific, this descending air causes a high pressure area in the East Pacific. The pressure difference between Tahiti in the east and Darwin in the west is a commonly used measure. It is used to describe fluctuations in the strength of the Southern Oscillation.

Also in the ocean the trade winds induce surface flows. In the region between the ITCZ and the equator the surface winds blow from the southeast. Due to the Coriolis force there the water flows to the right perpendicular to the wind, resulting in an eastward flow. This flow is called the Equatorial Counter Current. North of the ITCZ and south of the equator the winds result in the existence of the North and South Equatorial Currents that flow to the west. Water moves away from the equator and subducts in the subtropical gyres, forming a meridional cell of convecting water. This induces upwelling near the equator. Just below the sea surface the horizontal pressure gradient that results from the trade winds induces another eastward current. This jetlike current is situated at a depth of about 200m in the West Pacific and 40m in the East Pacific. It has velocities as high as 1.4 ms^{-1}.

The sea surface temperature is characterized by an east-west gradient. The trade winds keep this east-west gradient in balance, pushing warm water to the west and leaving relatively cold water in the east. Furthermore, the upwelling of cold water keeps the East Pacific cold as well. In the eastern Pacific the annual mean temperature is very cold for the tropics, with temperatures as low as $20°$ C. This is the so called 'cold tongue' region. At the other side of the basin, approximately west of the dateline the 'warm pool' is located. In this western Pacific region mean SSTs are higher than $28°$ C, and locally higher than $30°$ C.

The trade winds maintain the warm pool in the West Pacific, whereas cold water upwells in the East Pacific. This maintains the zonal SST gradient, with a warmer SST in the West Pacific. Deeper in the ocean, the temperature gradually decreases with depth until it reaches the so called thermocline. This thermocline is a sharp vertical temperature gradient around $20°$ C that divides the warm top layer and the cold deeper ocean. The subtropical cell of deeper water is important for the formation of this thermocline. In the eastern cold tongue area the average depth of the thermocline is only 50 meters. The thermocline slopes downward to the western warm pool area, where it reaches a depth of about 150 meters. In literature and in this thesis we often use the $20°$ C isotherm to define the depth of the thermocline.

Although the solar zenith passes the equator twice a year the seasonal cycle at the equator in the central and eastern Pacific is dominated by an annual component (Li and Philander, 1996). In the cold tongue area the east-west gradient in SST reaches a maximum in October and a minimum in April. In the warm pool region the seasonal cycle is very weak and bi-annual, with only small changes in SST and mean wind. However, the variability of the wind does show a seasonal cycle, with more variability in the Northern Hemisphere winter. This seasonal cycle is important in the theory of the triggering of El Niño events.

1.3   The Pacific Ocean – evolution of an El Niño

The ENSO cycle is a damped oscillation around the seasonal cycle in the equatorial Pacific ocean. In this thesis the ENSO cycle is described in terms of differences (anomalies) relative to the mean seasonal cycle. At first order, El Niño is not dependent on the seasonal cycle. Also, the first order relations between the mean ocean currents and El Niño are negligible. The strong SST gradient, the upwelling water at the equator, and the thermocline being close to the surface in the East Pacific are important to explain the ENSO phenomenon.

During an El Niño the mean state is disturbed. The origin of a disturbance is still a matter of debate. However, to understand the evolution of an event it does not matter where we start.

Suppose that, for some reason, the SST in the East Pacific becomes warmer than normal. Consequently, the zonal SST gradient is smaller than normal. This influences the strength of the trade winds; the westward blowing winds in the west Pacific weaken. Due to the reduced trade winds, some of the warm water volume that has been built up in the West Pacific flows back to the east. This reinforces the SST anomaly in the East Pacific. Furthermore, because of the eastward flow of the water, the thermocline becomes shallower in the West Pacific and deeper in the East Pacific, reducing the tilt. Also, the upwelling in the East Pacific reduces, and this water originates from a warmer mixed layer. The deeper East

a)

Convective loop

Equator

20°N

0°

20°S

120°E

80°E

160°W

120°W

80°W

Thermocline

b)

Increased
Convection

Equator

20°N

0°

20°S

120°E

160°E

160°W

120°W

80°W
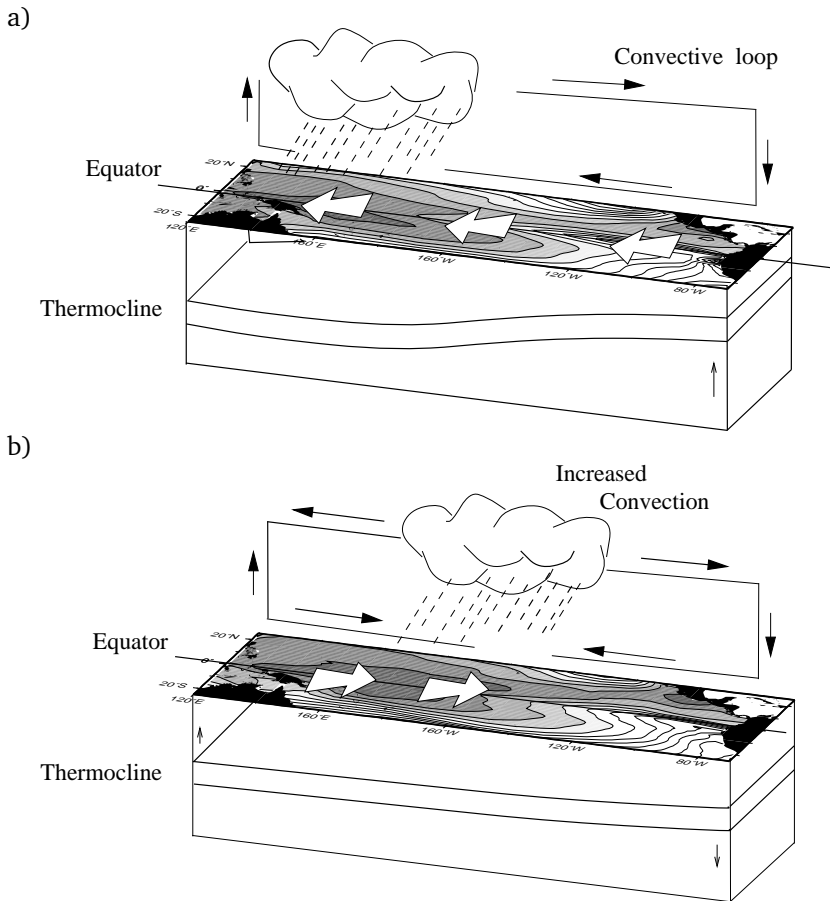
Thermocline

Fig. 1.1: a) Normal conditions in the equatorial Pacific region. The SST gradient, atmo-
spheric convection and tilt in the thermocline are in equilibrium. b) El Niño con-
ditions. The SST gradient is smaller, the convective cells have changed and the
thermocline is more flat. The figures were obtained from Vossepoel (1999), and
created after an example on the web-page of the Pacific Marine Environmental
Laboratory: http://www.pmel.noaa.gov

Pacific thermocline and reduced upwelling of cold water enhance the temperature anomaly in the East Pacific. The feedback loop between SST, wind and thermocline is closed. See also Figure 1.1b.

This positive feedback described above can induce temperature anomalies in the central to East Pacific as large as a few degrees. These anomalies can cover more than half of the equatorial Pacific basin. Such large anomalies can exist for a couple of months up to a year. These warm water anomaly events are called El Niño events.

The opposite of an El Niño also occurs, when the eastern Pacific SST becomes cooler than normal. A negative temperature anomaly in the East Pacific strengthens the trade winds. These stronger easterlies increase the tilt on the thermocline and enhance the upwelling of cold water in the east. This feedback causes the negative temperature anomaly to persist for a couple of months. Such a negative temperature anomaly event is called La Niña, 'the little girl'. Often, but definitely not always, a cold event follows a warm event. The opposite, a warm event following a cold event, occurs even less frequently.

The fact that El Niño peaks around Christmas is a second order relation between El Niño and the seasonal cycle. However, this seasonal dependence is not essential for the equations used in this thesis.

1.4   El Niño variability – characteristics

The knowledge about El Niño started with the absence of fish, noted by the Peruvian fisherman. Nowadays, with a definition that has slightly changed, ENSO is a well known term and it is studied frequently due to its importance for large parts of the world. Measurements in the equatorial Pacific basin are carried out on a structural basis. Seasonal and monthly forecasts are made routinely. More and more standardized measures are used to describe the state of the ocean.

Commonly used characteristics include for instance the pattern and amplitude of an SST anomaly. Furthermore, the mean time between two El Niño events and the time of the evolution of one event are often used to validate climate models and seasonal forecast models. Finally, in this thesis we also use the skewness of the SST anomalies (i.e., the degree to which warm anomalies are larger or smaller than cold anomalies).

The patterns of El Niño events are never exactly similar. However, often the big El Niño of 1997-1998 is used for illustration, because it was one of the strongest events of the last 150 years, and the first large El Niño that was exquisitely observed. Figure 1.2 shows the SST anomaly of December 1997. An El Niño pattern is clearly visible in the Pacific Ocean, with temperature anomalies up to 5 degrees Celcius in the cold tongue region. A measure that is often used to describe the El Niño pattern is the so called first Empirical Orthogonal Function (EOF), which shows the pattern of maximum variability of multiyear SST fields. As the SST variability near the equator is mainly caused by El Niño the pattern of the first EOF is comparable to this SST anomaly pattern, with a maximum in the central to east Pacific Ocean.

A commonly used measure for the strength of El Niño is the Niño3.4 index. This index denotes the average sea surface temperature anomaly in a region around the equator ($5°$ S-$5°$ N; $170°$ W-$120°$ W), where a value of Niño3 = 2K corresponds to a fairly strong El Niño.
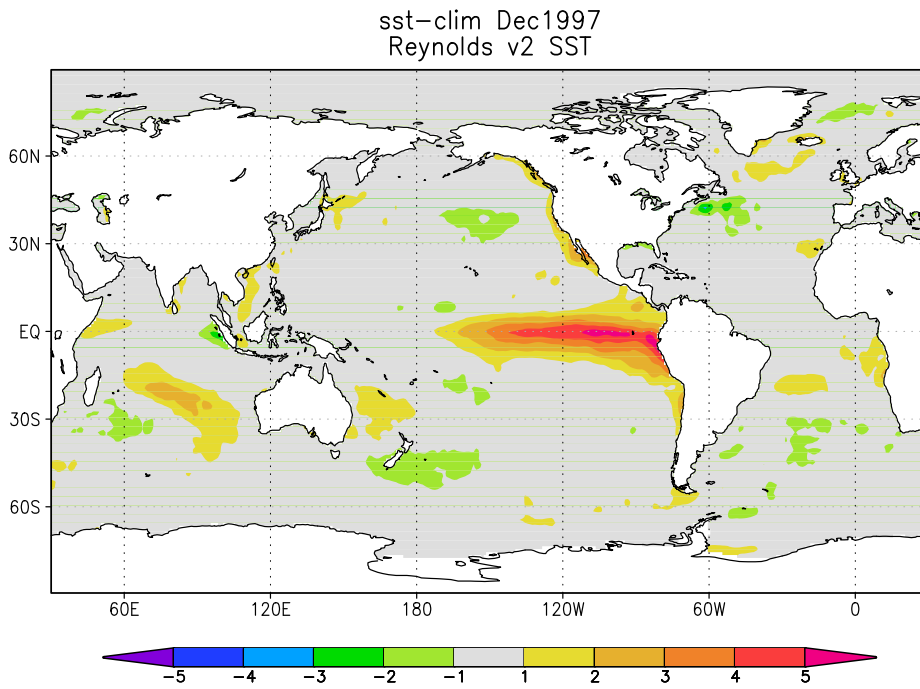
Fig. 1.2: SST anomaly pattern of December 1997, using Reynolds V2 SST data (Reynolds et al, 2002). Temperature anomalies are in $^\circ$ C.
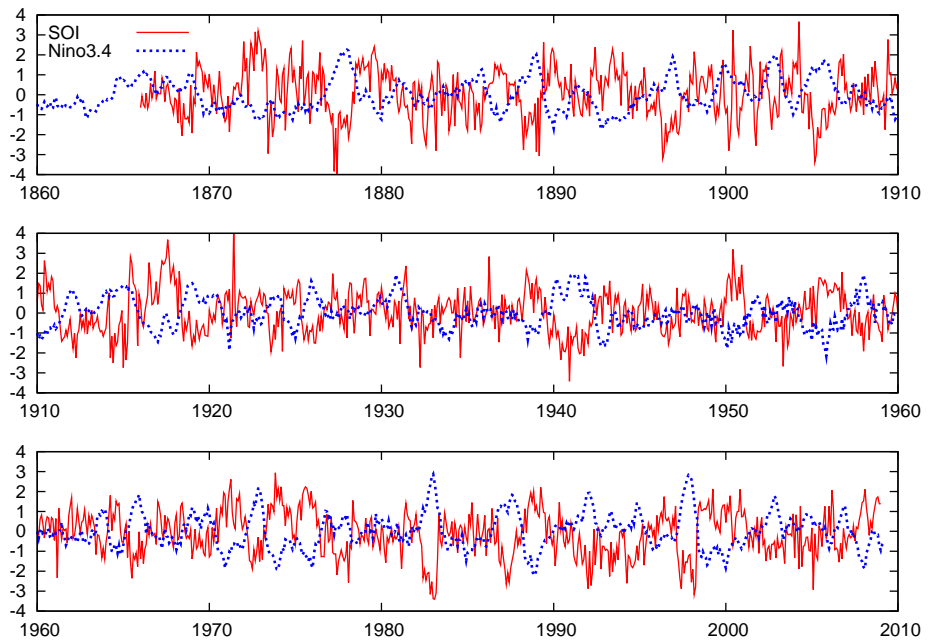
Fig. 1.3: Normalized SOI index and Niño3.4 index [K] (average sea surface temperature anomaly in 5° S-5° N; 170° W-120° W). The indices are clearly anti-correlated.

Sometimes different Niño-indices are used (Niño3, Niño4), corresponding to other regions around the equator. Another frequently used measure is the standard deviation (a measure of the spread in strength of El Niño) of the timeseries corresponding to the first EOF.

Together with a changing amplitude of an SST anomaly the pressure difference between the East and West Pacific changes as well. This so-called Southern Oscillation is measured by the Southern Oscillation Index (SOI). This index describes fluctuations around the normal pressure difference between Darwin and Tahiti. Other influences than El Niño cause fluctuations in the pressure at Darwin and Tahiti. Therefore we do not find a one-to-one relation between the Niño3 index and the pressure difference between these locations, but generally a negative correlation exists (Figure 1.3). As the SOI has been measured for a long time (since 1866), this measure is well known as well.

The frequency with which El Niño events occur is about once every 2-7 years. This could be the result of a series of events occuring by chance every now and then. Other hypotheses refer to a quasi-periodic oscillation resulting from the feedback between the ocean and atmophere, see Kessler (2002) for a discussion. The timeseries of the Niño3
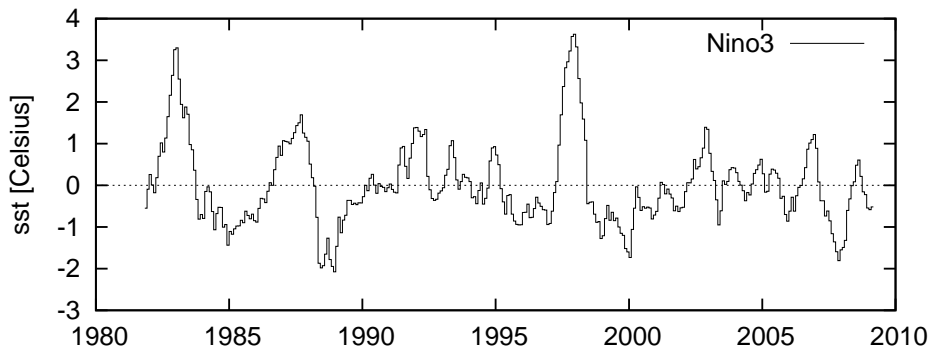
Fig. 1.4: Timeseries of the Niño3 index, using Reynolds V2 SST data (Reynolds et al, 2002). Temperature anomalies are in $^\circ$ C.

index clearly shows the occurrence of the El Niño and La Niña events every couple of years, see Figure 1.4.

Sometimes, the SST skewness is given as an extra measure for El Niño. In the East Pacific the SST skewness is strongly positive, see Figure 1.5. This describes the fact that in general positive SST anomalies in the East Pacific are stronger than negative SST anomalies. In other words, El Niño events are stronger than La Niña events.

1.5   Overview of theoretical models for ENSO – the Recharge Oscillator

Although the ENSO phenomenon is well known by local people near the coast of Equador and Peru for ages, more physical explanations for the phenomenon were put forward only in the 20th century. Since then more and more comprehensive theories are developed and models are built with increasing complexity.

The first one who argued that El Niño and the Southern Oscillation are part of the same phenomenon is Berlage (1957). Although this interpretation turned out to be important for the discussion on the ENSO phenomenon, his physical interpretation in terms of advection of warm anomalies induced by the trade winds is not correct. A better interpretation was given in the sixties by Bjerknes (1966). He recognized that ENSO is a result of ocean-atmosphere interaction in the tropical Pacific. An anomalously weak equatorial zonal SST gradient induces anomalous westerlies over the tropical Pacific. These anomalous westerlies in turn create the warm SST over the eastern Pacific and thus weaken the SST gradient.

The ocean feedback loop between SST and thermocline depth was explained in more detail by Wyrtki (1975). He suggested that the buildup of sea level (an indicator of heat content) over the equatorial Pacific is related to the strengthening of the trade winds. Ac-
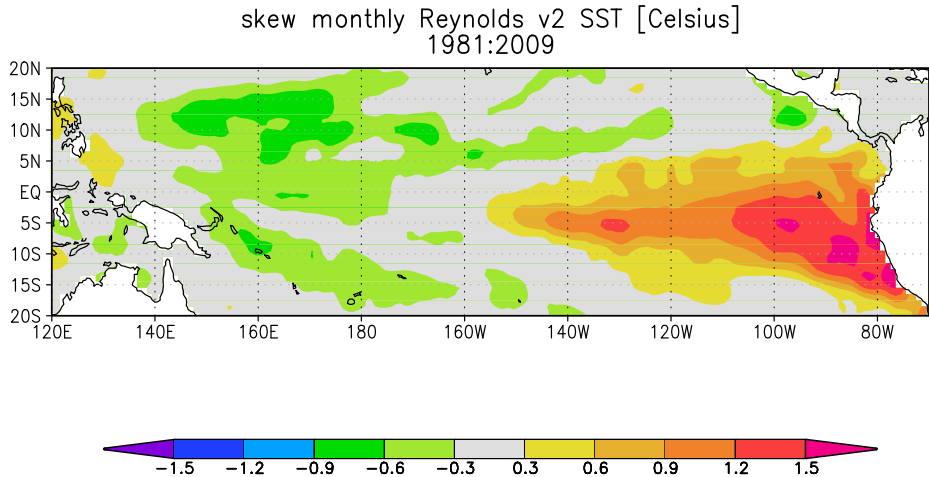
Fig. 1.5: SST skewness in the equatorial Pacific Ocean, using Reynolds V2 SST data (Reynolds et al, 2002).

cumulated warm water flows eastward in the form of Kelvin waves (equatorially trapped gravity waves allowed by linear equatorial ocean dynamics) to initiate an El Niño event.

Cane and Zebiak (1985) combined the former two views on the ENSO cycle. They hypothesise that the aftermath of a warm event leaves the thermocline along the whole equator shallower than normal. **?** suggested that over the next few years the equatorial Kelvin waves can move enough of the warm water to the eastern end of the equatorial Pacific to initiate the next event. In this hypothesis they couple three variables: wind, SST and thermocline depth.

With this theory the idea of the recharge oscillator was born (Jin, 1997). This oscillator views ENSO as a two-dimensional dynamical system. The two variables which are $90°$ out of phase are the eastern Pacific SST and the mean equatorial Pacific thermocline depth. A phase diagram of these two variables is shown in Figure 1.7 and will be explained later.

A warmer than normal East Pacific SST (and thus weaker gradient in SST) sets up an anomalous mean wind stress. The mean wind stress in turn influences the east-west gradient in thermocline depth:

$$h_E - h_W = \kappa \tau_x \tag{1.1}$$

where h_E and h_W are the mean thermocline depths in the East and West Pacific respectively, τ_x is the zonally integrated windstress and κ is a constant.

An important consideration in the recharge oscillator view is the time scale of the thermocline adjustment. The mean thermocline depends on mass adjustment, where water

flows into or out of the equatorial region:

$$\frac{dh_W}{dt} = -rh_W - F_{\tau_x} \tag{1.2}$$

where r is a damping term and F is the zonally integrated wind stress. This term represents the so-called Sverdrup transport, i.e., the wind induced transport of water in or out the equatorial region. This transport, that leads to changes in mean thermocline depth, is a slow ocean process. This is different from the time scale of changes in the tilt of the thermocline, which is relatively short.

Jin (1997) explains that the variation in SST depends on three terms. The first one is the local thermocline depth that determines the subsurface temperature through upwelling. The second term is an advective feedback from wind anomalies, influencing SST by anomalous currents. The third one is damping of SST fluctuations through the mean climatological upwelling and heat exchange between the ocean and the atmosphere.

Finally, the atmosphere responds to SST anomalies. In the above described view a time-delay is present in the response of the western Pacific to wind stress changes and in the response of the East Pacific SST to thermocline anomalies. It it assumed that the tilt in the thermocline responds quasi-instantaneously to wind stress anomalies and that no time-delay is present in the upwelling of cold water from the thermocline.

Burgers et al (2005) showed that the finite time it takes for a Kelvin wave to propagate a signal through the thermocline to the surface in the East Pacific contributes significantly to the coupled oscillator. Curiously, inclusion of the extra time delay leads to the same damped oscillator equations as derived in Jin (1997), only with different interpretations of the coefficients. The coupled equations will be described in more detail in Chapter 2.

In these conceptual models it is assumed that ENSO has only one timescale (~ 4 years). However, we can also interpret ENSO in terms of a two-stage process, i.e., the evolution of one event (~ 2 years) and the time between two events (> 4 years). It is not yet clear which view fits the observations best.

Starting with El Niño conditions, one cycle in the recharge oscillation can be described as follows, see also Figure 1.6. The thermocline in the East Pacific is deeper than normal, corresponding to a positive SST anomaly and an eastward wind stress anomaly. Due to the Coriolis force and Sverdrup transport water moves away from the equator, causing the thermocline to rise. As the thermocline has become shallower the SST anomaly and consequently the wind stress anomaly are reduced back to zero. However, now the thermocline is no longer in equilibrium with the wind stress. This directly causes the tilt of the thermocline to increase. The increased tilt of the thermocline induces a negative SST anomaly in the East Pacific, which immediately enhances the westward trade winds. Now, the Coriolis force and Sverdrup transport induce water transport towards the equator, causing the thermocline to deepen again. The thermocline in the East Pacific is at its average depth, which reduces the SST anomaly to zero. Consequently the wind stress anomaly is diminished as well. The tilt of the thermocline is too steep for this zero wind stress anomaly and has to reduce again. The discharge-recharge cycle can start all over again.

At first order, the interaction between the mean Pacific equatorial thermocline depth anomalies and the East Pacific SST demonstrated in Figure 1.6 is a classical damped oscillator. In SST-thermocline space, the oscillation roughly follows circular paths. Figure 1.7
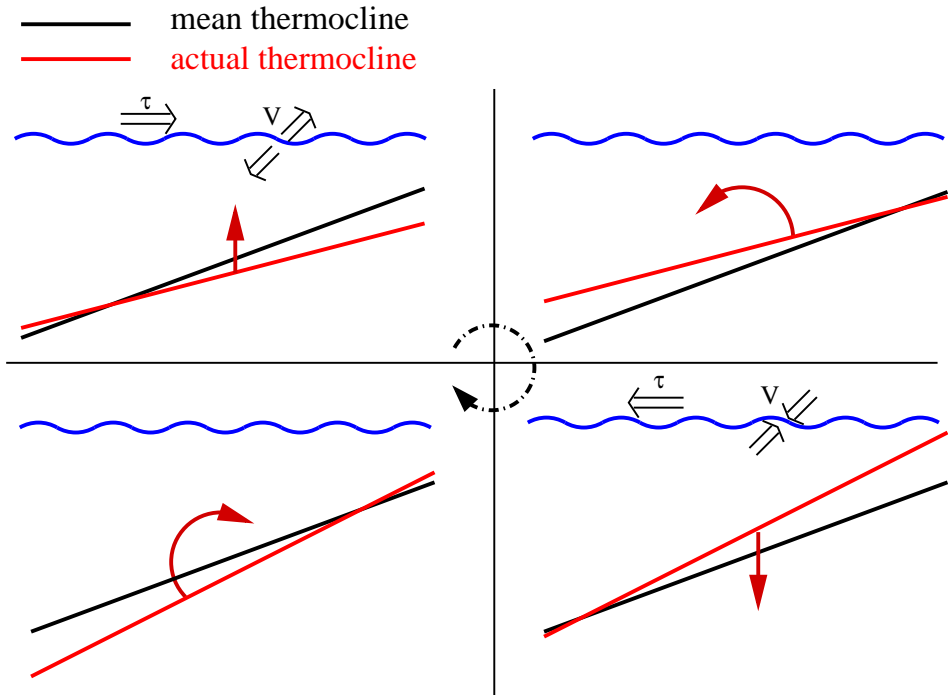
Fig. 1.6: Schematic of the recharge oscillator: vertical oceanic cross-section at the equator. The black line is the mean thermocline depth and the red line is the actual situation. Top left: El Niño situation with a thermocline that is deeper than normal in the East Pacific and an eastward wind stress anomaly (τ). Water moves off the equator (V), causing the thermocline to rise. Top right: neutral SST situation, with a the thermocline that is shallower than normal and a wind stress anomaly that is reduced to zero. The thermocline is no longer in equilibrium with the wind stress and the tilt of the thermocline will increase. Bottom right: La Niña situation with an increased tilt of the thermocline, and enhanced westward trade winds (τ). Water is transported towards the equator (V), causing the thermocline to deepen again. Bottom left: neutral SST situation, where the thermocline in the East Pacific is at its average depth, and the tilt in the thermocline is very steep. The wind stress anomaly is diminished as well. The tilt will reduce.
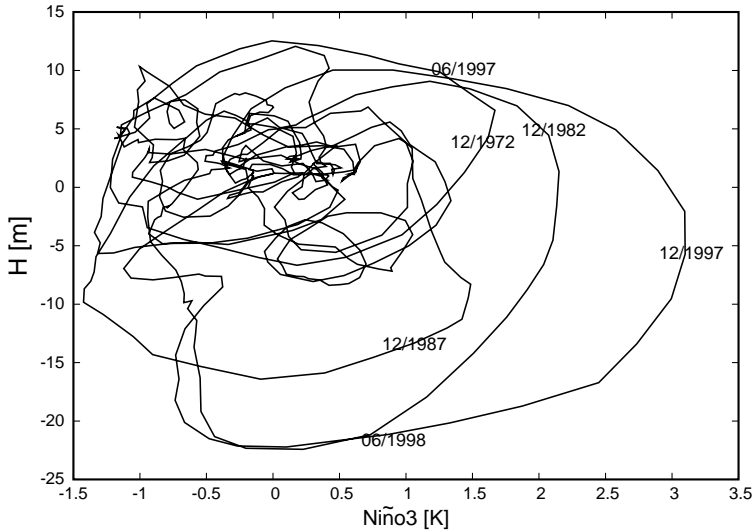
Fig. 1.7: A phase diagram of SST anomalies in the eastern equatorial Pacific (Niño3) versus the zonally averaged mean thermocline depth anomaly H using observational analysis data from 1960-2004 (Ingleby and Huddleston, 2007). Time increases clockwise along the trajectory.

shows such a phase diagram. For the mean thermocline depth, anomalies in the mean equatorial thermocline are used, averaged for $5°$ N - $5°$ S and $120°$ E - $90°$ W. The SST anomalies of the East Pacific are averaged over the Niño3 region ($5°$ N - $5°$ S, $150°$ W - $90°$ W), since this corresponds more or less to the ENSO pattern.

Nowadays, the recharge oscillator model is often used to describe the basic concept of the El Niño – Southern Oscillation. Coupled climate models are much more advanced than this two-dimensional dynamical system. Intermediate Complexity Models like the Zebiak-Cane model (Zebiak and Cane, 1987) and the Gmodel (Burgers et al, 2002) solve simplified equations of motion on a realistic grid. These models describe the ENSO phenomenon in much more detail. A version of the Gmodel will be discussed in Chapter 2.

1.6   Research questions and set-up of the study

The El Niño – Southern Oscillation is a complex phenomenon. For large parts of the world it is important to forecast the development of this system. Therefore we first need to understand the system.

To make better seasonal forecasts and projections into a future climate for El Niño we

need reliable models. The Global Climate Models (GCMs) that are currently in use have become more and more advanced. However, to what extend are they realistic enough for reliable projections? Are some models better than other ones?

To address this, we first study ENSO in observations. This is necessary for understanding the feedbacks between the ocean and atmosphere. Then, we compare climate models to observations. The focus is on assessing the necessary basic ingredients a model should represent correctly. However, diagnosing the degree to which GCMs represent the necessary processes well is severely complicated by the model complexity. Therefore, we choose a strategy where we diagnose the GCM behaviour by linkage to a relatively simple conceptual ENSO model, and study the characteristics of this framework.

Figure 1.8 shows a conceptual model of ENSO with interactions between the relevant variables zonal wind stress (τ_x), SST and thermocline depth (Z_{20}), see also Fedorov and Philander (2001); Burgers and van Oldenborgh (2003). The recharge oscillator, described in Section 1.5 is a mechanistic picture of the feedbacks between these variables. In our set-up, we will build a set of linear and nonlinear equations representing the feedbacks shown in Figure 1.8.

The simplest representation of the feedbacks shown in Figure 1.8 is by means of linear equations (or 'couplings') expressing the mutual dependence of relevant variables. The linear couplings include the feedbacks between SST and wind stress, the dependence of SST on thermocline depth and the dependence of the thermocline depth on wind stress anomalies (Figure 1.8a). In addition, different descriptions of the driving external atmospheric noise term and the internal nonlinear response of wind stress to SST are investigated (Figure 1.8b).

In this simplified model coupling strengths are fitted from observations and GCMs. This allows an assessment to what extent GCMs are similar to observations. Chapter 2 is dedicated to the explanation of this method that will be used in the rest of this thesis.

We first apply this method to the assessment of the effect of climate change on ENSO projected by GCMs. As our climate changes, we whish to determine possible scenarios for the evolution of ENSO. It is still unknown what the response of ENSO will be on global warming. In Chapter 3 we show ENSO characteristics for climate projections into a warmer climate. We select the best projections based on their model performance in a current climate scenario. We do not just select models based on ENSO characteristics like amplitude, period and pattern, but rather on the mechanisms behind it as described by the coupling diagram in Figure 1.8.

After selecting models based on their linear dynamics, we can use the best models to evaluate the relevant feedbacks in a warmer climate. So far, we investigated mechanisms and linear feedbacks between the ocean and atmosphere in a current climate scenario. In Chapter 4 these linear feedbacks are studied using climate scenarios for a warmer, future climate. Differences in feedbacks between a current and a future climate scenario are highlighted. With this we investigate the reliability of the ENSO projections in a warmer climate.

The linear dynamics that maintain the ENSO cycle are relatively well understood. One of the remaining questions concerns the fact that in general El Niño is larger than La Niña. In Chapter 5 the influences of some atmospheric properties on this nonlinear effect are
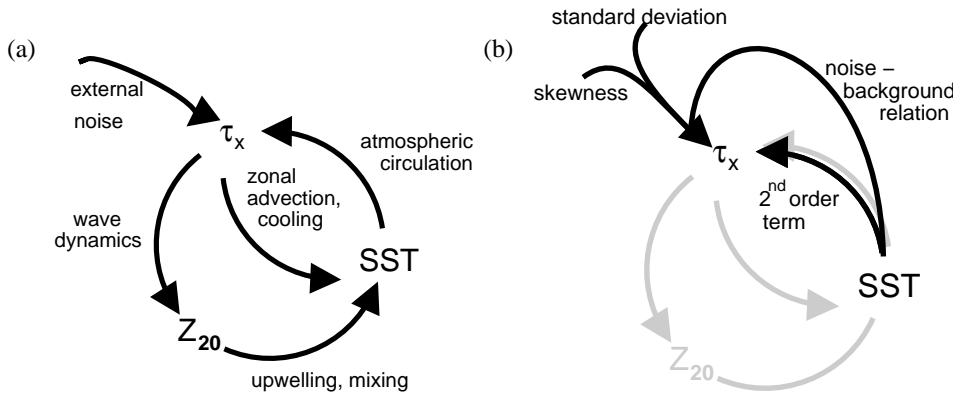
Fig. 1.8: The main feedbacks between wind stress (τ_x), SST and thermocline depth (Z_{20}) in the ENSO cycle and the external noise term. a) linear feedbacks and b) the contribution of noise properties and nonlinear terms examined in this thesis.

studied in observational data.

The question that arises now is whether the models that have been selected based on their best linear dynamics also model the above mentioned nonlinearity adequately. In Chapter 6 we compare the nonlinearities arising from atmospheric properties in models with that in observations.

We now know to what extent GCMs are similar to observations in the sense of the different parts in the ENSO feedback loop. However, we also want to know the influence of different coupling and atmospheric noise parameters on the ENSO cycle separately. It is difficult to investigate this in multi-model ensemble or climate change scenario runs; in such runs GCM parameters and mean climate state both influence the feedback cycle. In Chapter 7 the importance of different parts in the linear ENSO feedback loop on variations in the ENSO cycle is quantified, using an ensemble of runs from one GCM in which parameters in the ocean and atmosphere are perturbed. This enables us to investigate the variations in the feedback cycle that are caused by GCM parameters that are not principally controlled by variations in the mean climate state.

Finally, in Chapter 8 we discuss the results of the investigations that are described above. We summarize the new method exploring ENSO used in this thesis and give advice for future research.

2. A CONCEPTUAL MODEL OF ENSO

2.1 Introduction

We want to test the reliability of GCMs by comparing them to observations. As a first check, we compare the coupling strengths between the ocean and atmosphere in GCMs with that in observations. This enables us to check the reliability of the feedbacks in the GCMs. Next, we use a conceptual ENSO model to test the influence of differences in coupling strengths between observations and different models. The conceptual model uses the coupling strengths between the ocean and atmosphere and atmospheric noise terms that are fitted from either observational data or GCM output.

In the conceptual model, the variation in SST is described with a linear SST anomaly equation, see Fig 1.8a. Anomalies in SST are expressed as a function of zonal wind stress anomalies and thermocline depth anomalies. A damping term restricts the growth of SST anomalies.

The zonal wind stress (τ_x) is the atmospheric component that is dynamically most important (Philander, 1990). In turn two terms determine the zonal wind stress anomalies to a large extent: SST anomalies and atmospheric noise, see also Fig 1.8. The first order wind stress response to SST anomalies is described with a linear statistical equation, referred to as the 'linear atmosphere model'. A nonlinear atmospheric response is described with a second order term in the statistical atmosphere model.

The atmospheric noise term is described using the observed or GCM modelled wind stress on the one hand, and the quantity described by the (nonlinear) statistical atmosphere on the other. This noise is simply calculated as the observed/GCM modelled wind stress that is not captured by the (non)linear atmosphere model, i.e., the residual term. It is described by the first two non-zero statistical moments: standard deviation and skewness. The noise terms depends on the background SST as well.

To complete the main feedback loop shown in Fig 1.8 we include the coupling between zonal wind stress and thermocline depth. Zonal wind stress anomalies force, among others, eastward travelling Kelvin waves (equatorially trapped gravity waves allowed by linear equatorial ocean dynamics. Kelvin waves propagate a signal through the thermocline to the surface in the East Pacific. In the conceptual model we represent this coupling with a single number for the Kelvin wave speed.

We solve basic relations between oceanic and atmospheric variables on a grid using a a so-called Intermediate Complexity Model (ICM). In this ICM the evolution of the oceanic variables is described by the shallow water equations. Besides, part of the relations are em-

bedded using empirical statistical equations (equations describing the couplings displayed in Figure 1.8). The conceptual model is thus embedded in the ICM.

The ICM is based on the so called Gmodel (Burgers et al, 2002; Burgers and van Oldenborgh, 2003). It consists of three components in the equatorial Pacific region, represented on 2D-grids, see Figure 2.1. Between the deeper ocean and the shallow ocean the shallow water equations are solved two-dimensionally. The bottom layer represents the thermocline depth in which Kelvin waves can travel from west to east. Interaction between the thermocline-field and the SST-field (middle layer) takes place locally, from single grid-points in the thermocline to single grid-points in the SST-field. From the SST-field patterns are projected on the wind stress field (top layer). This is not a point-by-point coupling, as wind stress responds to SST gradients rather than to local SSTs. In contrast, forcing of the thermocline by the wind stress anomalies is again local. Finally, a two-dimensional field of physically consistent wind stress noise drives ENSO.

The linear and nonlinear coupling strengths between SST, Z_{20} and τ_x and the atmospheric noise terms are fitted to either observations or GCM output. These terms are added to the ICM in a number of stages, allowing increasing complexity of the ICM. First, the linear coupling strengths and noise terms are implemented. Next, the nonlinear atmospheric wind stress terms are added one by one to the originally linear reduced model and the ENSO properties in the ICM are studied.

The description of the ICM is organised as follows. Details of the linear feedbacks are given in Section 2.2. Characteristics of the atmospheric noise term are discussed in Section 2.3. The nonlinear atmospheric feedbacks are investigated in Section 2.4. Furthermore, the structure of the complete ICM in which these these feedbacks and noise characteristics are combined is described in more detail in Section 2.5.

2.2   Linear feedbacks between SST, Z_{20} and τ_x

The linear feedbacks include a linear SST anomaly equation, a linear statistical atmosphere model and a Kelvin wave speed.

2.2.1   The linear SST anomaly equation

The response of SST to zonal wind stress anomalies $\tau_x'(x,y,t)$ and thermocline anomalies $Z_{20}'(x,y,t)$ (see Figure 1.8a) is described with a local linear SST anomaly equation:

$$
\begin{aligned}
\frac{dT'}{dt}(x,y,t) &= \alpha(x,y)\, Z_{20}'(x,y,t-\delta(x,y)) + \\
&+ \beta(x,y)\, \tau_x'(x,y,t) - \gamma(x,y)\, T'(x,y,t).
\end{aligned}
\tag{2.1}
$$

$T'(x,y,t)$ is the local SST anomaly. Upwelling and mixing of thermocline temperature anomalies are parameterised by α (nonlinear terms in this process are very small in observational data). The parameter β describes the effects of zonal advection, upwelling, evaporation and variations in mixed-layer depth on SST, neglecting nonlinear terms. The damping parameter γ is a relaxation term proportional to the SST anomaly. An example
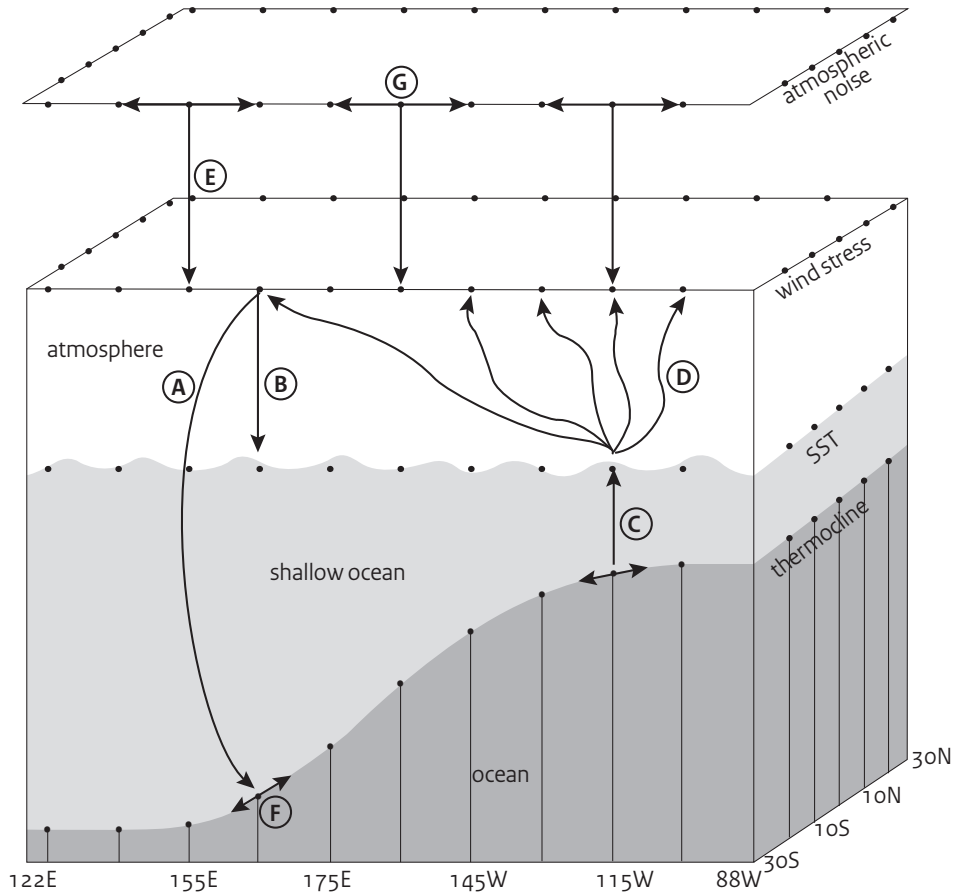
Fig. 2.1: Schematic of the ICM. From bottom to top the layers denote: the thermocline layer between the shallow ocean and the deeper ocean, the SST layer on top of the ocean, a wind stress layer and a layer with atmospheric noise. The exchange of information is local from wind stress to the thermocline (A) and to SST (B) and from the thermocline to SST (C). SST box-averages project wind stress patterns on the wind stress (D). Atmospheric noise drives the ENSO cycle (E). Two-dimensional equations are solved on the thermocline layer (F). The atmospheric noise is spatially and temporally coherent (G).

of a damping process is the cloud feedback, where a higher SST in the western Pacific provides more evaporation, more clouds, a decrease in insolation and consequently lower SSTs. Heat fluxes play a role as well, but are implemented indirectly as a damping term in the SST equation.

The finite upwelling time lag δ is prescribed from observations (Zelle et al, 2004) and varies from less than one month east of $130°$ W to 5 months at the date line; this also agrees well with lag correlations of most model data. For models that did not represent this spatial pattern of δ well, $\delta=0$ was used. For observations, the SST equation explains 60-80% of the variance of SST between approximately $8°$ S - $8°$ N. Results are shown in the next chapters.

Although the linear model fits the SST evolution well, nonlinear effects that are not included in Eq. 2.1 are known to play a role, especially in the central Pacific (e.g. Boulanger et al, 2001). An example of such a nonlinearity is nonlinear dynamical heating in the central Pacific (Jin et al, 2003). This term both depends on and contributes to SST.

2.2.2   The linear atmosphere model

The atmosphere is described by a statistical relationship between regionally averaged SST anomalies and zonal wind stress anomaly patterns, which is the most important atmospheric forcing. The relationship uses n equal-sized boxes along the equator in $5°$ S–$5°$ N, $140°$ E–$80°$ W. Such a model is called a 'linear statistical atmosphere model' (e.g. Von Storch and Zwiers, 2001, §8.3):

$$\tau'_x(x,y,t) = \sum_{i=1}^{n} A_{1,i}(x,y)T'_i(t) + \epsilon_1(x,y,t) \tag{2.2}$$

where $\tau'_x(x,y,t)$ is the domain-wide zonal wind stress anomaly and $T'_i(t)$ are SST anomalies averaged over separate regions $i = 1, 2, ..., n$. The patterns $A_{1,i}(x,y)$ are the domain-wide regression coefficients between the wind stress patterns and regional SST anomalies. Mathematically, we solve this matrix equation by numerically maximising the wind stress explained by the patterns $A_{1,i}$, thereby minimising the noise component $\epsilon_1(x,y,t)$. For this linear statistical atmosphere model this is mathematically equivalent to dividing the regression of wind stress on the SST-anomalies in the boxes by the covariance matrix of the SST anomalies between the boxes. With this statistical representation of the atmosphere a wind stress pattern $A_{1,i}(x,y)$ corresponds to an SST anomaly in one of the boxes, being insensitive to the SST anomalies in the other boxes. [Usually the SST anomalies are correlated.] The subscript 1 refers to the linear model, and a nonlinear equivalent $A_{2,i}(x,y)$ will be introduced below. The term $\epsilon_1(x,y,t)$ denotes the residual noise by random wind stress variations and represents a stochastic forcing to the model. In our ICM (see later) this is not white noise at each time step, as the wind varies only on weekly time scales. As the ICM is integrated in time steps of 8 hours, the forcing varies slowly compared to other processes and the equations can be solved using the normal method for equations with additive noise. Section 2.3 is devoted to the properties of this noise term.

The response to each box should to first order be a Gill-type pattern (Gill, 1980): westerly wind response to the east of the SST anomaly, weaker easterly response to the west, and possibly to the north and south of the SST anomaly. The strength of the response

should depend on the background temperature: due to the nonlinear nature of convection the wind response is stronger over warm water than over colder water (e.g. Burgers and van Oldenborgh, 2003). The zero-line of the wind response is to the east of the heating anomaly (Clarke, 1994), which in turn is usually located to the west of the SST anomaly due to the temperature gradient and background wind.

2.2.3 Representation of the thermocline response

Horizontal motion in the upper layers of the ocean is described with the so-called shallow water equations. These are the equations that are solved in the ocean model of the ICM (Figure 2.1), see Section 2.5. The lowest order solution for these equations is the eastward travelling, non-dispersive shllow water or Kelvin wave that travels through the thermocline.

Variability in the thermocline depth influences SST. These thermocline anomalies are set up by variability in the zonal wind stress. Subsequently they travel eastward through the thermocline in the form of Kelvin waves. It is therefore important to determine the speed of these waves, which equals $c = \sqrt{g'H}$, where H is the mean thermocline depth and the reduced gravity is given by $g' = g(\rho_2 - \rho_1)/\rho1)$ with ρ_1 and ρ_2 the density in the upper ocean layer and the layer below the thermocline. A value of $c = 2.5\mathrm{ms}^{-1}$ is normally found to describe observations well.

In the 1.5-layer ocean model used in this thesis and explained in Section 2.5 the ocean wave dynamics are described by the gravest baroclinic mode, the first Kelvin wave. The speed of this Kelvin wave is fitted to optimise ocean dynamics in the un-coupled versions of the extended Gmodel in the region 5° S-3° N, 150° E-110° W, i.e., satisfying a maximum in the correlation between GCM and ICM thermocline anomalies. This region is selected as in this region the thermocline is relatively important compared to the wind stress response to SST and the damping, and the SST-equation explains enough of the variance (>0.4).

2.3 Atmospheric noise properties

ENSO can be viewed either as a stable damped mode or as an unstable self-sustained mode. The ENSO feedback system used in this thesis is close to stability and affected by external noise in the form of wind variations. The role of external noise in the form of atmospheric stochastic forcing has already been studied extensively. Blanke et al (1997) suggested that the addition of atmospheric noise increases ENSO irregularity and that the ocean is sensitive to the spatial coherence of noise fields.

In this thesis atmospheric noise is constructed by subtracting the wind stress calculated with Equation 2.2 from the total observed wind stress. Properties of this residue are calculated separately from the statistical atmosphere model. These residuals are added to the wind stress forcing in this (intrinsically stable) atmosphere-driven ENSO model. The timescale on which the stochastic noise terms vary (1 week) is much longer than the integration time-step of the Gmodel (1/3 day). The characteristics of noise can be described in several ways, ranging from quite simple to more advanced descriptions. In this study the noise terms are characterised with statistical parameters.

This description of atmospheric noise does not include a dynamical structure, i.e., equatorial travelling noise patterns like the ones associated with the Madden-Julian Oscillation (MJO). However, partly because the ocean acts as a low pass filter, this description of atmospheric noise is quite realistic. When the ocean model used in this study is forced with observed wind stress it shows similar SST characteristics compared to when the model is forced with noise characterised as above. Some GCMs have nonlinear aspects such that the ICM represents the GCMs less well than observations.

In the original, linear version of the Gmodel the external noise was represented simply by adding red plus white noise to the SST Niño-indices instead of explicitly changing the wind forcing by adding noise to the wind stress. [The use of red and white noise appears a better approximation for the autocorrelation of the residuals than only adding white noise (Burgers and van Oldenborgh, 2003).] Effectively, this relatively simple description of noise is a method to simulate the effect of perturbations of the coherent wind fields associated with the Niño-indices. The effect of this parameterization of the noise on the ENSO cycle is very similar to that of the full noise field in terms of wind stress (Burgers and van Oldenborgh, 2003). However, in this study we aim to get more insight in the details of the full noise field. A better parameterization of the spatial variability of the noise field on smaller scales over the whole equatorial Pacific is then needed. Rather than applying noise to the Niño-indices, we explicitly describe the full noise field in terms of a larger number of two-dimensional atmospheric forcing parameters.

One possibility to describe the full noise field is by using EOFs (Perez et al, 2005). We did not use this approach, since the standard deviation and skewness of this EOF-based noise field can not easily be brought in agreement with observations. Moreover, patterns of the first few noise-EOFs give rise to spurious long-distance correlations. These correlations give undesirable effects on the ENSO cycle in the ICM. To avoid this effect we developed a method in which the standard deviation, skewness and spatial and temporal correlation of the noise are preserved.

2.3.1   Noise amplitude properties

In this study the noise has been modelled as a stochastic field with spatially prescribed standard deviation and skewness, which are the first two non-zero statistical moments of the noise. The statistical parameters of the stochastic field are derived from the obtained residuals $\epsilon_1(x, y, t)$. From these the 2-dimensional fields for standard deviation and skewness are calculated.

The standard deviation is simply the amplitude of the noise. Near the equator the noise standard deviation is highest in the West Pacific where temperatures are highest. Westerly (i.e., eastward) wind noise is the sum of shorter time scale westerly wind events (WWEs) such as storms (often associated with the MJO) or tropical cyclones. These occur on a background state of easterly trade winds plus the state of ENSO. Even on monthly time scales this translates into a positive skewness of the noise. Thus, in the warmer West Pacific strong, short time scale WWEs occur frequently. These cause the distribution of zonal wind stress to be positively skewed.

2.3.2 Noise spatial- and temporal correlation coefficients

Blanke et al (1997) showed that spatial coherence of noise influences the ENSO cycle. The spatial correlation ensures that events are correlated in a physically plausible way rather than than being unphysical random noise. Burgers and van Oldenborgh (2003) show that also time-correlation strongly influences the amplitude of ENSO. The time correlation that is due to other processes in the equatorial Pacific accounts for the long lasting, larger scale anomalies (Burgers and van Oldenborgh, 2003; Cravatte et al, 2003). Therefore in this study the noise has been modelled with prescribed spatial and temporal correlation structures in the equatorial Pacific basin.

Results in this study are not very sensitive to the exact two-dimensional patterns of the spatial and time-correlations of the noise field but an estimate is needed for the implementation of the noise field in the Gmodel (see Section 2.5). The spatial and time-correlations are estimated from 25 equally distributed locations between 30° S-30° N, 120° E-270° E, that is, 5 locations zonally times 5 locations meridionally. This number of locations was enough to cover the whole basin.

2.4 Nonlinear atmospheric feedbacks

The atmosphere is represented by a statistical model of wind stress that consists of a combination of a deterministic and a stochastic term (Eq. 2.2). Both parts can be either a linear or nonlinear function of SST anomalies. In this study we consider two non-linear extensions to the atmospheric component discussed in the previous section: a second order term in the statistical atmosphere model and the dependence of wind stress noise on the background SST via a reformulation of the A-coefficients in Eq. 2.2 (see Figure 1.8b). We restrict the investigation in this study to non-linearities related to atmospheric noise and wind response to SST, elaborating on existing studies by e.g., Lengaigne et al (2004), Eisenman et al (2005), Vecchi et al (2006), Kug et al (2008) and Gebbie et al (2007). Non-linearities in the ocean model are not considered. For both deterministic and stochastic wind stress terms, the functional relationships to SST anomalies are found empirically.

2.4.1 State-dependent wind stress response to SST

The nonlinear response of wind stress to SST is represented by the second term of a Taylor expansion in the statistical atmosphere model:

$$
\begin{aligned}
\tau'_x(x,y,t) &= \sum_{i=1}^{n} A_{2,i}(x,y)T'_i(t) + \\
&+ \sum_{j=1}^{m} B_j(x,y)T'^2_j(t) + \epsilon_2(x,y,t,state)
\end{aligned}
\tag{2.3}
$$

where the patterns $A_{2,i}(x,y)$ and $\epsilon_2(x,y,t,state)$ differ only slightly from the patterns $A_{1,i}(x,y)$ and $\epsilon_1(x,y,t)$ in Eq. 2.2. The term '$state$' will be explained in the next section. The patterns $B_j(x,y)$ are the domain-wide wind stress regression patterns onto the squared

SST anomalies in the boxes $j = 1, 2, ..., m$. These m boxes do not necessarily have to be similar to the n boxes of the linear representation. This is desirable as nonlinear terms might act in a specific region near the equator that must be covered by one box. Note that with the addition of the second order term in the statistical atmosphere model the first two non-zero statistical moments of the noise $\epsilon_2(x, y, t, state)$ also change slightly.

We expect a nonlinear signal near the mean edge of the warm pool. Kessler and Kleeman (2000) already showed this phenomenon in a much simpler model, where wind stress similar to that of the Madden-Julian Oscillation develops a rectified, additional SST anomaly, which contains a response additional to the linear response. This leads to cooling in the West Pacific and warming in the East Pacific. In other words, the zonal gradient is smaller and therefore more westerly winds can occur, even resulting in a mean westerly wind. The result is confirmed by Lengaigne et al (2003) who show [in an atmospheric general circulation model] that the eastward displacement of the warm pool induces an eastward shift of convection, which in turn promotes the occurrence of WWEs. The additional WWEs result in a net westerly response.

2.4.2 State-dependent atmospheric noise properties

In the previous description of noise $\epsilon_1(x, y, t)$ in terms of standard deviation $\sigma(x, y)$ and skewness $S(x, y)$, the noise does not depend on the background SST. However, for instance Kug et al (2009) already suggested that state-dependent noise is directly induced by the low-frequency wind anomaly, which is caused by SST associated with ENSO. In Eq. 2.3 this state-dependence is represented by the term '$state$' in $\epsilon_2(x, y, t, state)$.

A simple method for obtaining an SST dependency is to split the noise timeseries into three equally likely categories depending on the ENSO phase. These three ENSO phases are defined as high, normal or low SST in the central Pacific (El Niño, neutral or La Niña), where all three categories are equally likely by definition. Then, for each of these three phases the standard deviation and skewness fields are computed separately. A similar alteration can be made from $\epsilon_1(x, y, t)$ to $\epsilon_1(x, y, t, state)$.

2.5 Setup of the Intermediate Complexity Model

The influence of atmospheric noise and the nonlinear wind stress response to SST on ENSO is studied with an Intermediate Complexity Model (ICM). This ICM is based on the so called Gmodel (Burgers et al, 2002; Burgers and van Oldenborgh, 2003). The extended version of the Gmodel uses a more comprehensive conceptual model of ENSO than the original one (Figure 1.8b).

The extended Gmodel consists of a linear 1.5-layer reduced-gravity ocean model. It solves the shallow water equations (Gill, 1982). The model domain ranges from $30°$ S to $30°$ N and $122°$ E to $68°$ W, on a $2° \times 1°$ longitude-latitude grid with realistic coast lines, see Figure 2.1. In the reduced-gravity ocean model a Kelvin wave speed is parameterised. Apart from this ocean model the ICM consists of the statistical atmosphere model and the SST equation. The ICM is driven by wind stress noise obtained from the statistical

atmosphere model. As the ICM runs are not time consuming, for each combination of parameter settings the ICM is run for at least 400 years, with a spin-up time of 10 years.

The driving noise terms are prescribed with standard deviation, skewness and correlations as described in the above sections. Reconstructed fields with these three or four characteristics (without or with prescribed skewness) are used as noise fields. Technically, this noise field is implemented by a diffusion operator. This operator generates a spatially correlated field from an uncorrelated noise field that is drawn randomly from a normal distribution with prescribed standard deviation over the whole basin. Optionally, for a non-zero skewness the field is then distorted to the observed skewness. For details of the implementation, see the next section.

The value for the Kelvin wave speed that results in the best ocean dynamics is determined from a forced version of the Gmodel. In this version the SST-equation parameters in the Gmodel are fitted to output from each GCM separately. The forcing is represented by the two-dimensional zonal wind stress anomaly timeseries of the respective ensemble members. For the GCM data different Kelvin wave speeds between 1.8 ms^{-1} and 2.6 ms^{-1} are tested for the highest average correlation between the Gmodel-thermocline depth and the thermocline depth of each ensemble member.

For a selection of GCMs and for observations the fitted components are coupled together, resulting in different versions of the extended Gmodel. Simulations are performed with these different versions of the extended Gmodel. Nonlinearities and noise characteristics are added one by one. Using these tuned reduced models we estimate the influence of the similarities and dissimilarities of atmospheric noise and the nonlinear response of wind stress to SST.

2.6 Reconstruction of noise fields

The idealised noise fields used as input in the ICM should have the same standard deviation, skewness and correlations as the original noise field $\epsilon_1(x, y, t)$ or $\epsilon_2(x, y, t)$ derived from observations and GCM simulations. This is obtained in four successive steps, with $N_1(x, y, t)$, $N_2(x, y, t)$ and $N_3(x, y, t)$ as intermediate steps.

1. Standard deviation: Gaussian distributed random numbers $\varepsilon(x, y)$ (with a standard deviation that equals 1), with x and y varying along the domain, are multiplied by the standard deviation of the original noise field $\sigma(x, y)$:

$$N_1(x, y, t) = \varepsilon(x, y)\sigma(x, y) \tag{2.4}$$

2. Spatial correlation lengths a_x and a_y: the field obtained by Equation 2.4 has to be convolved with a two-dimensional normal distribution with prescribed spatial correlation lengths (a_x and a_y) in order to get a noise field with desired spatial correlations:

$$N_2(x, y, t) \sim a_x a_y \int dx' dy' N_1(x', y', t) e^{-\frac{(x-x')^2}{2a_x^2} - \frac{(y-y')^2}{2a_y^2}} \tag{2.5}$$

In practice, a diffusion operator is used for the convolution. The diffusion operator is designed to ensure that the standard deviation of $N_2(x, y, t)$ ($\sigma'(x, y)$) is approximately the same as the original $\sigma(x, y)$ (Bonekamp et al, 2001).

3. Time correlation $(a_1(x, y))$: the first order time-correlation at lag 1 is imposed by applying:

$$N_3(x, y, t) = \frac{a_1(x, y)N_2(x, y, t - 1) + N_2(x, y, t)}{\sqrt{a_1(x, y)^2 + 1}} \tag{2.6}$$

Note that the standard deviation of $N_3(x, y, t)$ is equal to the standard deviation of $N_2(x, y, t)$ ($\sigma'(x, y)$).

4. Skewness $(S(x, y))$: in order to preserve the standard deviation $\sigma'(x, y)$ but additionally obtain the desired skewness $S(x, y)$, we solve the equation

$$\begin{aligned}
\epsilon(x, y, t) &= A(x, y) + B(x, y)\, N_3(x, y, t) + \\
&\quad + C(x, y)\, S(x, y)\, N_3(x, y, t)^2
\end{aligned} \tag{2.7}$$

for the constants $A(x, y)$, $B(x, y)$ and $C(x, y)$ so that for every location the time mean of $\epsilon(x, y, t)$ is zero, the standard deviation of $\epsilon(x, y, t)$ is $\sigma'(x, y)$ and the skewness of $\epsilon(x, y, t)$ is $S(x, y)$. The solution for $S(x, y) < \sqrt{8}$ is (derivation not shown):

$$A(x, y) = -C(x, y)\sigma(x, y)^2 S(x, y)$$
$$B(x, y) = \sqrt{\cos(2\phi/3) + \sqrt{3}\sin(2\phi/3) - 1}$$
$$C(x, y) = \frac{-\cos(\phi/3) + \sqrt{3}\sin(\phi/3)}{\sqrt{2}\sigma(x, y)S(x, y)}$$
with $\phi = -\arctan\left(\sqrt{8 - S(x, y)^2}/S(x, y)\right)$

With this equation the noise field is then transformed towards correct skewness.

These 4 steps are repeated every time that the wind stress field in the ICM is calculated. The resulting fields are added as driving noise terms to the Gmodel.

3. EL NIÑO IN A CHANGING CLIMATE: A MULTI-MODEL STUDY

In many parts of the world, climate projections for the next century depend on potential changes in the properties of the El Niño — Southern Oscillation (ENSO). The current status of these projections is assessed by examining a large set of climate model experiments prepared for the Fourth Assessment Report of the Intergovernmental Panel on Climate Change. Firstly, the patterns and time series of present-day ENSO-like model variability in the tropical Pacific Ocean are compared with that observed. Next, the strength of the coupled atmosphere-ocean feedback loops responsible for generating the ENSO cycle in the models are evaluated. Finally, we consider the projections of the models with, what we consider to be, the most realistic ENSO variability.

Two of the models considered do not have interannual variability in the tropical Pacific Ocean. Three models show a very regular ENSO cycle due to a strong local wind feedback in the central Pacific and weak sea surface temperature (SST) damping. Six other models have a higher frequency ENSO cycle than observed due to a weak east Pacific upwelling feedback loop. One model has much stronger upwelling feedback than observed, and another one cannot be described simply by the analysis technique. The remaining six models have a reasonable balance of feedback mechanisms and in four of these the interannual mode also resembles the observed ENSO both spatially and temporally.

Over the period 2051–2100 (under various scenarios) the most realistic six models show either no change in the mean state or a slight shift towards El Niño-like conditions with an amplitude at most a quarter of the present day interannual standard deviation. We see no statistically significant changes in amplitude of ENSO variability in the future, with changes in the standard deviation of a Southern Oscillation Index that are no larger than observed decadal variations. Uncertainties in the skewness of the variability are too large to make any statements about the future relative strength of El Niño and La Niña events. Based on this analysis of the multi-model ensemble, we expect very little influence of global warming on ENSO.

3.1   Introduction

The El Niño – Southern Oscillation phenomenon (ENSO) is the largest and best known mode of climate variability that affects weather, ecosystems and societies in large parts of the world. The influence of increasing greenhouse gases on the properties of ENSO is a

critical question in determining the impacts of climate change at the regional scale. Because of the complexities of the physical processes involved, we must rely heavily on complex climate models which represent interactions between those processes explicitly. Here we assess ENSO simulations in the multi-model ensemble collected for the Intergovernmental Panel on Climate Change (IPCC) Fourth Assessment Report (4AR).

Observations and understanding of ENSO have progressed rapidly over the last decade (e.g. McPhaden et al, 1998; Neelin et al, 1998). The theoretical framework we will be using is sketched in Fig. 1.8 (Fedorov and Philander, 2001; Burgers and van Oldenborgh, 2003). The main positive feedback in the ENSO cycle is represented by the outer loop (Bjerknes, 1966). Wind anomalies in the central equatorial Pacific generate thermocline anomalies which travel to the east. In the eastern equatorial Pacific these upwell as sea surface temperature (SST) anomalies, which in turn give rise to wind anomalies in the central Pacific. There is a secondary feedback loop in the central Pacific (Wyrtki, 1975; Picaut et al, 1996), whereby SST is affected directly by wind anomalies via advection, anomalous upwelling, evaporation and mixed-layer depth anomalies. These central Pacific SST anomalies in turn influence the wind. The whole system is close to stability and affected by external noise in the form of wind variations. While this conceptual model represents radiative feedbacks (Yu and Boer, 2002) only as damping terms, we should note the climate models examined all have complex representations of clouds and radiation.

Most climate models now show ENSO-like oscillations in the tropical Pacific and the properties of the modelled time series in the current climate may be compared with that observed. However, there are many different physical ways in which models can produce interannual oscillations. Using the ENSO theory outlined in Chapter 1, we first evaluate whether the main nodes in Fig. 1.8 have the correct variability. Next, we compare the strength of the linear couplings in the models to the observations. The changes in ENSO properties under global warming can then be assigned confidence levels using these findings.

Previous complex model studies (e.g. Meehl et al, 1993; Knutson et al, 1997; Tett, 1995; Timmermann et al, 1999; Collins, 2000a,b) have used a wide range of techniques to evaluate the model ENSO behaviour and found a wide range of responses to increasing greenhouse gases from no change to significant changes in the amplitude, frequency and skewness of ENSO. As an example of more recent work in the manner of the study we present here, Zelle et al (2005) analysed the links of the feedback chains quantitatively in the NCAR CCSM 1.4 model. They found that in spite of very reasonable overall ENSO properties, this coarse resolution model suffers from a number of flaws that cast doubt on the projected ENSO properties: the wind response is too narrow in latitude leading to a more stable ENSO cycle; the wind response does not depend on the background temperature, and the central Pacific surface cycle is too strong compared with the Bjerknes feedback loop. By examining the key physical processes responsible for ENSO properties in the models, we can build confidence in their predictions of changes in properties in a warmer world. Ultimately we should attach formal likelihoods to different model projections in order to make probabilistic predictions of future climate (e.g. Murphy et al, 2004).

The outline of this chapter is as follows. First, the models and their output are introduced in Sect. 3.2. For these models we consider the overall ENSO properties: amplitude,

pattern, spectrum of the time series in SST in Sect. 3.3 and the corresponding amplitudes in zonal wind stress and thermocline depth in Sect. 3.4. Next, we discuss the most important linear couplings shown in Figure 1.8. We discuss the wind response to SST anomalies in Sect. 3.5 and the SST response to thermocline and wind anomalies in Sect. 3.6. The response to increasing greenhouse gases is discussed in Sect. 3.7 and we give a short set of conclusions in Sect. 3.8.

3.2 Models

The model set consists of the climate models that had made enough data available via the IPCC data center at PCMDI on April 15, 2005 (subsurface data for ECHAM5/MPI-OM and UKMO HadGEM1 was obtained directly from the modeling groups). The list is given in Table 3.1, including references to detailed information about the models. Properties of present-day ENSO are from the "Climate of the twentieth century" (20c3m) experiments except for the UKMO HadGEM1 model, for which the pre-industrial control (picntrl) was used. For the future climate we used the last 50 years of the SRES A2 experiments, except for FGAOLSg-1.0 and MIROC3.2 (hires), for which the SRES A1B was used, and GISS-EH and UKMO HadGEM1, which only had "1% increase per year to doubling" (1pctto2x) experiments available.

Observations are mainly taken from the Tropical Atmosphere Ocean (TAO) array of moored buoys (McPhaden et al, 1998), which has measured many variables at a relatively coarse grid. Most buoys have been deployed in the late 1980s, so that the length of the record is the main restriction. SST measurements go further back, the pattern of ENSO variations is compared to the SSTOIv2 analyses of Reynolds et al (2002) over 1981–2004 and the time series properties are evaluated against the reconstruction of Kaplan et al (1998) which covers the period 1856–2003. Finally, we use the NCEP tropical Pacific ocean reanalysis 1980–1999 (Behringer et al, 1998) for subsurface temperatures and the ERA-40 reanalysis (Uppala et al, 2005) for sea-level pressure (SLP) and zonal wind stress (τ_x).

3.3 SST variability in the tropical Pacific

Most of the climate models considered show ENSO-like oscillations in the tropical Pacific. We compare the SST expression of these oscillations in the current climate with that observed by calculating the first EOF over the region $10°$ S–$10°$ N, $120°$ E–$90°$ W, as this captures the main pattern, period and amplitude of SST variability. It excludes the coastal El Niño which models do not simulate, presumably because the thermocline is too deep as a consequence of the absence of stratus clouds. Despite this limitation, the characteristic examples shown in Fig. 3.1 show that many models can capture SST variability well.

In Table 3.2 the main features are summarized for all models. In the SSTOIv2 analysis (1981–2004) the first EOF explains 65% of the variance and matches the cold tongue upwelling region along the equator (Fig. 3.1a). The corresponding time series of the Kaplan analysis (1856–2003) has a broad peak in the spectrum spanning periods from 2.5 to 6 years. The standard deviation is 0.20 (with the EOF pattern normalized to one) and the

skewness is 0.54; this means that SST anomalies are in general larger during El Niño than during La Niña.

The GISS-AOM and GISS-ER models do not appear to simulate any ENSO variability and are not considered in the rest of the paper. This is most likely due to the ocean resolution being too coarse to describe the equatorial wave guide. We should note however that other coarse resolution models can simulate some ENSO variabiliy (Collins, 2000a) and that the highest ocean resolution does not guarantee the best simulation by this measure.

In the models CCSM3 (Otto-Bliesner and Brady, 2001) and CGCM3.1(T47) the SST variability pattern is displaced to the west, the peak in the spectrum is at slightly higher frequencies than in the observations, the amplitude is lower than observed and the skewness close to zero (e.g. Fig. 3.1b). These are well-known (but not fully understood) effects of a coarse-resolution atmosphere model (van der Vaart, 1998; Guilyardi et al, 2004; Zelle et al, 2005). The CSIRO-Mk3.0 (Cai et al, 2003), GFDL-CM2.0 (Wittenberg et al, 2005), GISS-EH (Schmidt et al, 2006), INM-CM3.0 (Volodin and Diansky, 2004), MRI-CGCM2.3.2 and PCM (Meehl et al, 2001) models also have a too short ENSO period but do not display all the features described above.

The models CNRM-CM3, FGOALS-g1.0 (Yu et al, 2004) and IPSL-CM4 (Codron et al, 2001) display an unrealistically sharp ENSO peak in the spectrum, with variability mainly in the eastern Pacific (illustrated in Fig. 3.1c with the CNRM-CM3 results). These models all have a larger ENSO amplitude than observed and negative skewness. This behaviour resembles the one observed in intermediate complexity models above the first Hopf bifurcation (Dijkstra, 2000). The ENSO cycle then is a self-sustained regular oscillation that has not yet reached the chaotic stage. It is affected very little by atmospheric noise. The HadGEM1 model (Johns et al, 2004) also has a narrowly peaked spectrum, but a lower amplitude and positive skewness.

The remaining models, ECHAM5/MPI-OM (Keenlyside et al, 2005), GFDL-CM2.1 (Wittenberg et al, 2005), MIROC3.2 (K-1 model developers, 2004) and HadCM3 (Collins, 2000a), (Figs 3.1d-f) resemble the observed ENSO reasonably well in SST variability. A noteworthy result is that the high-resolution version of MIROC3.2 has a much more realistic skewness than the medium resolution version.

3.4   Variability in wind stress and thermocline depth

While the variability of SST is a useful indicator of the gross characteristics of ENSO, the mechanisms which generate the coupled nature of the mode must be examined in order to fully evaluate model reliability. Hence we examine the variables displayed in Fig. 1.8 by computing the standard deviation of the grid box SST variability at the location of the maximum of the first SST EOF, the standard deviation of zonal wind stress at the location of the maximum of the zonal wind response to this SST EOF, and the standard deviation of the depth of the $20°$ C isotherm at these two positions as a measure of the depth of the thermocline. Numerical values are shown in Table 3.3 with uncertainties quantified by the 95% confidence interval obtained using a bootstrapping approach with 7-month moving blocks. For the observations we use single buoys from the TAO array which we note are only available from the rather active last 20 years. Both factors lead to higher observed

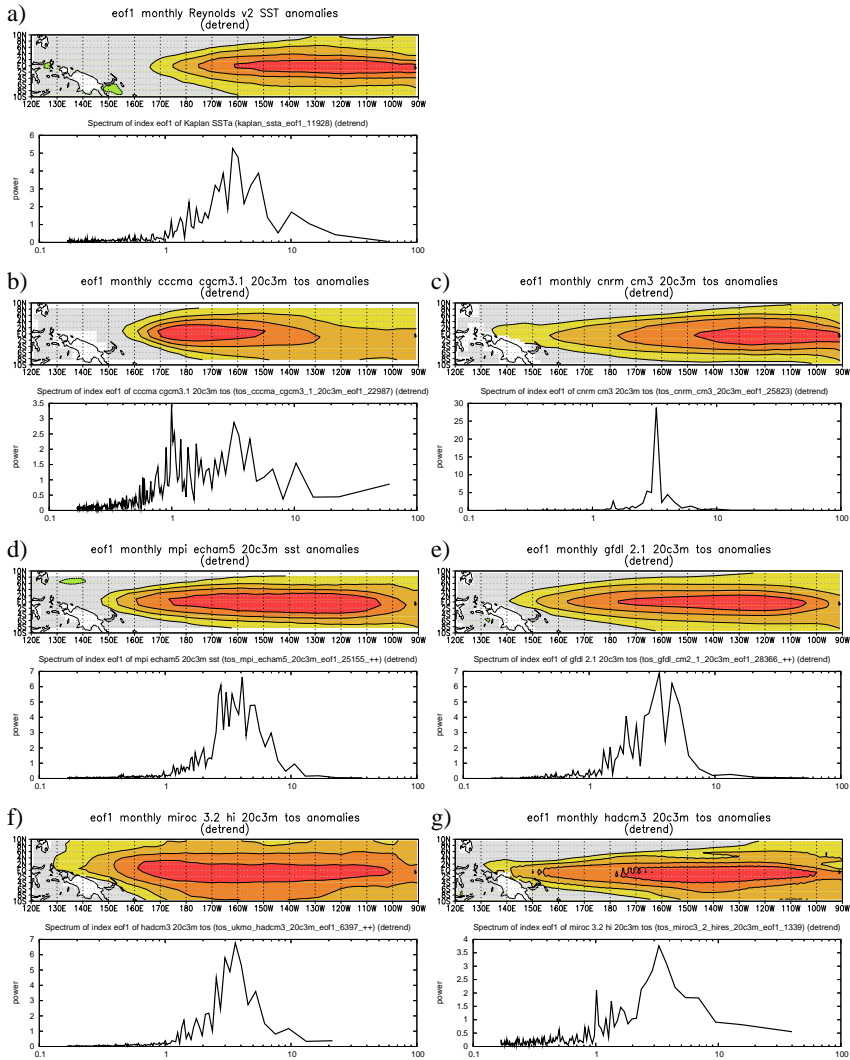*Fig. 3.1:* Examples of the first EOF of detrended SST in the region 10° S–10° N, 120° E–90° W and the spectrum of its corresponding time series. The pattern is normalized to have unit amplitude and the contour interval is 0.2. a) Observations: the pattern of SSTOIv2 and the time series of Kaplan SST, b) CGCM3.1(T47), c) CNRM-CM3, d) ECHAM5/MPI-OM, e) GFDL-CM2.1, f) MIROC3.2(hires) and g) HadCM3.

variability, especially in wind stress and SST, than can be expected from a long model simulation.

In many models thermocline variability is underestimated in comparison with the observations although we should note the caveat above regarding the length and period of the observed record. The wind stress variability depends strongly on the weather noise, so that the low variability in many models can be due either to a too weak ENSO signal or too little internal atmospheric variability (many models fail to simulate intraseasonal variability for example). Exceptions are CNRM-CM3 and FGOALS-g1.0, which overestimate the SST variability, and HadCM3 and ECHAM5/MPI-OM, which seem well-balanced.

There are various instances in which a reasonable SST variability is generated from zonal wind stress and thermocline variability that is much lower than observed. These sensitivities will be explored in more detail in Sect. 3.6.

3.5   Wind response to SST perturbations

The amplitude of zonal wind stress variability in Table 3.3 is a combination of the slow variations that are part of the ENSO cycle and high-frequency weather noise integrated to the monthly time scale. To separate these contributions, the response of the atmosphere model to SST variations along the equator is examined. This may be done by regressing the zonal wind stress onto the first EOF of SST computed in Sect. 3.3. However, the length of the simulations allows for a more detailed treatment. For each model we construct a statistical atmosphere model with as basis n equal-sized boxes along the equator in $5°$ S–$5°$ N, $140°$ E–$80°$ W (e.g. Von Storch and Zwiers, 2001, §8.3), see Eq. 2.2. The patterns show the average atmospheric response to an SST anomaly in this box only. For comparison with observations we only show results for $n=3$ boxes. More detailed plots with n up to eight (for long runs with multiple ensemble members) confirm the findings.

The ERA-40 data have been analyzed with three boxes (Figs. 3.2): western Pacific (warm pool), central Pacific (approximately equal to Niño4) and eastern Pacific (cold tongue, similar to Niño3). We see that the response to a temperature anomaly in the central box is indeed stronger than the response to an anomaly in the eastern box. In both of these regions the longitudinal offsets cancel: the zero wind stress anomaly line is near the middle of the SST anomaly. The response to the western box is "drowned" in the noise with only 45 years of data and only small SST variability.

The atmospheres of the climate models are less noisy as there is more data to construct the statistical atmosphere model. The responses are very diverse (Figs. 3.2 and 3.3). Almost all models show a weaker positive atmospheric response than the reanalysis when SST anomalies are present in the central or eastern Pacific. Only the MRI-CGCM2.3.2 model has a stronger response, with peak values twice those found in ERA-40. The CCSM3, CGCM3.1(T47), MIROC3.2(hires), HadCM3 and HadGEM1 models have a peak response that is only slightly weaker than the reanalysis, whereas the PCM model hardly shows any response at all. The weak response in most models explains why thermocline variability is in general lower than observed, although the exceptions (CNRM-CM3, FGOALS-g1.0, and INMCM3.0) show that there are other factors as well. A weak wind response will also suppress the non-linear aspects of ENSO in the ocean.

The equatorial negative response to the east of the SST anomaly in the central Pacific is also (much) weaker than observed in most models. Only the CCSM3, GFDL-CM2.0, GFDL-CM2.1 and HadGEM1 models have the same magnitude. The off-equatorial response is important in setting the time scale of the ENSO cycle. The negative patterns of the Rossby wave response in the Gill pattern are hardly visible in the reanalysis, but much stronger in many models, especially CNRM-CM3 and MIROC3.2(medres). This is partly due to the much narrower latitudinal response in the models, a well-known problem with low resolution atmospheres (Guilyardi et al, 2004; Zelle et al, 2005), although not necessarily improved at higher resolutions. In general the narrower response leads to a shorter and more stable ENSO cycle. The northern off-equatorial response is positive rather than negative in the FGOALS-g1.0, HadCM3 and HadGEM1 models.

The location of the response is more easterly than in observations in most models. Only in ECHAM5/MPI-OM, the GFDL models, IPSL-CM4 and MRI-CGCM2.3.2 the offset is zero, as observed. FGOALS-g1.0 shows a westerly offset. In most models the response is stronger over warmer water, as expected. Only in CCSM3 the strength is largest over the cold tongue (which in this model is in the central Pacific).

The response to SST anomalies in the western Pacific is stronger than in the reanalysis in most models. However, this is likely a problem in the reanalysis rather than the climate models, as SST variability is small in the warm pool, which means the response cannot be determined well by this technique.

3.6   SST response to wind and thermocline perturbations

Most models have a wind response to SST anomalies that is too weak, and hence less thermocline variability than observed. There are three ways to obtain SST variability with a realistic amplitude from a weak wind response. Either SST responds more strongly to thermocline variability in the cold tongue, or SST responds more strongly to local wind anomalies on the edge of the warm pool, or SST damping is reduced. These processes have been separated by fitting the simple local SST equation (Eq. 2.1) (Burgers and van Oldenborgh, 2003) to both observations and GCM output.

In the TAO data the SST model Eq. (2.1) explains 60–80% of the variance along the equator (Fig. 3.4a), from $170°$ E where surface processes dominate to $110°$ W in the cold tongue where upwelling variability determines SST. The TAO buoy at EQ, $95°$ W has only 80 months of observations, so the uncertainties in the fit parameters are quite large. In the climate models (examples are shown in Figs. 3.4b–f) the fraction of explained variance is similar in most models: higher when there is little weather noise (CNRM-CM3, FGOALS-g1.0), and usually lower in models with a weak ENSO (GISS-EH, MIROC3.2(hires)). In general the SST model fits the data reasonably well in the region where ENSO is active.

In Figs. 3.5, 3.6 and 3.7 the values of the parameters α, β and γ^{-1} are plotted as a function of longitude, averaged over the equatorial wave guide $3°$ S–$3°$ N. In the GISS-EH model the parameters fluctuated so wildly that they have not been plotted. The other models are shown in three groups. The first one has wind stress sensitivities in the central Pacific β that are within 50% of those obtained from the TAO data, the second group is within a factor two and the third one outside of that.

ERA40

CCSM3

CGCM3.1(T47)

CNRM-CM3

CSIRO-Mk3.0

ECHAM5/MPI-OM

FGOALS-g1.0

GFDL-CM2.0

GFDL-CM2.1

-0.02 -0.016 -0.012 -0.008 -0.004 0.004 0.008 0.012 0.016 0.02
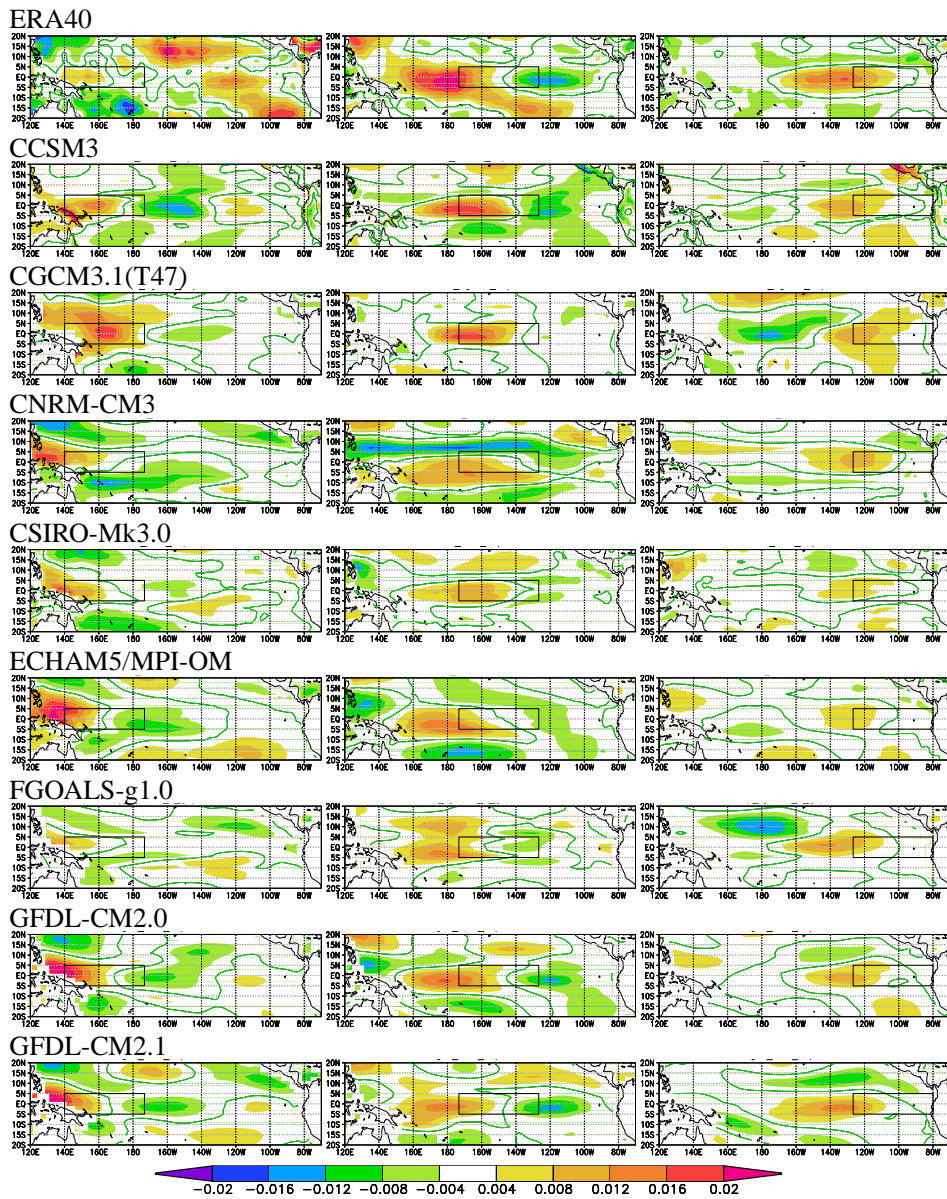
Fig. 3.2: The zonal wind stress response $[\mathrm{Nm}^{-2}\mathrm{K}^{-1}]$ to SST anomalies in three equal-sized boxes in $5°$ S–$5°$ N, $140°$ E–$80°$ W.

GISS-EH

INM-CM3.0

IPSL-CM4

MIROC3.2(hires)

MIROC3.2(medres)

MRI-CGCM2.3.2

PCM

HadCM3

HadGEM1
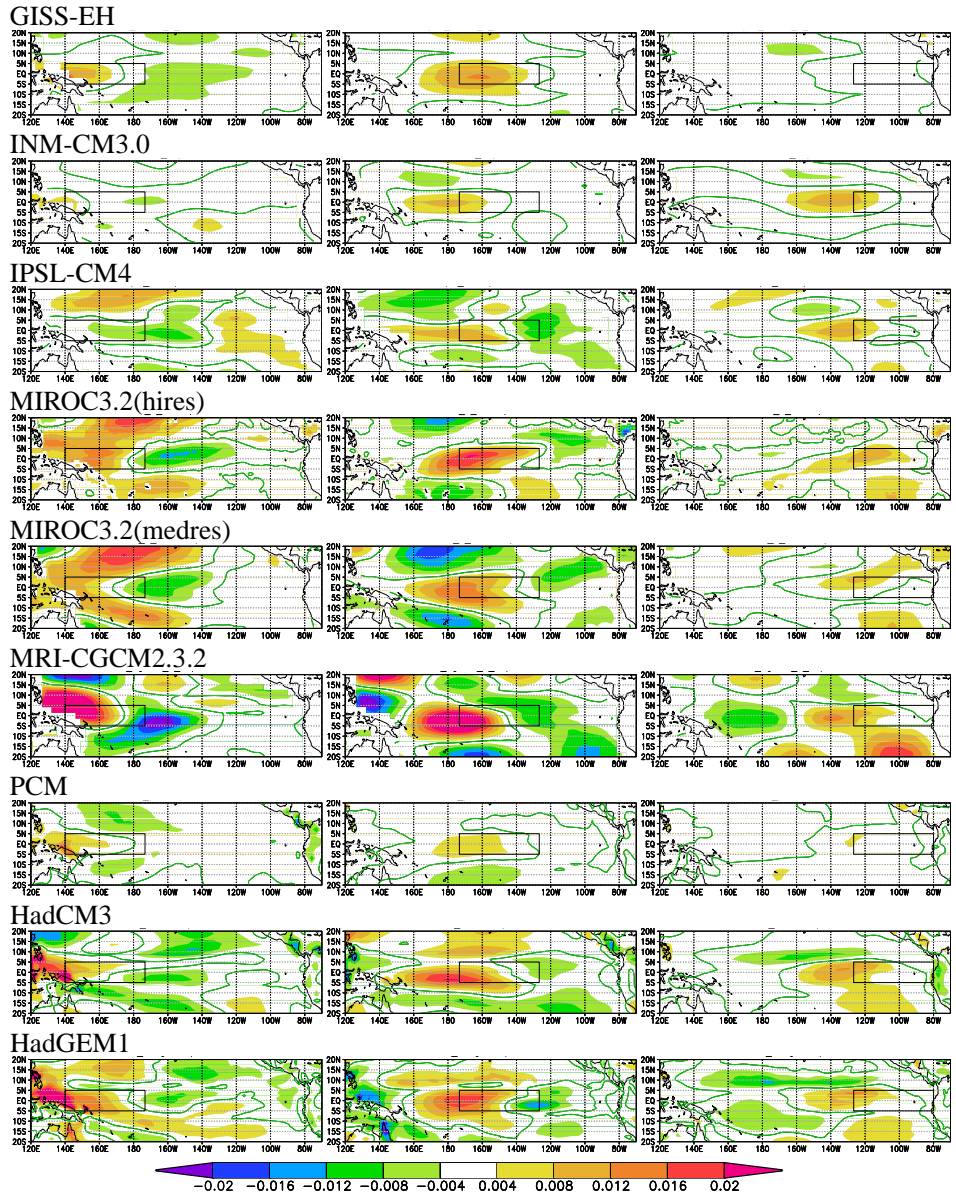
Fig. 3.3: continuation of Fig. 3.2
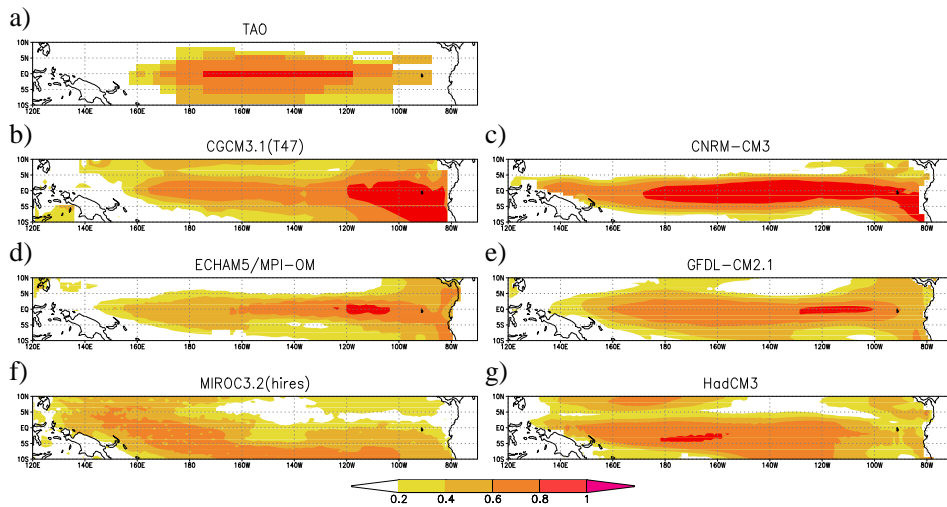
Fig. 3.4: Fraction of SST variance explained by the simple SST model Eq. 2.1 over an AR1 model ($\alpha = \beta = 0$) in **(a)** TAO data, **(b)** CGCM3.1(T47), **(c)** CNRM-CM3, **(d)** ECHAM5/MPI-OM, **(e)** GFDL-CM2.1 **(f)** MIROC3.2(hires) and **(g)** HadCM3.

We see that in most models, the weak zonal wind response found in Sect. 3.5 is compensated by an enhanced sensitivity of SST to zonal wind stress β and a longer damping time γ^{-1}, whereas the sensitivity to thermocline depth variations α clusters around the value deduced from observations. A notable exception to this pattern is the MRI-CGCM2.3.2 model, in which the thermocline sensitivity is a factor three stronger than observed. In this model the damping term is stronger than in most other models (and close to the value fitted from observations) to keep the ENSO amplitude reasonable.

The models with a very regular ENSO cycle (CNRM-CM3, FGOALS-g1.0 and IPSL-CM4) all have weak damping and strong wind feedback. Most models with a short ENSO cycle (CCSM, CSIRO-Mk3.0, CGCM3.1(T47), INM-CM3 and PCM) have too strong wind sensitivities in the central Pacific to compensate for the weak wind response. As the thermocline feedback is not enhanced, this implies that ENSO in these models is much more surface-driven than in the observations. SST in the HadGEM1 and GISS-EH models is not described well by Eq. (2.1).

The models with spectra that most resemble observations (ECHAM5/MPI-OM, GFDL-CM2.1, HadCM3, MIROC3.2 and to a lesser extent GFDL-CM2.0) show SST sensitivities comparable to observations in the relevant regions: wind stress in the central Pacific, thermocline in the eastern Pacific.
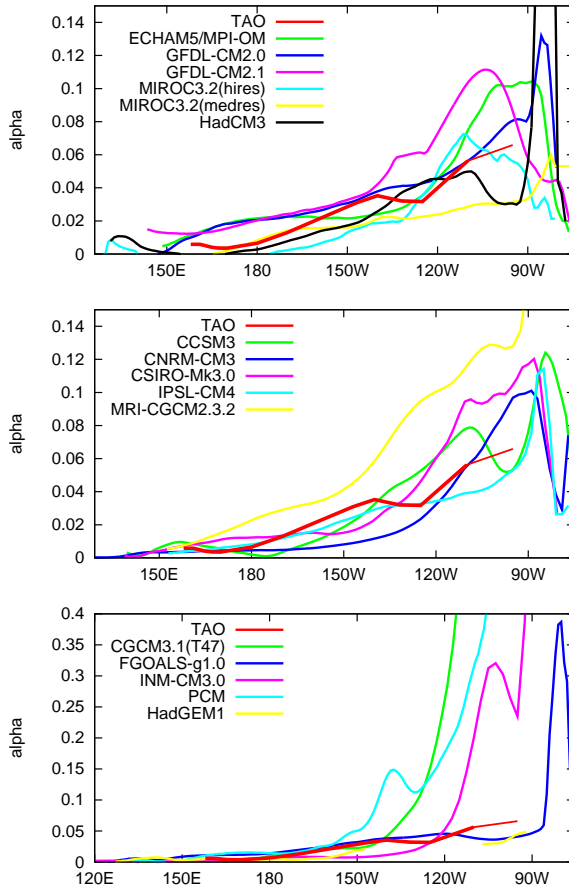
Fig. 3.5: The parameter α $(\text{km}^{-1}\text{month}^{-1})$ that describes the effect of thermocline anomalies on SST in Eq. 2.1 averaged over $3°$ S–$3°$ N in the TAO observations and the climate models. Note the change of scale in the third panel.
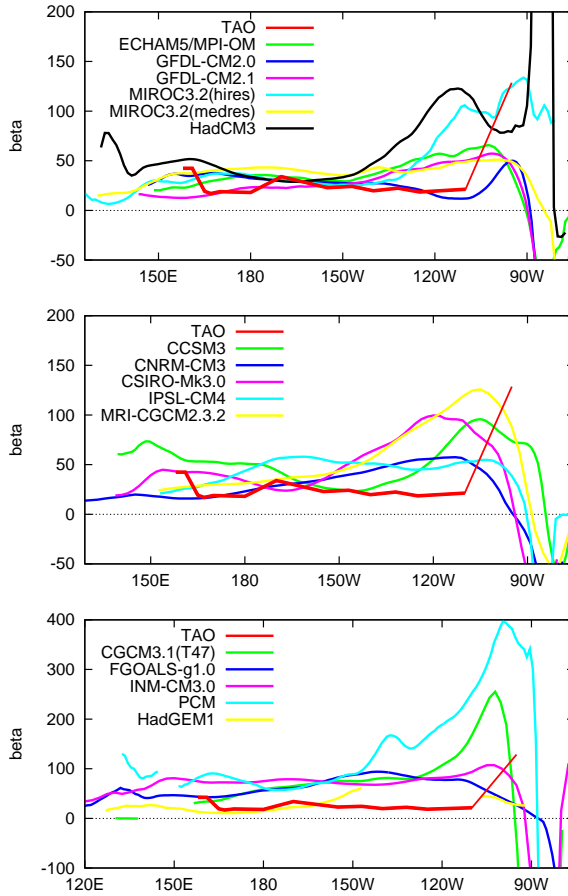
Fig. 3.6: The parameter β $(\mathrm{KPa}^{-1}\mathrm{month}^{-1})$ that describes the effect of wind stress anomalies on SST in Eq. (2.1) averaged over $3°$ S–$3°$ N in the TAO observations and the climate models. Note the change of scale in the third panel.
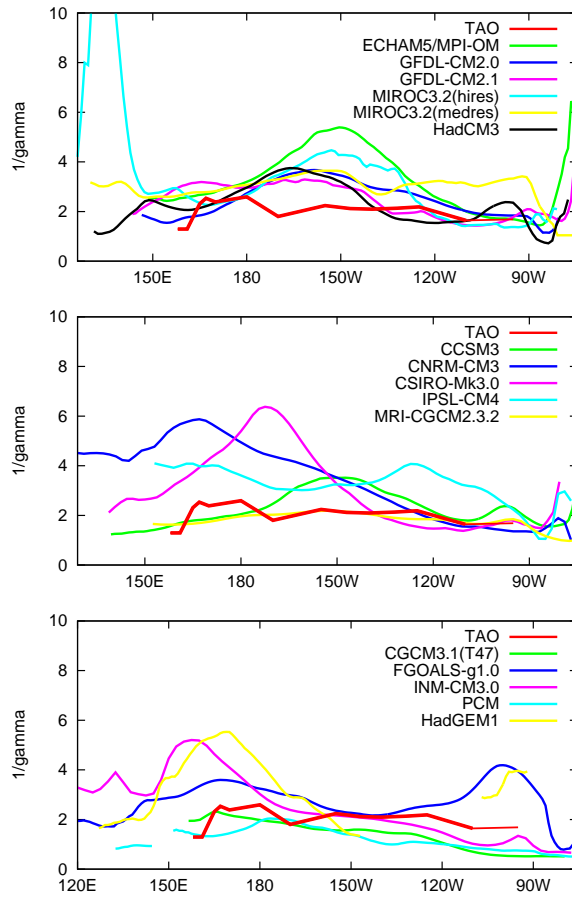
Fig. 3.7: The damping time γ^{-1} (months) in Eq. 2.1, averaged over 3° S–3° N in the TAO observations and the climate models.

3.7   ENSO in a warmer climate

After assessing the representation of ENSO in the current climate we next turn to the projections for the next century. Specifically, projected changes in the mean state, amplitude and skewness are considered. The SST expression of the ENSO cycle is not the most convenient index as it is mixed with the global warming signal itself. Instead, we use a pressure index comparable to the Southern Oscillation Index (Walker and Bliss, 1932; Berlage, 1957): the time series of the first EOF of SLP normalized to standard deviation over the area $30°$ S–$30°$ N, $30°$ E–$60°$ W. In order to minimize the influence of weather noise a 5-month running mean is applied. In the ERA-40 reanalysis this index is strongly correlated with the traditional Darwin-Tahiti SOI ($r = -0.91$). For scenario experiments the pattern obtained in the current climate is projected onto the SLP field of the future (in the IPSL and MIROC3.2(hires) models, the second EOF corresponds to the Southern Oscillation). The patterns are in general very realistic (Fig. 3.8) and do not change significantly under global warming.

For ENSO variability and skewness the first EOF of SST in the region $10°$ S–$10°$ N, $120°$ E–$90°$ W with a 10yr running mean subtracted was also considered. The results were identical to the ones obtained with the SLP index.

In Table 3.4 the results are shown as the difference in the mean value of the indices in the future climate divided by the standard deviation of the current climate, the ratio of the standard deviations, and the skewness. The future climate is represented by the last 50 years of the scenario run (SRES A2, SRES a1B or 1%/year compounded CO_2 increase). Uncertainty estimates (95% limits) have been computed with a moving block bootstrap procedure. The subjective confidence level attached to the prediction (medium, high) reflects whether ENSO in the model seems to be based on the same physical processes as in the observations, as determined in the previous sections.

As in previous studies (e.g. Collins, 2004), changes in the mean state range from more La Niña-like conditions to more El Niño-like mean conditions. The low-resolution models CGCM3.0(T47), GISS-EH, INM-CM3, IPSL-CM4 and PCM project a change to more La Niña-like mean conditions, but these all have been assigned a lower confidence level due to either a too regular cycle or too much of a surface-driven ENSO cycle. In most of these models this shift is due to a large change in the Indian Ocean or off-equatorial Pacific Ocean projecting onto the ENSO pattern. The only model in which the time change in surface pressure resembles the Southern Oscillation is INM-CM3.0, however, in the stabilisation period after 2100 this model switches to a more El-Niño-like state.

CCSM3, CNRM-CM3, ECHAM5/MPI-OM, FGOALS-g1.0, the MIROC3.2 models and MRI-CGCM2.3.2 show a shift to on average more El Niño-like mean conditions. Almost all these shifts are about one quarter of the interannual standard deviation. (The much larger shift in the high resolution version of the MIROC3.2 model is due to a discontinuity between the twentieth century run and the SRES A1B run; the scenario run indicates a much smaller shift in the mean state.) Again, only in ECHAM5/MPI-OM and MRI-CGCM2.3.2 the shift resembles the Southern Oscillation pattern.

The remaining models, CSIRO-Mk3.0, both GFDL models and the Hadley Centre models HadCM3 and HadGEM1 show no significant change to a more El Niño or La Niña-like

climatology.

The trends in sea-level pressure are not necessarily consistent with the trends in SST, as investigated by others (e.g. Guilyardi, 2006; Merryfield, 2006). Quite a few models show warming in the cold tongue, but no change in SLP, or even a shift to La Niña (CGCM3.1(T47), IPSL-CM4). This could be understood as a change ΔT in the cold tongue having less effect on air pressure than the same change in the warm pool. As the main reason for this study is the effect of ENSO on the weather, we consider the pressure trends to be the more important ones.

The range in forecasts for the SLP variability is just as large. The CCSM3, CGCM3.0(T47), FGOALS-g1.0, MIROC3.2(medres) and PCM models have statistically significant less variability in the last 50 years of the scenario runs; the ECHAM5/MPI-OM, GFDL-CM2.0, MRI-CGCM2.3.2 and HadCM3 models show more activity and the other models (CNRM-CM3, CSIRO-Mk3.0, GFDL-CM2.1, GISS-EH, INM-CM3, IPSL-CM4, MIROC3.2(hires) and HadGEM1) have no significant change in standard deviation under global warming. The difference between the two versions of the GFDL model (a factor 1.21 ± 0.12 higher standard deviation in CM2.0 and 0.88 ± 0.13 in CM2.1) shows that the change in variability is due to small details of the model, similar to that seen in Collins (2000b). Note that the changes are of the same order as those observed in the SOI over the period 1866–2004, so that the predicted change in standard deviation is often only significant with more than one ensemble member, and hence unobservable in reality.

Due to the limited number of years (50) in the future period, only the FGOALS-g1.0 and MRI-CGCM2.3.2 models show a shift in skewness that is statistically significantly different from zero. However, even the models that resemble reality most do not reproduce the observed skewness of SST, thermocline depth and zonal wind stress very well, so they are unlikely to contain correctly the nonlinear mechanisms that determine the differences between El Niño and La Niña. We therefore do not attach much significance to the fact that these models do not show much change in skewness.

3.8 Conclusions

We have studied ENSO-like oscillations in the equatorial Pacific in the 19 climate models that had made data available in the PCMDI archive at the time of submission. First, the similarity of these oscillations with the observed ENSO cycle has been determined. Two models (GISS-AOM and GISS-ER) do not show ENSO-like variability and are excluded from the analysis.

Three models (CNRM-CM3, FGOALS-g1.0 and IPSL-CM4) show very regular oscillations with negative skewness, in contrast to the real irregular ENSO cycle with positive skewness. These models seem to operate in a different dynamical regime than the point close to stability that the observed ENSO is thought to occupy. Another group of models (CCSM3, CGCM3.1(T47)), has a more westerly ENSO pattern than observed, a shorter period, a lower amplitude and no skewness. Other models (CSIRO-Mk3.0, GFDL-CM2.0, GISS-EH, INM-CM3, MRI-CGCM2.3.2, PCM) share most of these properties, which often occur in coarse-resolution models. ECHAM5/MPI-OM, GFDL-CM2.1, MIROC3.2 and HadCM3
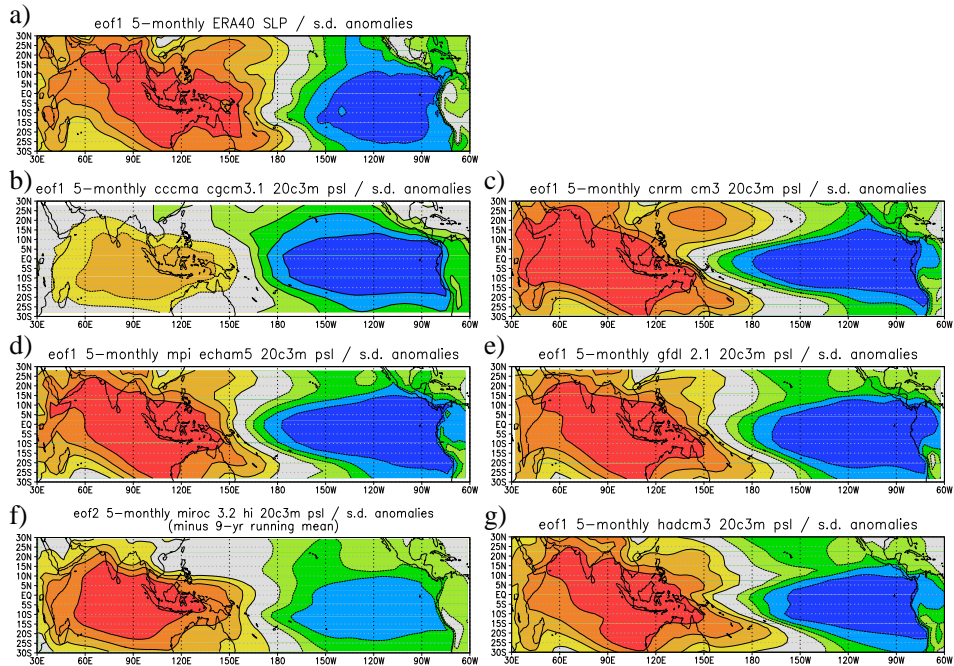
Fig. 3.8: First EOF of normalized sea-level pressure over the region $30°$ S–$30°$ N, $30°$ E–$60°$ W ($\alpha = \beta = 0$) in **(a)** TAO data, **(b)** CGCM3.1(T47), **(c)** CNRM-CM3, **(d)** ECHAM5/MPI-OM, **(e)** GFDL-CM2.1, **(f)** MIROC3.2(hires) (second EOF) and **(g)** HadCM3.

display the most realistic time series properties. HadGEM1 is unlike other models with a fairly narrow spectral peak but positive skewness.

The reasons for these diverse modelled ENSO cycles become clearer when considering the strength of the zonal wind response to equatorial SST anomalies and the SST response to wind and thermocline depth anomalies. Most models show a zonal wind response that is weaker and more confined in latitude than the observations. This is compensated by a stronger direct SST response to wind anomalies and weaker damping of surface temperature than the observations indicate, whereas the reaction to thermocline depth anomalies is similar to estimates from TAO data. In these models ENSO is therefore more surface-driven than thermocline-driven. A different mixture occurs in the MRI model, in which SST reacts very strongly to both wind and thermocline depth anomalies, and is more damped to obtain a realistic SST variability. The ECHAM5/MPI-OM, GFDL-CM2.0, GFDL-CM2.1, MIROC3.2 and HadCM3 models show a fairly realistic balance between the two feedback loops of the ENSO cycle and the forecasts from these models are considered most reliable.

In these models the forecasts for the mean state of ENSO in 2051–2100 in an SRES A2 scenario range from no change (four models) to a small shift (25% of the standard deviation) towards more El Niño-like conditions (two models) in surface pressure. The variability projections vary from a slight increase, by 15% (three models), through no change (two models) to a decreases by 15% (one model). The possible changes are of the same size as the observed decadal variability over the last century and only statistically significant for multiple ensemble members. It will therefore be difficult to verify with only one realization of reality. The statistical and systematic errors in skewness are too large to say anything with any degree of certainty about the relative strength of El Niño and La Niña events in a future climate.

This is only a first assessment of the characteristics of ENSO variability in climate models, covering what we judge to be the most important aspects. In the conceptual model of the ENSO cycle of Fig. 1.8 we have not considered the characteristics of the external noise, nor the relationship between zonal wind stress anomalies and thermocline perturbations. The seasonal cycle has been neglected throughout. Apart from this simplified picture the radiation and latent heat contributions to SST variability should be studied in more detail. The causes of changes in ENSO properties in the modelled future climate have also not been investigated in this study but should be a priority for future work. The next chapter addresses the feedback relationships.

Tab. 3.1: The models considered here. The ocean resolution is the resolution along the equator. The number of ensemble members refers to runs with different initial conditions. For most models, ocean data was available only for a single ensemble member.

Name	Originating group(s)	Country	Resolution atmosphere	Resolution ocean	Ensemble members	Reference
CCSM3	NCAR	USA	T85L26	$1.125° \times 0.27°$ L40	6	Collins et al (2006b)
CGCM3.1(T47)	CCCMA	Canada	T47L31	$1.85° \times 1.85°$ L29	1	Kim et al (2002)
CNRM-CM3	Météo-France/CNRM	France	T63L45	$2° \times 0.5°$ L31	1	Salas-Mélia et al. (2005)[1]
CSIRO-MK3.0	CSIRO	Australia	T63L18	$1.875° \times 0.84°$ L31	1	Gordon et al (2002)
ECHAM5/MPI-OM	MPI	Germany	T63L31	$1.5° \times 1.5°$ L40	3	Jungclaus et al (2006)
FGOALS-g1.0	LASG/IAP	China	T42L26	$1° \times 1°$ L33	3	Yu et al (2004)
GFDL-CM2.0	GFDL	USA	$2.5° \times 2°$ L24	$1° \times 1/3°$ L50	3	Delworth et al (2006)
GFDL-CM2.1	GFDL	USA	$2.5° \times 2°$ L24	$1° \times 1/3°$ L50	3	Delworth et al (2006)
GISS-AOM	NASA/GISS	USA	$4° \times 3°$ L12	$4° \times 3°$ L16	2	Lucarini and Russell (2002)
GISS-EH	NASA/GISS	USA	$5° \times 4°$ L20	$2° \times 2°$ L16	5	Schmidt et al (2006)
GISS-ER	NASA/GISS	USA	$5° \times 4°$ L20	$5° \times 4°$ L13	9	Schmidt et al (2006)
INM-CM3.0	INM	Russia	$5° \times 4°$ L21	$2.5° \times 2°$ L33	1	Volodin and Diansky (2004)
IPSL-CM4	IPSL	France	$2.5° \times 3.75°$ L19	$2° \times 1°$ L31	1	Marti et al (2005)
MIROC3.2(hires)	CCSR, NIES, FRCGC	Japan	T106L56	$0.28° \times 0.1875°$ L47	1	K-1 model developers (2004)
MIROC3.2(medres)	CCSR, NIES, FRCGC	Japan	T42L20	$1.4° \times 0.5°$ L43	3	K-1 model developers (2004)
MRI-CGCM2.3.2	MRI	Japan	T42L30	$2.5° \times 0.5°$ L23	5	Yukimoto and Noda (2002)
PCM	NCAR	USA	T42L18	$2/3° \times 1/2°$ L32	2	Washington et al (2000)
UKMO-HadCM3	UKMO	UK	$3.75° \times 2.5°$ L19	$1.25°$ L20	2	Gordon et al (2000)
UKMO-HadGEM1	UKMO	UK	$1.875° \times 1.25°$ L38	$1° \times 1/3°$ L40	1	Johns et al (2004)

[1] Salas-Mélia, D., Chauvin, F., Déqué, M., Douville, H., Gueremy, J. F., Marquet, P., Planton, S., Royer, J. F., and S., T.: Description and validation of the CNRM-CM3 global coupled model, CNRM Working Note 103, 2005.

Tab. 3.2: Properties of the first EOF and associated time series (PC) of detrended monthly SST in the region 10° S–10° N, 120° E–90° W. The pattern denotes the longitudes of the contour of 80% of the peak value, the period denotes the height of the power spectrum at 50% of the peak value.

Analysis/model	Pattern	Period (yr)	Amplitude	Skewness
SSTOIv2/Kaplan	160° W–<90° W	2.5–6	0.25	0.54
CCSM3	160° W–100° W	2–2.5	0.22	−0.06
CGCM3.1(T47)	170° E–150° W	2.5–5	0.14	0.08
CNRM-CM3	160° W–<90° W	3.1–3.5	0.48	−0.13
CSIRO-Mk3.0	160° E–95° W	2–4	0.27	0.04
ECHAM5/MPI-OM	175° W–105° W	2.5–7	0.47	0.08
FGOALS-g1.0	180°–105° W	3.0–3.3	0.57	−0.18
GFDL-CM2.0	175° E–115° W	1.5–3.5	0.32	0.14
GFDL-CM2.1	180°–105° W	2–6	0.39	0.31
GISS-AOM	140° E–<90° W	1–10	0.09	−0.01
GISS-EH	150° W–100° W	1.5–4	0.16	−0.20
GISS-ER	170° W–<90° W	2.5–8	0.07	−0.18
INM-CM3.0	150° E–155° W	1.5–9	0.34	0.42
IPSL-CM4	175° W–100° W	2.2–2.7	0.28	−0.12
MIROC3.2(hires)	160° E–100° W	2.5–7	0.17	0.63
MIROC3.2(medres)	155° E–105° W	3–10	0.25	0.16
MRI-CGCM2.3.2	180°–105° W	1.8–3.5	0.26	0.55
PCM	145° W–100° W	1.5–5	0.23	0.21
UKMO-HadCM3	175° W–100° W	2.5–5	0.32	0.21
UKMO-HadGEM1	145° W–110° W	4.1–4.4	0.17	0.15

Tab. 3.3: The amplitude (standard deviation) of monthly SST and thermocline variability at the maximum of the first SST EOF, and amplitude of zonal wind stress and thermocline variability (approximated by the depth of the 20° C isotherm) at the point of maximum wind response. The errors denote the 95% confidence interval.

Model	lon	SST (K)	z_{20} (m)	lon	τ_x (10^{-3} Pa)	z_{20} (m)
TAO (1983–2004)	110° W	1.7±0.5	26±5	170° W	22±4	18±5
NCEP (1980–1999)	115° W	1.5±0.4	28±6	170° W	13±2	17±3
ERA40 (1957–2002)				170° W	18±2	
Kaplan (1854–2004)	112° W	0.9±0.1				
CCSM3	125° W	1.33±0.09	19.9±1.0	170° W	12.3±0.2	12.1±0.8
CGCM3.1(T47)	170° W	0.76±0.05	8.7±0.5	170° E	13.2±0.7	5.8±0.3
CNRM-CM3	120° W	2.31±0.13	40.8±1.9	170° W	17.5±1.3	22.7±2.1
CSIRO-Mk3.0	140° W	1.24±0.10	26.2±3.5	160° W	10.0±0.7	11.6±2.6
ECHAM5/MPI-OM	140° W	1.78±0.06	27.0±0.6	160° E	18.2±0.5	17.8±0.3
FGOALS-g1.0	120° W	3.23±0.09	29.1±1.6	170° W	17.4±0.4	21.8±1.4
GFDL-CM2.0	150° W	1.22±0.06	16.3±1.1	160° E	19.9±0.9	12.2±0.8
GFDL-CM2.1	130° W	1.91±0.18	27.8±2.9	170° E	24.1±1.2	17.3±1.9
GISS-EH	100° W	1.31±0.03	11.0±0.6	155° W	9.9±0.2	8.1±0.5
INM-CM3.0	160° W	1.69±0.11	11.3±0.7	155° W	13.4±0.7	25.3±1.8
IPSL-CM4	130° W	1.33±0.10	14.8±1.3	155° W	10.1±0.6	10.7±0.9
MIROC3.2(hires)	160° W	0.57±0.06	9.3±0.6	160° E	8.7±0.6	8.1±0.7
MIROC3.2(medres)	140° W	0.73±0.03	15.8±0.6	160° E	9.5±0.3	5.2±0.2
MRI-CGCM2.3.2	150° W	1.05±0.05	16.8±0.4	180°	22.7±0.6	11.9±0.3
PCM	120° W	1.51±0.10	17.1±1.2	180°	11.1±0.4	10.5±1.0
UKMO-HadCM3	130° W	1.55±0.09	33.2±1.6	180°	14.8±0.7	10.0±0.7
UKMO-HadGEM1	130° W	1.28±0.10	22.7±2.1	170° E	13.0±0.7	8.5±0.7

Tab. 3.4: The change in mean value normalized to the standard deviation, the ratio of the standard deviation and change in skewness of the SLP pattern between the current climate and the last 50 years of a scenario experiment. Positive values denote El Niño, negative La Niña. The errors denote the 95% CL interval. The MIROC3.2(hires) Δ mean is unreliable due to a discontinuity.

Model	Confidence	Scenarios		Δ mean	Δ s.d.	Δ skewness
CCSM3		20c3m	sresa2	0.61±0.08	0.81±0.05	0.04±0.27
CGCM3.1(T47)		20c3m	sresa2	-0.38±0.16	0.75±0.09	-0.06±0.31
CNRM-CM3		20c3m	sresa2	0.46±0.22	1.09±0.11	-0.09±0.29
CSIRO-Mk3.0		20c3m	sresa2	0.07±0.15	1.03±0.10	0.05±0.32
ECHAM5/MPI-OM	high	20c3m	sresa2	0.22±0.12	1.14±0.08	-0.15±0.20
FGOALS-g1.0		20c3m	sresa1b	0.12±0.09	0.64±0.04	-0.18±0.14
GFDL-CM2.0	high	20c3m	sresa2	0.02±0.23	1.21±0.12	0.12±0.29
GFDL-CM2.1	high	20c3m	sresa2	-0.10±0.16	0.88±0.13	-0.03±0.46
GISS-EH		20c3m	1pctto2x	-0.34±0.12	1.00±0.09	-0.03±0.35
INM-CM3.0		20c3m	sresa2	-0.76±0.19	0.92±0.15	0.42±0.49
IPSL-CM4		20c3m	sresa2	-0.45±0.20	1.10±0.12	-0.07±0.29
MIROC3.2(hires)	medium	20c3m	sresa1b	(1.13±0.20)*	0.97±0.17	-0.29±0.58
MIROC3.2(medres)	medium	20c3m	sresa2	0.25±0.10	0.86±0.07	0.12±0.27
MRI-CGCM2.3.2		20c3m	sresa2	0.25±0.11	1.26±0.07	-0.23±0.16
PCM		20c3m	sresa2	-0.12±0.11	0.89±0.07	0.08±0.29
UKMO-HadCM3	high	20c3m	sresa2	0.00±0.20	1.16±0.13	0.07±0.35
UKMO-HadGEM1		picntrl	1pctto2x	0.01±0.23	1.10±0.13	-0.15±0.34

4. SHIFTS IN ENSO COUPLING PROCESSES UNDER GLOBAL WARMING

Global warming may shift the properties and dynamics of El Niño. We study the shifts in ENSO couplings in IPCC-AR4 coupled general circulation climate models. First, we compare the ENSO period, pattern and amplitude and the mean state of the Pacific Ocean between the current climate and a high CO_2 climate. Next, shifts in ENSO couplings between sea surface temperature (SST), thermocline depth and wind stress are discussed. Although the mean state shifts, the overall ENSO properties do not change much. Changes in the mean state affect the feedback loop. Higher mean SST provides higher damping through cloud feedback. The shallower thermocline and mixed layer depth increase SST sensitivity to thermocline variability and wind stress. Wind response to SST variability increases where the mean SST has increased the most. However, the higher damping and more stable atmosphere compensate the other changes and the residual change in ENSO properties is relatively small.

4.1   Introduction

El Niño — Southern Oscillation (ENSO) is a climate phenomenon that affects large parts of the world. It is therefore important to gain more insight into the behaviour of El Niño in a future, warmer climate. Projections of the properties of ENSO in a future climate are made with general circulation models (GCMs). Most models that describe ENSO reasonably well in the current climate show only small changes in the behavior of ENSO (Chapter 3). This can be the result of two very different scenarios: either the strength of the couplings remains similar to the current values in spite of the changing background state, or they change in such a way that the effects cancel in overall ENSO properties.

Recently, mean state, period, pattern and amplitude of ENSO in an enhanced greenhouse gas (GHG) scenario of the IPCC-AR4 GCMs have been analyzed (e.g., Guilyardi, 2006; Merryfield, 2006; van Oldenborgh et al, 2005). Guilyardi (2006) analyzed the ENSO amplitude and frequency and found no consistency in changes in a GHG scenario in a range of GCMs, although he did find a trend to a more thermocline-driven mode. Furthermore, he showed that a higher El Niño amplitude is related to a weaker mean zonal wind stress (τ_x). The relationship between ENSO period and the pattern of the anomalous zonal wind stress

---

This chapter is based on the paper "Shifts in ENSO coupling processes under global warming" by S. Y. Philip and G. J. van Oldenborgh, published in *Geophysical Research Letters* 2006, **33**, L11704.

has been examined by Kirtman (1997), Zelle et al (2005), and Capotondi et al (2006). They have shown that a broader meridional pattern is associated with longer periods. Capotondi et al (2006) have also examined the dependency of the ENSO period upon the longitudinal position of the wind stress, and have shown that models with westward displaced anomalous wind stresses tend to have a shorter period. Merryfield (2006) linked changes in sea surface temperature (SST) to changes in SST variability. His results indicate that a higher mean SST or a stronger temperature difference between east and west intensify SST variability. In Chapter 3 we investigated the feedback loop between SST, wind stress and thermocline depth in the current climate, and this allowed to identify a subset of six most reliable models. In these models we showed that the mean sea level pressure (SLP) state and amplitude of ENSO do not change much in a GHG scenario.

   In the present chapter we investigate whether and how the underlying mechanisms of ENSO change. We analyze for GCMs the feedback loop between SST, thermocline depth and wind stress as described in Chapters 1 and 2 . We compare a GHG scenario with the 20th century, and investigate the connection with changes in mean states of SST, thermocline and wind stress. Furthermore, we connect changes in the feedback loop and mean states to changes in ENSO pattern, amplitude and period.

4.2   Models

The set of models we use in this study is a selection of the AR4 climate models that were available via the IPCC data centre. The selection consists of ECHAM5/MPI-OM (ECHAM5), GFDL_CM2.0 (GFDL2.0), GFDL_CM2.1 (GFDL2.1), MIROC3_2(medres) (MIROC) and UKMO-HadCM3 (HadCM3). These models have enough data available for the GHG scenario (sresa1b), with a doubling of CO_2 up to 2100 and stabilisation afterwards, and they were found in van Oldenborgh et al (2005) to have the most realistic description of the mechanisms of ENSO in both pattern and feedback strength in the current climate. The simulation for the current climate (20c3m) has been used in van Oldenborgh et al (2005). The period used for the warmer climate is 2200-2300 except for HadCM3 where we used 2100-2200.

4.3   Overall properties

First, we analyze the overall properties of ENSO where we compare the differences between the current climate and a climate with doubled CO_2 concentration. Besides period, pattern and amplitude we will also analyze the mean states of SST, zonal wind, thermocline depth and mixed layer depth (MLD).

4.3.1   Period, pattern and amplitude

The pattern and period of ENSO are defined as the first EOF of SST and the full width at half height of the spectrum of the principal component of the leading EOF. The changes in pattern and period between a current and a future climate are very small (e.g., van Oldenborgh et al, 2005; Guilyardi, 2006; Merryfield, 2006).

Tab. 4.1: Amplitude 20th century and relative change in amplitude between the 20th and 23rd centuries of SST in the NINO3, the NINO3.4 and the NINO4 regions.

model	scenario	NINO3	NINO3.4	NINO4
ECHAM5	20c3m	1.34±0.04	1.41±0.05	1.23±0.04
	change	+10%±8%	+22%±8%	+27%±8%
GFDL2.0	20c3m	0.97±0.07	1.05±0.08	0.94±0.07
	change	+4%±12%	+2%±13%	−14%±13%
GFDL2.1	20c3m	1.29±0.12	1.33±0.12	1.16±0.09
	change	−14%±14%	−17%±14%	−28%±12%
HadCM3	20c3m	0.94±0.05	0.99±0.06	0.87±0.05
	change	−5%±11%	+7%±11%	+22%±9%
MIROC	20c3m	0.52±0.03	0.54±0.04	0.52±0.03
	change	−23%±9%	−17%±10%	−15%±9%

The amplitude of El Niño is defined as the standard deviation of SST in a 5° S-5° N region in the Pacific Ocean. The amplitudes in the NINO3 (150° W-90° W), NINO3.4 (170° W-120° W) and NINO4 (160° E-150° W) regions show no consistent change (see Table 4.3.1). This is consistent with earlier results (van Oldenborgh et al, 2005; Guilyardi, 2006; Merryfield, 2006). The amplitude in the MIROC model is quite small and the pattern extends too far to the west. The skewness is not considered since this property is not modelled well.

Overall, the changes in these ENSO properties are not large.

4.3.2   Mean states

Comparing the 20th and the 23rd century, the mean SST rises more at the equator than in the subtropics, see also Liu et al (2005, Fig. 1). For GFDL2.0 and GFDL2.1 this rise is about the same in the central Pacific as in the coastal zone. ECHAM5 and HadCM3 show a higher increase in temperature in the east than in the west. The warming in MIROC corresponds clearly with the ENSO pattern in SST. However, only ECHAM5 and MIROC show a significant shift in SLP pattern in sresa2 2050-2100, towards a pattern that resembles an El Niño event (van Oldenborgh et al, 2005).

In all models the mean zonal wind stress between 10° S-10° N becomes weaker (0-40%) in the 23rd century (not shown). It also becomes more symmetrical around the equator and the area of convection shifts somewhat to the east.

As an approximation for the thermocline, (the division between warm and cold water) we use an isotherm. For all five models z_{24} (23rd century) or z_{20} (20th century) is a good approximation for the maximum gradient of the thermocline. The approximation becomes less accurate west of 160° W where the thermocline becomes more diffuse but also less important for the coupling with the atmosphere due to the deeper mean value. We checked for one model (GFDL2.1) that the maximum gradient of the thermocline behaves the same as in the TAO observations (McPhaden et al, 1998), namely a trend to smaller maximum
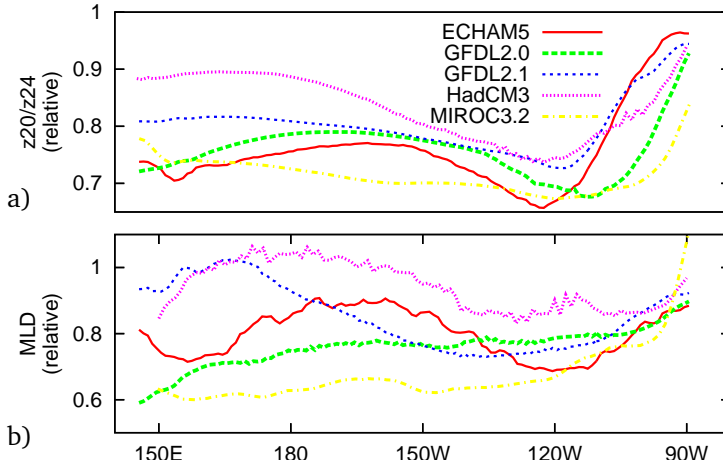
Fig. 4.1: **(a)** Relative change in thermocline depth approximated by z_{20} (20th century) and z_{24} (23rd century) (upper panel) and **(b)** mixed layer depth, estimated by the average of the monthly values of z(SST-0.5).

gradients during La Niña. Except for HadCM3, where the thermocline depth remains about the same, the whole thermocline shoals in a warmer climate, and shoals more in the west, see Fig. 4.1a. The reduction of the thermocline slope is directly related to the weaker mean zonal wind stress that is observed in all models.

Another result of the weaker mean zonal wind stress is the reduction in MLD, defined as z(SST-0.5), see Fig. 4.1b. Due to the weakened wind and stronger stratification the depth of the mixed layer decreases.

In general, we see that in a warmer climate the mean state of the Pacific ocean changes considerably.

4.4   ENSO mechanisms

So far, we discussed the gross characteristics of ENSO. We find that although mean states do change considerably, changes in ENSO properties are small. In order to understand why these changes are so small we investigate the mechanisms behind them. The most important mechanisms that affect El Niño are the SST response to thermocline and wind variabilities and the wind response to SST perturbations.

4.4.1   SST variability

First we examine SST variability caused by thermocline anomalies, wind stress anomalies and damping. The simple SST equation Eq. 2.1 (Burgers and van Oldenborgh, 2003) ex-

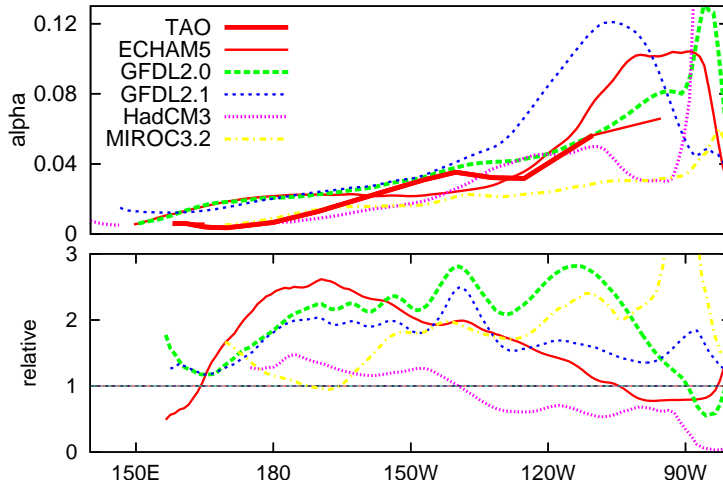*Fig. 4.2:* Sensitivity of SST to thermocline variability α [Km^{-1}] for the 20c3m scenario (top) and the relative change in the warmer climate (bottom).

plains about 60-80% of the total variance in the TAO data and all five models. For future scenario runs we use z_{24} in stead of z_{20}.

Results for the current climate are presented in van Oldenborgh et al (2005). These results are now compared to the sensitivities of SST in a doubled CO_2 scenario. The fitted coefficients of the linear SST equation in the current climate and the relative change between the current and the future climate are shown in Figs. 4.2-4.4. Statistical uncertainties of the fitted parameters are in the order of 10% in the regions where they are the most important.

The influence of thermocline depth variations is most important in the east Pacific where the thermocline is shallowest. The sensitivity to the thermocline depth, α, (see Fig. 4.2) becomes about two times higher in all models except in the HadCM3 model. The overall higher sensitivities in the models can be related to the shoaling of the thermocline as a whole (Fig. 4.1). A shallower thermocline exerts a larger influence on SST. For HadCM3 the shoaling is not as clear as for the other models.

Fig. 4.3 shows β, the sensitivity of SST to wind stress, which is most important in the central Pacific. Almost all models show an increase in sensitivity to wind stress variability, especially in the central Pacific. The increased sensitivity of SST on wind stress may be related to the shallower oceanic MLD in a warmer climate (see Fig. 4.1).

All models show an increase in the damping term γ in the central Pacific (see Fig. 4.4). This is partly due to a shift of the convection to the central Pacific, since at higher temperatures clouds extend more to the east, see Fig. 4.5. For HadCM3 the change in the latent heat flux is equally important. ECHAM5 is an exception with no change in cloud-cover
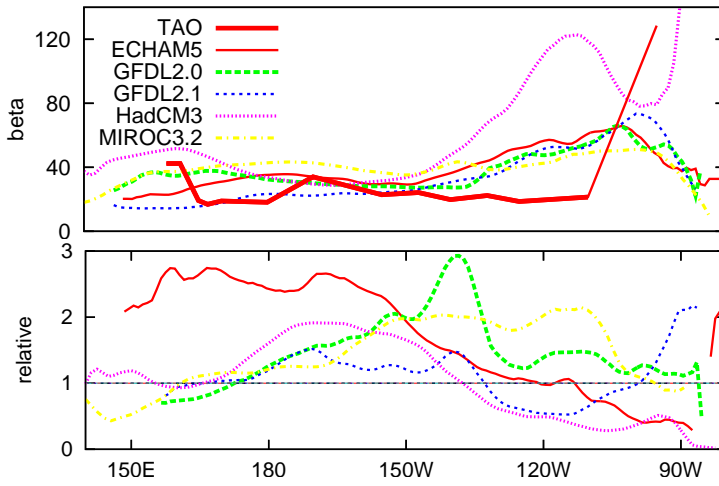
Fig. 4.3: Sensitivity of SST to wind stress variability β [KPa^{-1}] for the 20c3m scenario (top) and the relative change in the warmer climate (bottom).
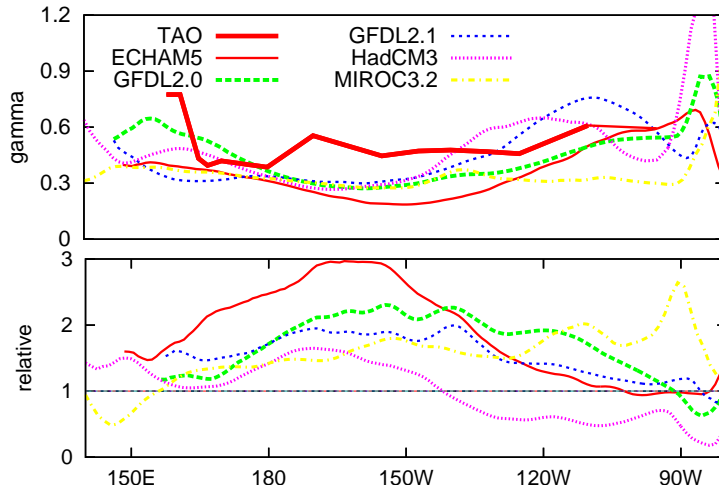
Fig. 4.4: Damping term γ [month^{-1}] for the 20c3m scenario (top) and the relative change in the warmer climate (bottom).
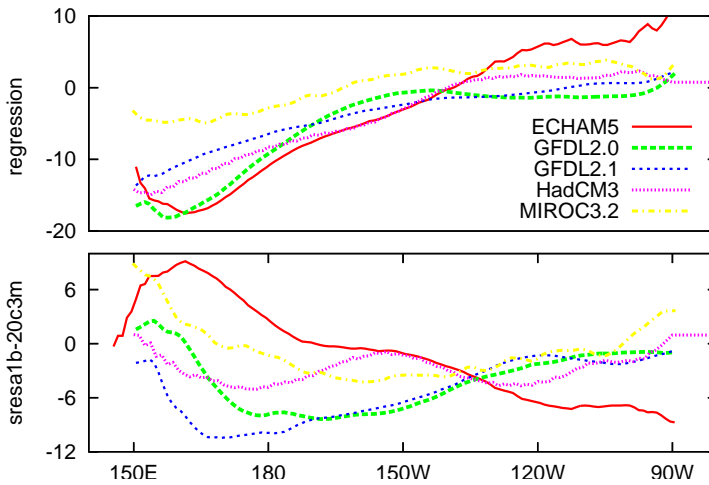
Fig. 4.5: Regression of the downward shortwave radiation with local SST, averaged over
5° S-5° N in the 20th century (upper panel) and absolute difference between the
23rd and 20th centuries.

feedback in the central Pacific.

Overall, we find roughly a doubling of the coupling strengths and damping in the areas
where they are most important.

4.4.2   Zonal wind stress response to SST variability

Another important feedback in the ENSO cycle is the response of the wind to SST anomalies
along the equator. A change in this response influences the properties of the ENSO cycle.
This wind sensitivity to SST anomalies is examined with a linear statistical atmosphere
model with as basis n equal-sized boxes along the equator in 5° S–5° N, 140° E–80° W (e.g.
Von Storch and Zwiers, 2001, §8.3), see Eq. 2.2. The model is defined as the response
of the atmosphere on a SST anomaly in one of the boxes only. In this study we compare
the atmospheric response to SST anomalies in $n=3$ boxes separately for the climate of the
20th century and the doubled CO_2 scenario. The central box corresponds approximately
to NINO4, the eastern box to NINO3 and the patterns are clear enough to study with one
ensemble member for all five models.

In our models the change in wind response to SST anomalies along the equator is
consistent with the change in mean SST for the most localized warmings (see Fig. 4.6 and
Liu et al (2005, Fig. 1)): GFDL2.0 and GFDL2.1 have a stronger maximum wind stress
response of 100% and 30%, respectively, in the central Pacific where the SST rises the
most. In the eastern Pacific the wind response reduces somewhat. ECHAM5 has a stronger

response in the east (50%) where the SST also rises the most, and a weaker response in the central part (-20%). In HadCM3, where warming is about equal along the whole equator, the wind response is higher along the whole equator. The decrease in wind response is strongest in MIROC3.2 where the rise in SST is almost the same in all NINO regions.

Overall, wind response to SST variability increases where the mean SST has increased most, but decreases where SST increases less. This is a combination of two effects. First, a warmer background temperature provides higher evaporation and a stronger wind response. This explains the spatial pattern of the changes. Second, the response as a function of a heating anomaly becomes about two times weaker everywhere along the equator in a doubled CO_2 climate (not shown). This can be attributed to the fact that the equatorial atmosphere becomes more stable. **?** argue that, following the Clausius-Clapeyron scaling, the dry stability in the tropics increases as the temperature and the low-level moisture increase.

4.5   Conclusions

A previous study of El Niño in a future, warmer climate showed only small changes between the climate of the 20th century and a warmer climate in overall properties like period and amplitude of ENSO. It is tempting to conclude that El Niño will not change significantly. However, it was not clear how to interpret this result since the overall properties of the projected warmer climate differ clearly from the 20th century.

In this study we show that although the overall ENSO properties do not change much, ENSO couplings are very different. In five GCMs with most reliable physics related to El Niño, the feedback loop between SST, wind stress and thermocline does change in greenhouse warming simulations following changes in the mean state. The mean SST, wind stress and thermocline show changes in the same direction. The mean SST increases more in the tropics than in the subtropics. The mean wind stress decreases and the convection cell shifts eastward. In the ocean the thermocline becomes shallower.

These changes in mean states affect the feedback loop in these five GCMs as follows. SST sensitivity to thermocline variability increases since the thermocline is shallower, and the response of SST to wind stress becomes larger partly due to the decreased mixed layer depth. On the other hand, the higher mean SST provides higher damping through cloud feedback. The response of the wind stress to SST variability becomes only stronger near locations where the mean SST has increased the most. This is the result of the local higher background temperature, which increases the response of the wind stress on SST, counteracted by the overall lower response of wind on heating, which decreases the response of the wind stress. All these changes are visible in at least four of the five GCMs, although their location and precise strength differ. Besides these main factors other (nonlinear) mechanisms undoubtedly also play a role.

We see that these changes impact with large amplitudes on the overall properties, but with opposing signs. The residual change is almost zero and depends on the details of ENSO in the GCMs.

ECHAM5
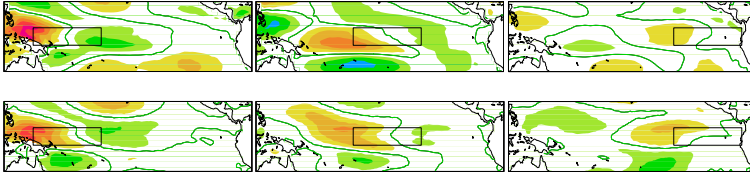
GFDL2.0
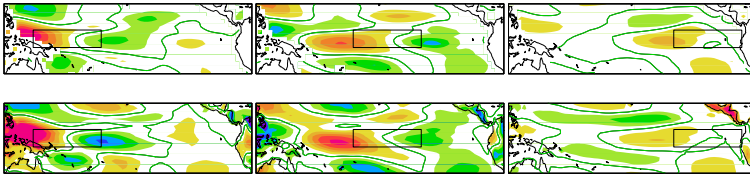
GFDL2.1
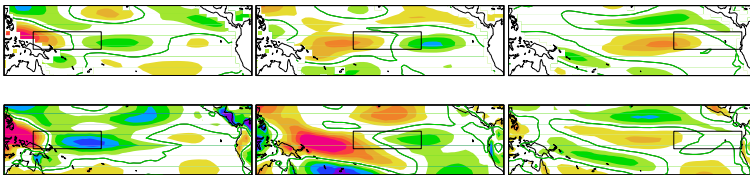
MIROC
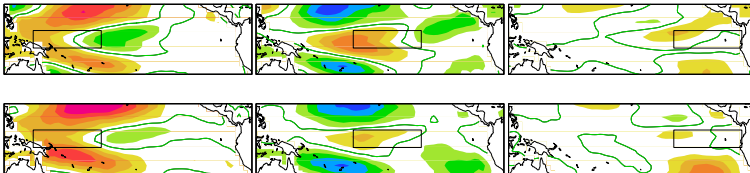
HadCM3
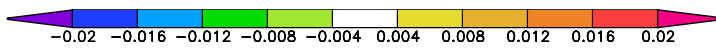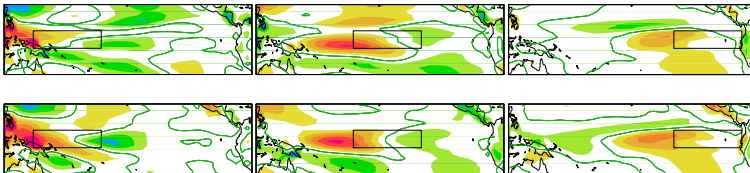
Fig. 4.6: Wind response to SST anomalies in $120°$ E-$70°$ W, $20°$ S-$20°$ N for three boxes. Upper ones are current climate, lower ones are doubled CO_2 climate.

5. SIGNIFICANT ATMOSPHERIC NONLINEARITIES IN THE ENSO CYCLE

The nonlinearities that cause El Niño events to deviate more from the mean state than La Niña events are still not completely understood. In this paper we investigate the contribution of one candidate mechanism: ENSO nonlinearities originating from the atmosphere. The initially linear Intermediate Complexity Model of the equatorial Pacific ocean in which all couplings were fitted to observations describes the ENSO cycle reasonably well. In this linear model we systematically introduce extra terms in the atmospheric component. These are the nonlinear response of mean wind stress to SST anomalies, the skewness of the driving noise term in the atmosphere and the relation of this noise term to the background SST or the ENSO phase. The nonlinear response of mean wind stress to SST in the ENSO region is found to be the dominant term influencing the ENSO cycle. However, this influence is only visible when noise fields are used that are fitted to observed patterns of prescribed standard deviation and spatial decorrelation. Standard deviation and skewness of noise do have a dependence on the ENSO phase, but this has a relatively small influence on the ENSO cycle in this model. With these additional nonlinearities in the representation of the atmosphere a step forward has been made towards building a realistic reduced complexity model for ENSO.

5.1 Introduction

Theoretical explanations for the climate phenomenon El Niño – Southern Oscillation (ENSO) have been developed and models have become more advanced and more reliable. Although El Niño forecasts are reasonably reliable up to about three to nine months ahead (depending on the season), the physical mechanisms determining the onset of an event and nonlinearities in the ENSO phenomenon are not yet well understood. A major nonlinearity is the larger magnitude of the positive sea surface temperature (SST) anomalies, El Niño, compared to the negative SST phase, La Niña. Defined with respect to the mean state, La Niña events occur more frequently than El Niño events but are weaker. The relative importance of the atmospheric contribution to the atmosphere-ocean coupled ENSO cycle for this nonlinear behavior is still a subject of discussion.

Different types of nonlinearities have been discussed in previous studies. Kessler and

Kleeman (2000) found evidence that the location of the edge of the warm pool is a measure of the size of the area where Madden-Julian Oscillation (MJO) events occur. Through feedbacks in the ocean and atmosphere oscillating MJO events result in a mean westerly wind, which in turn enlarges the area where the MJO events occur. This strengthens the positive feedback between wind and SST during El Niño, but weakens it during La Niña, giving rise to the observed asymmetry. Jin et al (2003) claim that nonlinear dynamical heating is an important nonlinearity in the eastern Pacific. During El Niño easterlies in the east Pacific enhance vertical advection of anomalous warm water that accelerates the surface warming, whereas during La Niña westerlies in the east Pacific reduce upwelling and slow down the surface cooling.

Most Intermediate Complexity Models (ICMs) like the Cane-Zebiak model (Zebiak and Cane, 1987) have a nonlinearity in the oceanic and/or atmospheric part. In the Cane-Zebiak model, for example, the nonlinearity in the ocean is characterized by a nonlinear coupling between SST and the thermocline depth. This is based on the observation that around the thermocline the temperature is a very nonlinear function of depth. The assumption is then made that raising or lowering the thermocline also has a nonlinear effect on SST. However, such a nonlinear coupling between SST and the thermocline depth is not very clearly seen in observations (not shown). Toniazzo et al (2008) Nevertheless, these models describe characteristics of the ENSO cycle like amplitude, frequency and sometimes also skewness in SST better than linear models. Also, there is evidence that nonlinearities in the atmosphere play a role as well, e.g., the wind stress response to SST anomalies is not linear everywhere, and noise components in the wind that drive anomalies in the ocean can depend strongly on the background SST, like in the model of Kleeman et al (1995). The representations of the atmosphere and atmospheric couplings to SST in ICMs range from totally linear to strongly nonlinear. Often the non-linear component is not as strongly constrained by observations as the dominant linear response.

Most state-of-the-art climate models do not simulate the ENSO skewness correctly. Even if the balance between El Niño and La Niña events is reasonable, the nonlinearities in other aspects differ from observations, casting doubt on the correctness of the representation of the nonlinearities in these models (van Oldenborgh et al, 2005, and Chapter 3). Therefore, in this study we investigate some nonlinearities in the atmospheric dynamics in observations and re-analyses.

One of the most obvious nonlinearities in the atmospheric dynamics is the difference in response of wind stress to positive or negative SST anomalies. Here we can distinguish between the mean response of wind stress to SST and higher moments that characterize the atmospheric noise driving the ocean dynamics. Previous studies have approached these nonlinearities in the atmospheric dynamics in several ways. Sura et al (2005) already demonstrated that a simple linear system with multiplicative noise (i.e., noise with an amplitude depending on the background state) can result in a non-Gaussian distribution. The application can be found in Sura et al (2006), who show that for mid-latitude SST anomalies inclusion of a multiplicative noise term does result in skewed SST. The net effect of multiplicative noise is thus a nonlinear response of the atmosphere. Therefore throughout this chapter multiplicative noise is ranged among nonlinear effects.

Perez et al (2005) studied the difference between the influence of additive and multi-

plicative noise in the atmosphere driving the ocean on the ENSO probability density function. For the additive noise they used 25 empirical orthogonal functions (EOFs) of noise in the wind stress component with a stochastic forcing amplitude that is a linear function of the Niño3 index (5° S–5° N, 150° W–90° W). They show that the dynamics of the system are different for additive and multiplicative stochastic forcing and additive forcing alone does not reproduce the variability well. Eisenman et al (2005) use westerly wind events (WWEs) with fixed spatial structure and duration. They show that the influence of WWEs is enhanced when the occurrence of WWEs is no longer only additive but has a deterministic part which is purely a function of the warmpool extent. The modulation of the occurrence of WWEs by the large-scale equatorial SST field enhances the low frequency component of WWEs. The mechanism behind this is that for higher SSTs more WWEs can occur and accumulation of these WWEs can induce a warming event. The effect of migration of WWEs with the warmpool (Gebbie et al, 2007) is shown to be important for ENSO dynamics, where eastward migration and modulation of WWEs during a warm event enhance the amplitude of ENSO. Tziperman and Yu (2007) discuss a parameterization of the nonlinear modulation of pattern, amplitude and timing of WWEs by SST. They find that WWEs are not totally additive but partly multiplicative since ENSO and the seasonal cycle dominate the characteristics of the WWEs. Lengaigne et al (2004) made an analysis of WWEs in a coupled general circulation model. They show that the coupled response is strongly sensitive to WWEs and one of the responses to a WWE is an eastward displacement of the warmpool.

In this study we want to investigate the influence of nonlinearities that are fitted to observations of the ENSO cycle. For this, we take the opposite approach to studies that start from a model and tune nonlinear properties of the atmosphere such that the model output resembles observations the best. We first deduce the nonlinear properties of the atmosphere from observations, and next use a tuned Intermediate Complexity Model (ICM) to investigate the effects of each nonlinear term on the ENSO cycle. The starting point of the study is the ICM consisting of the linear feedbacks studied in van Oldenborgh et al (2005), completed with a linear ocean model (Burgers et al, 2002). In this model, noise is represented in the form of Gaussian perturbations of the wind patterns corresponding to the Niño3 and Niño4 indices, taking into account the correlation between the Niño3 and Niño4 indices and the temporal correlation of the observed wind patterns (Burgers and van Oldenborgh, 2003). This model performs reasonably well with only linear dynamics but nonlinearities in the ENSO cycle are obviously not represented. In our study some nonlinearities are added in order to build a more realistic ICM and obtain more insight in the dynamics of ENSO.

In this chapter the atmosphere is represented by a statistical model of wind stress that consists of a combination of a deterministic and a stochastic term. The deterministic term can be either a linear or nonlinear function of SST anomalies. The stochastic term is defined in terms of the standard deviation and skewness of noise, each of which are two-dimensional functions of SST, and have realistically prescribed spatial and time correlations. For both deterministic and noise wind stress terms, the functional relationships to SST anomalies are found empirically. Using this model the following terms that lead to a nonlinear model are studied:

1. the dependence of the mean westerly wind anomaly on background SST; in practice this can be done by investigating the nonlinear response of wind stress to SST.

2. the standard deviation and skewness of the atmospheric noise distribution.

3. the relation between this noise distribution and background SST.

The questions addressed in this chapter are: does an ICM with coupling parameters fitted to observations describe the ENSO cycle well, including nonlinearities? And which of the nonlinear aspects of the atmosphere mentioned above is most important in generating the skewness in SST in the ENSO cycle?

The methodology of this study and the model are described in Section 5.2. In Section 5.3 we describe the different characteristics of the atmospheric noise. Implications of these characteristics for the ENSO cycle are shown in Section 5.4. Finally we discuss the results and conclude in Section 5.5.

5.2   Method of investigation

In Figure 1.8 a conceptual model of ENSO is shown, with feedbacks between zonal wind stress (τ_x), SST and thermocline depth (Z_{20}). The ICM that is built from this conceptual model is based on the so called Gmodel (Burgers et al, 2002; Burgers and van Oldenborgh, 2003). The linear couplings between SST and wind stress, and the dependence of SST on thermocline depth (Figure 1.8a) were investigated in detail by van Oldenborgh et al (2005). In order to complete the reduced model, the different descriptions of the driving external atmospheric noise term and the internal nonlinear response of wind stress to SST are investigated (Figure 1.8b). The findings are added one by one to the originally linear reduced model and the ENSO properties in the complete reduced model are studied.

The description of the model is organized as follows. Details of the statistical atmosphere are given in Section 5.2.1. Characteristics of the external noise term are discussed in Section 5.2.2-5.2.3. Furthermore, the linear fit parameters in the ocean model are described in more detail in Section 5.2.4 and the data and different types of model experiments are discussed in Section 5.2.5.

5.2.1   Statistical atmosphere: mean response to background SST

The atmosphere is described by a statistical atmosphere model where local SST anomalies result in zonal wind stress patterns, which is the most important atmospheric component. Nonlinearities are added to a linear statistical description of the atmosphere.

Our starting point is a linear statistical atmosphere model where wind stress anomalies are described as a direct response to SST anomalies in separate regions near the equator, see Eq. 2.2.

In this study, SST variations are summarized as the average temperature anomalies in $n = 2$ equal-sized boxes (more boxes would give too much noise) along the equator in 5° S–5° N, 160° E–90° W. With this choice $T'_i(t)$ corresponds approximately to the Niño-indices, with $T'_1(t) \approx$ Niño4 and $T'_2(t) \approx$ Niño3. The motivation for this choice will be explained in Section 5.3. The effects of temperature anomalies in the two boxes on wind stress are

investigated separately. For the linear statistical atmosphere model this is mathematically equivalent to dividing the regression of wind stress on the Niño-indices by the covariance matrix of the Niño-indices: the two wind stress patterns then correspond to an SST anomaly in one of these two boxes only and not to anomalies in the other box.

A nonlinear version of the statistical atmosphere has been constructed by including the next term in a Taylor expansion, see Eq. 2.3. In this study the linear part is defined as above, whereas for the nonlinear part we use $m = 1$ over the area 5° S–5° N, 145° W–118° W. This is approximately the western half of Niño3. The motivation for this choice will be explained in Section 5.3.1. The nonlinear part can be seen as the integrated effect of the nonlinear dependence of the mean wind stress to SST anomalies, resulting in an extra mean westerly wind anomaly during both warm and cold events.

In the experiments where we use the nonlinear statistical atmosphere, the quadratic term in the atmosphere is the only nonlinear term in the model. Since in the ICM this term is never compensated by nonlinear damping terms, we cut off the nonlinear statistical atmosphere term at an SST anomaly index of $\pm 2K$, which corresponds to a fairly strong El Niño/La Niña. Results are qualitatively robust when we vary the cut off around this value of $\pm 2K$.

The wind stress patterns for observational data $A_2(x, y)_i$ and $B(x, y)_i$ are shown in Section 5.3.1.

5.2.2   Statistical atmosphere: characteristics of noise

An observed atmospheric noise is constructed by subtracting the wind stress calculated with Equation 2.2 or 2.3 from the total observed wind stress. The characteristics of noise are characterized with statistical parameters.

From the noise fields the 2-dimensional fields for standard deviation and skewness are calculated as explained in Chapter 2. These fields are shown in Section 5.3.2.

The spatial correlation length (defined as the the zonal or meridional width at a correlation of 1/e) of the noise has been calculated to be 36 degrees in longitude (a_x) and 6 (between 10° N and 10° S) to 8 (higher latitudes) degrees in latitude (a_y). A good approximation of the time-correlation coefficient at lag 1 time unit (one model week) $a_1(x, y)$ is given by a function that varies linearly along the equator and exponentially along the meridionals as $a_1(x, y) = 1.1(1 + x/8N_x)/\exp(\frac{1}{6}|y - \frac{1}{2} - \frac{1}{2}N_y|)$ with x,y ranging from 1 to N_x and 1 to N_y respectively and N_x=84, N_y=30. This gives correlations around 0.9 near the equator and 0.1 near the northern and southern edges of the domain.

Reconstructed fields with these three or four characteristics (without or with prescribed skewness) are used as noise fields. For details of the implementation, see Chapter 2.6.

5.2.3   Dependence of noise characteristics on the ENSO cycle

In order to complete the description of noise characteristics and their dependence on the ENSO cycle, the relationship between the standard deviation and skewness of the noise and the ENSO phase has been investigated. Note that the dependence of the mean wind stress response on the ENSO phase is described by the nonlinear statistical atmosphere.

Concerning the standard deviation and skewness, the timeseries of the noise is split into three categories depending on the ENSO phase. These three ENSO phases are defined as high, normal or low SST in the central box (El Niño, neutral or La Niña), where all three categories are equally likely by definition. Then, for each of these three phases the standard deviation and skewness fields are computed separately. The implementation of the noise fields in the reduced ENSO model is the same as described in the previous section, except that the parameters are selected on the basis of the category in which the SST anomaly falls: positive, neutral or negative.

5.2.4 Patterns of linear fit parameters

The 2-dimensional fitted parameters deduced from SODA data and used in the Gmodel are shown in Figure 5.1. SST variability caused by thermocline anomalies (α) is strongest in the east Pacific where the thermocline is shallowest. The response of SST to wind stress anomalies (β) plays a role in SST variability in both the eastern and central Pacific. However, the wind stress variability in the eastern Pacific is much smaller, so this term is most important in the central Pacific. The absolute damping (γ) is strongest in the east Pacific, but compared to the other terms damping is very large in the West Pacific. This is likely an effect of the cloud feedback that is strongest over the warmer West Pacific where cloud formation takes place (Philip and van Oldenborgh, 2006).

5.2.5 Data and experiments

The ocean parameters are fitted to the monthly SODA 1.4.2/3 $0.5°$ ocean re-analysis dataset (Carton and Giese, 2008), which is a mixture between observations and model calculations.

For the statistical atmosphere, weekly ERA40 data (Uppala et al, 2005) have been used. With 45 years of weekly ERA40 data the linear response to SST anomalies in 2 boxes in the Pacific Ocean can be resolved. Using more, smaller, boxes gives rise to too much noise in the response patterns. Since each of the boxes cover more than one third of the zonal extend, the longitudinal extent of these two boxes is quite large compared to the equatorial Pacific ocean.

The ICM (see Chapter 2.5) is driven by atmospheric noise as described above. In the context of this model, the effects of the nonlinearities have been investigated in isolation and together, keeping the modelled dynamics of the ocean linear. In Table 5.1 the different types of ICM experiments are listed with their abbreviations used throughout the text. The first category of experiments differs in the linear or nonlinear statistical atmosphere; *lin-* and *nonlin-*experiments. The second category distinguishes between relatively simple noise on the Niño-indices or a distribution of spatial noise fields on the wind stress, either characterized by standard deviation or by standard deviation and skewness; *nino-*, *full-sd-* and *full-skew-*experiments. In the last category the full noise fields can be chosen to be dependent or independent on the phase of the ENSO cycle; *fix-* and *phase-*experiments. For readability in the rest of this chapter the three types of noise will be referred to as 'nino noise', 'full sd noise' and 'full skewed noise'. All combinations have been explored but in
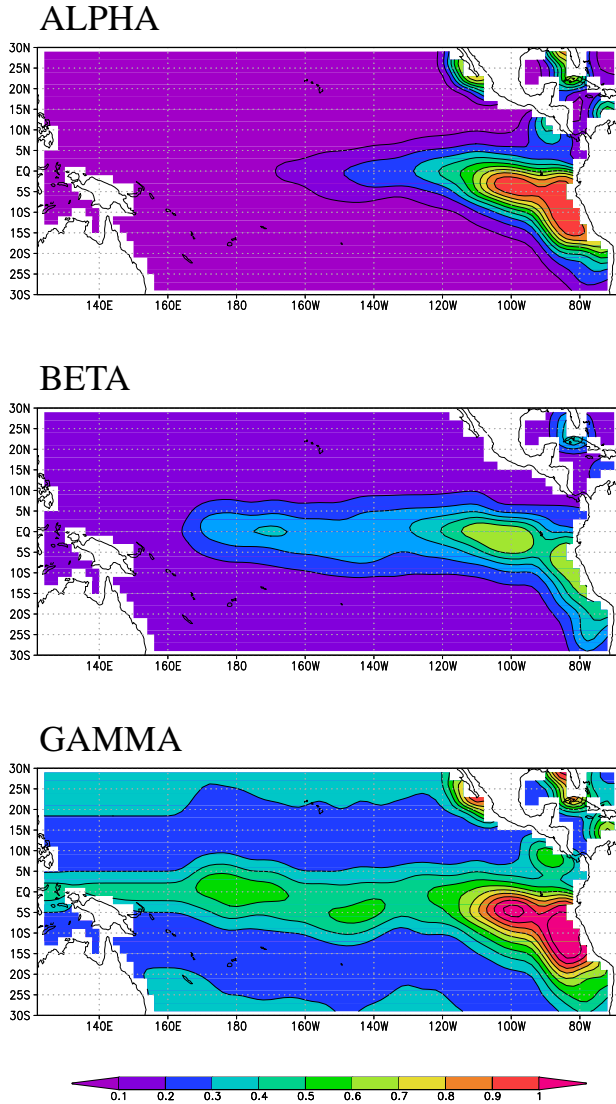
Fig. 5.1: 2-dimensional parameters as described in Equation 2.1, deduced from SODA data. α is the SST response to thermocline anomalies $[0.1 \mathrm{Km}^{-1}\mathrm{month}^{-1}]$, β is the SST response to wind variability $[100 \mathrm{KPa}^{-1}\mathrm{month}^{-1}]$ and γ is the damping $[\mathrm{month}^{-1}]$.

this chapter only the most interesting results are discussed in detail. The model run length for every experiment is 400 years, so that we have a balance between statistical errors and run time. The most important ENSO parameters that can change in the ICM by adding different types of noise are the first EOF, the period and skewness of SST. These diagnostics from the ICM output are compared with observations.

Tab. 5.1: Different types of ICM experiments including abbreviations.

Characteristic	abbreviation	explanation
Statistical	*lin*	linear statistical atmosphere (Eq. 2.2)
atmosphere	*nonlin*	nonlinear statistical atmosphere (Eq. 2.3)
Noise	*nino*	red plus white noise on the SST anomalies
	full-sd	noise on the wind stress field with prescribed standard deviation, spatial correlations and time correlation
	full-skew	noise on the wind stress field with prescribed standard deviation, skewness, spatial correlations and time correlation
ENSO phase	*fix*	noise field is independent on the ENSO phase
	phase	noise depends on the ENSO phase, e.g., El Niño, neutral, La Niña

5.3   *Atmospheric ENSO response and noise*

The standard Gmodel experiment with ocean parameters and a linear statistical atmosphere fitted to observations (*lin/nino/fix*) is driven by noise that has a relatively simple description, i.e. red and white noise on the Niño-indices. The linear relationship between SST and deterministic wind stress for the two boxes ($A_2(x, y)_i$ in Equation 2.3 with $i = 1, 2$) is shown in Figure 5.2a-b. The linear response $A_1(x, y)_i$ in Equation 2.2 differs only slightly from the first order term $A_2(x, y)_i$ and is not shown. The patterns resemble somewhat a Gill-type pattern (Gill, 1980), but differ in many details such as the relative strengths of the equatorial poles and the off-equatorial structure (see also van Oldenborgh et al, 2005). The linear wind response to a positive SST anomaly in the western box is directed eastward in the western Pacific and westward in the east Pacific. The wind response to a positive SST anomaly in the eastern box is eastward in the central Pacific.

The response to an SST anomaly in the western Pacific is stronger than the response to the same anomaly in the eastern Pacific. This is caused by the non-linear response of convection to SST depending on the background temperature (e.g., Philip and van Oldenborgh, 2006, and Chapter 3). Over high SST a small SST anomaly gives a larger latent heat release than the same SST anomaly over a lower SST. The wind stress response is proportional to the heat source, hence it is stronger in the western Pacific.

a)

b)

c)
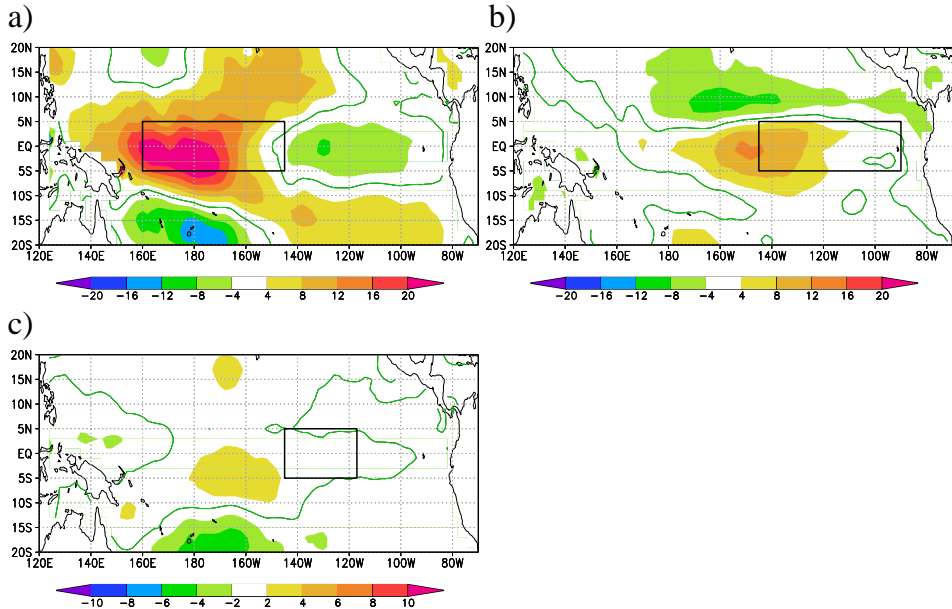
Fig. 5.2: Wind response $[10^{-3}\mathrm{Nm}^{-2}\mathrm{K}^{-1}]$ to an SST anomaly in the box only. a) linear wind response to an SST anomaly in the Niño4 region, b) linear wind response to an SST anomaly in the Niño3 region and c) quadratic wind response to an SST anomaly in the left half of the Niño3 region. Positive means a wind anomaly to the east, negative means a wind anomaly to the west. Note the difference in scale between the linear and nonlinear response.

The wind stress patterns of the statistical atmosphere in the Pacific Ocean are relatively stationary and not sensitive to the exact location and size of the boxes. If for instance two equal sized boxes between 180° E–80° W instead of 160° E–90° W are used the overall wind stress patterns are located at the same position (not shown, see also van Oldenborgh et al, 2005). The standard deviation of the remaining noise fields is somewhat lower for the Niño-based atmosphere than for the atmosphere based on the alternative boxes mentioned before. Therefore it is reasonable to use the statistical atmosphere based on approximately the standard Niño-indices.

In the next subsections the noise component and statistical atmosphere as derived from observations are discussed in detail.

5.3.1   Nonlinear atmospheric response

Figure 5.2c shows the observed second order term of the statistical atmosphere in the box that selects the western half of the Niño3 region, i.e. the quadratic response to an SST anomaly $B_1(x, y)_1$ in Equation 2.3. Like the linear wind stress response, the pattern of the nonlinear wind stress response is quite stationary and most of the variance of the noise that can be described by quadratic terms is explained by adding only this box. It shows a positive, eastward response of the wind to both positive and negative SST anomalies, with a maximum situated at the edge of the warm pool. This implies that the average westerly (eastward) wind response in the central Pacific during El Niño is larger than the easterly (westward) response to an equal-strength La Niña. This can be understood in terms of the background SST, with a larger effect of convective activity over a larger warm pool area during El Niño. Whereas the linear wind response to SST anomalies assumes a constant background SST, the nonlinear response shows the effect of the change in background SST, especially at the edge of the warm pool. During El Niño the convection zone is enlarged and the response is enhanced. Since the response is positive, this results in an enhancement of the westerly anomalies during El Niño. On the other hand, during La Niña the convection zone is reduced and the response is lower. Since the response during La Niña is negative the net effect is again positive.

Kessler and Kleeman (2000) already showed this phenomenon in a much simpler model, where wind stress similar to that of the Madden-Julian Oscillation develops a rectified SST anomaly additional to the linear response. This leads to cooling in the West Pacific and warming in the East Pacific. In other words, the zonal gradient is smaller and therefore more westerly winds can occur, resulting in a mean westerly wind. The result is confirmed by Lengaigne et al (2003) who show in an atmospheric general circulation model that the eastward displacement of the warmpool induces an eastward shift of convection, which in turn promotes the occurrence of WWEs. The additional WWEs result in a net westerly response.

5.3.2   The full noise field

The noise field of observational data can be calculated either based on the linear statistical atmosphere (Equation 2.2), or based on the nonlinear statistical atmosphere (Equation 2.3). From the noise field the standard deviation and skewness are determined. The fields corresponding to the nonlinear statistical atmosphere are shown in Figure 5.3. The figures corresponding to the linear statistical atmosphere are qualitatively the same and not shown.

Standard errors Δ in standard deviation σ and skewness S are approximated with $\Delta_\sigma = \sigma/\sqrt{2N}$ and $\Delta_S = \sqrt{6/N}$ respectively, where N is the number of independent values. As we use 45 years of observations and 400 years of model data and using a temporal decorrelation length of 4 weeks for noise and 6 months for SST the numbers of independent values become: $N_{\mathrm{noise-observed}} = 540$, $N_{\mathrm{noise-Gmodel}} = 2400$, $N_{\mathrm{SST-observed}} = 90$ and $N_{\mathrm{SST-Gmodel}} = 400$. For the observational noise fields with $N_{\mathrm{noise-observed}} = 540$ this gives a standard error of 0.03σ for the standard deviation and 0.11 for the skewness.
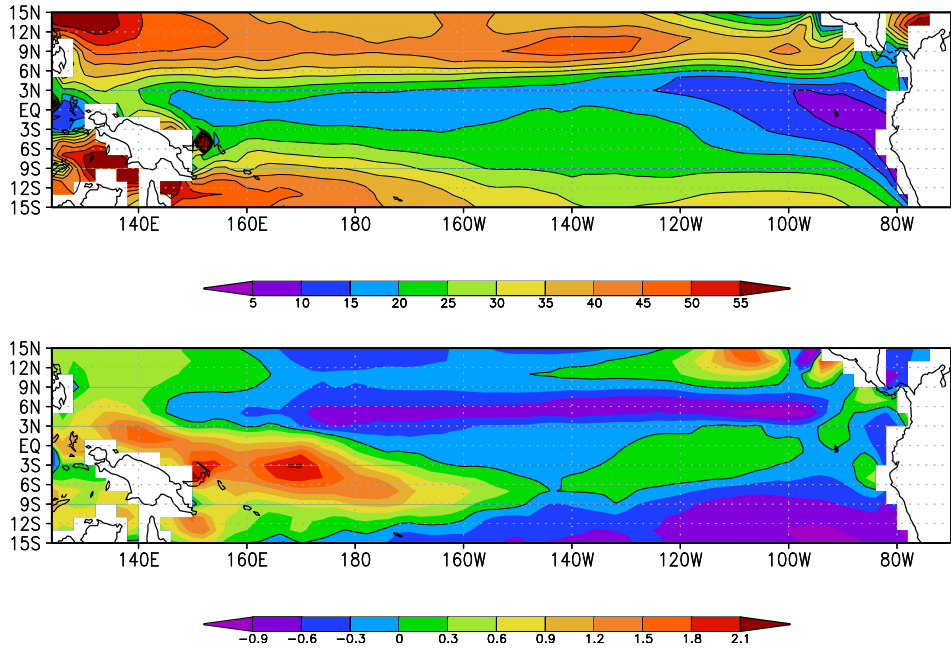
Fig. 5.3: Standard deviation $[10^{-3}\mathrm{Nm}^{-2}]$ (top) and skewness (bottom) of noise used to describe the nonlinear atmosphere. Positive skewness means stronger westerly than easterly anomalies.

As can be seen in Figure 5.3 the noise amplitude is lowest in the eastern equatorial region where the background SST (not shown) is lowest. Furthermore, the skewness shown in Figure 5.3 reflects stronger westerly wind anomalies than easterly wind anomalies in the West Pacific. This describes the fact that WWEs are westerly, not easterly. The region of the highest skewness is located slightly south of the equator, which is in accordance with the location of the highest climatological SST (not shown).

The driving noise fields are constructed as described in Section 5.2.2 and Chapter 2.6, with standard deviation (and optionally skewness), and spatial and temporal decorrelation scales prescribed from observations. We checked that the constructed noise field reproduces the standard deviation of the observed noise quite well. The skewness is reproduced by definition.

5.3.3   *ENSO-phase dependent noise*

First we show that the standard deviation and skewness of the observed noise depends on the ENSO-phase. The noise standard deviation and skewness of the warm- and cold-SST phases ($\sigma_{\mathrm{warm}}, \sigma_{\mathrm{cold}}, S_{\mathrm{warm}}$ and S_{cold}) are compared to noise standard deviation and skewness of the neutral phase ($\sigma_{\mathrm{neutral}}$ and S_{neutral}). Figure 5.4 shows the differences of the standard deviation as $(\sigma_{\mathrm{warm}} - \sigma_{\mathrm{neutral}})/(\sigma_{\mathrm{warm}} + \sigma_{\mathrm{neutral}})$ and $(\sigma_{\mathrm{cold}} - \sigma_{\mathrm{neutral}})(\sigma_{\mathrm{cold}} + \sigma_{\mathrm{neutral}})$. A value of 0.1 thus means an increase in standard deviation of 22%, a value of -0.1 means a decrease of 18%. White areas mark non-significant changes with respect to the neutral phase. One can see that not only the mean westerly wind stress increases during El Niño, as shown in Section 5.3.1, but also the amplitude of the noise becomes stronger for higher temperatures. The standard deviation of the noise in the El Niño phase is up to 35% higher than for neutral temperatures, especially in the West Pacific where the standard deviation is already higher than in the east equatorial Pacific. On the other hand, for La Niña the amplitude is up to 25% weaker.

Figure 5.5 shows the skewness of noise for the warm, neutral and cold SST ENSO phases. During El Niño significant changes can be found in the central Pacific: westerlies are spread out over a larger area since the area of the warm pool is extended. During La Niña a significant reduction in skewness of the noise is seen in the West Pacific. The higher skewness in the west equatorial Pacific during neutral conditions than El Niño conditions is statistically significant. This is in agreement with Monahan (2008) who shows that the skewness of zonal wind stress is highest for intermediate values of the ratio of the mean and the standard deviation of zonal wind stress. In an idealized stochastic boundary layer model he demonstrates that the skewness is determined by both the nonlinearity of the relationship between winds and wind stresses and the non-Gaussian shape of the vector wind distribution.

5.4   *Implications for the ENSO cycle*

In Figure 5.6 the first EOF, spectrum of the corresponding principal component (PC1) (which indicates the period of the ENSO cycle) and skewness of SST of the linear ICM *lin/nino/fix*-experiment are shown and compared to observations. Standard errors are 0.26 in the observed skewness of SST and 0.12 for the ICM SST skewness. In addition to the significance level of the spectrum, there is an error in the power of the spectrum due to sampling (not shown). Comparing the spectra of different Gmodel runs to each other it appears that the widths of the spectra are robust, but single peaks cannot be interpreted in terms of dynamics.

The maximum of the first EOF of the *lin/nino/fix*-experiment is too far west, the period is too frequent and slightly peaked around 3 years and the skewness of this ICM is, as expected for a linear model, not discernible from sampling noise.

Overall, this ICM output is encouraging since the components of the ENSO cycle seem modelled well enough to approximate the main properties of ENSO. However, a better description of the driving noise component and the statistical atmosphere are required in order to improve the first EOF, the spectrum and the skewness of SST.
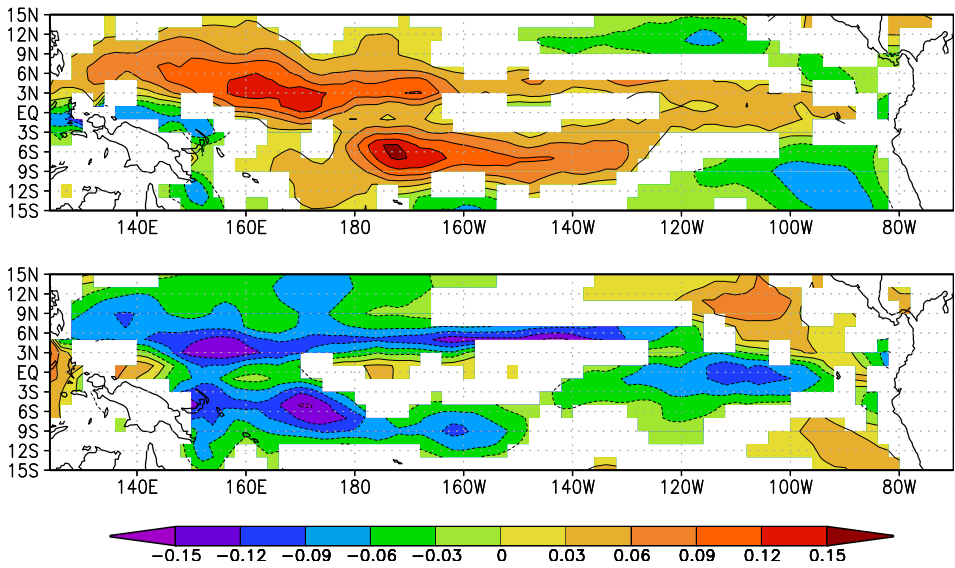
Fig. 5.4: Difference in standard deviation between the El Niño and neutral phase (top) and the La Niña and neutral phase (bottom) as $(\sigma_{\mathrm{warm}} - \sigma_{\mathrm{neutral}})/(\sigma_{\mathrm{warm}} + \sigma_{\mathrm{neutral}})$ and $(\sigma_{\mathrm{cold}} - \sigma_{\mathrm{neutral}})/(\sigma_{\mathrm{cold}} + \sigma_{\mathrm{neutral}})$, for noise used to describe the nonlinear atmosphere.
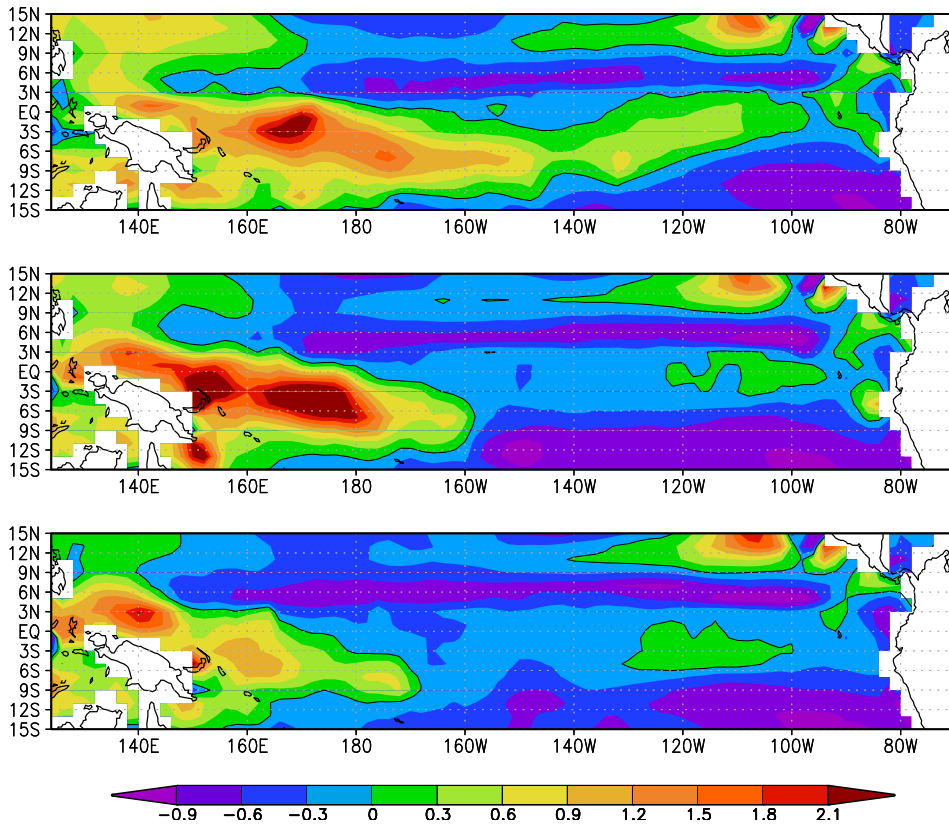
Fig. 5.5: Top to bottom: skewness of noise used to describe the nonlinear atmosphere for the warm, neutral and cold phase respectively.

Figures 5.7-5.9 show the most important implications of the nonlinear features discussed in this study for the ENSO cycle simulated by the ICM with nonlinear effects in the atmosphere added one by one.

Considering the first EOF of the ICM, adding a spatially distributed noise field on the wind stress field has the largest influence compared to the standard experiment *lin/nino/fix*. With the use of 'full sd noise' or 'full skewed noise' (all *full-sd-* and *full-skew-* experiments) the first EOF is strongly improved with respect to the *lin/nino/fix*-experiment. With a full noise field the maximum of the first EOF is no longer too far west. Although the pattern is spread out somewhat more westward than in the observations, it is in good agreement with the first EOF of observed SST. The result for the *lin/full-sd/fix*-experiment is shown in Figure 5.7. The EOFs for the other experiments are not shown, since differences of the first EOF between the *lin-* and *nonlin-*experiments and *fix-* and *phase-*experiments are much smaller than the difference between experiments with 'nino noise' and experiments with 'full sd noise'.

Next, the power spectrum of PC1 is investigated, see Figure 5.8. The period is affected most by adding 'full sd noise' to the ICM and by using the quadratic term in the atmosphere, and by the combination of the two. The influence of 'full skewed noise' and ENSO phase dependent noise is much smaller and results are not shown. For all experiments with a spatially distributed noise field the power spectrum has become a little broader. For all *nonlin/full*-experiments the maximum around 3 years is broadened and shifted to around 4 years.

Finally, the SST skewness of the ICM simulations is considered. SST skewnesses of a selection of experiments are shown in Figure 5.9. The simulations with linear statistical atmosphere show very low or even no significant SST skewness: the *lin/full-sd/fix*-experiment exhibits no significant SST skewness and the *lin/full-sd/phase*-experiment has a small signal in the west Pacific. Changing the noise field into a full skewed noise field results in a small SST skewness in the West Pacific. The effect of the use of the nonlinear statistical atmosphere is much larger, especially in combination with a full noise field. The SST of the ICM simulations is much more positively skewed, albeit only in the Central Pacific. Whereas the *nonlin/nino/fix*-experiment still shows only a small (significant) skewness, the SST of other *nonlin*-experiments turn out to be strongly skewed with skewnesses exeeding 1. The impact of using the nonlinear statistical atmosphere in combination with a 'full sd noise' field is very distinct. On the contrary, with phase-dependent noise or 'full skewed noise' SST skewness in the ICM shows only little changes, also in combination with other nonlinearities. Therefore only the *nonlin/full-sd/fix*-experiment is shown.

Overall, we recommend to use full noise fields with spatially varying standard deviation instead of simple noise terms on the SST indices in order to obtain more realistic ENSO characteristics like the first EOF and spectrum. However, using 'full sd noise', the nonlinearities in SST are seen to be dominated by the nonlinear statistical atmosphere, i.e. the nonlinear mean westerly wind response to SST in the ENSO region. This means that the integrated effect of the enhanced westerly wind events over the larger warm pool has a dominant influence on the difference in strength of El Niño relative to La Niña; other atmospheric aspects such as the skewness of the full noise fields are less important. Making the standard deviation (and alternatively skewness as well) of the noise dependent on the

EOF1
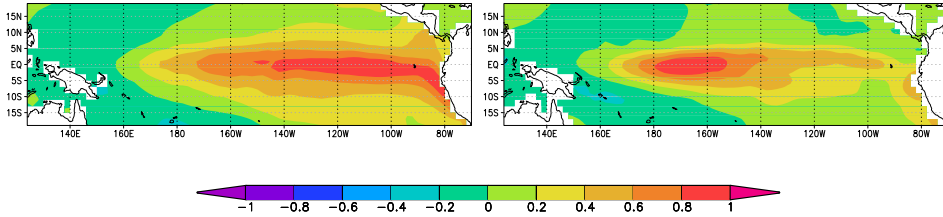
SPECTUM
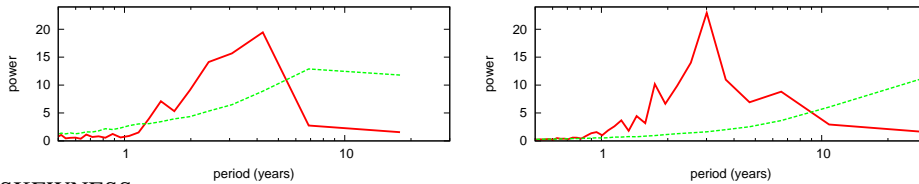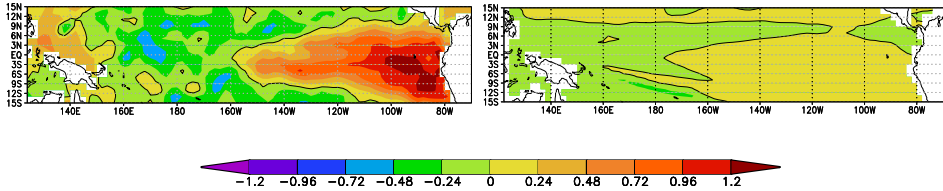
SKEWNESS

Fig. 5.6: First EOF, spectrum and skewness of SST of re-analysis (left) (Uppala et al, 2005) and of the linear ICM (right). Green lines in the spectrum figures denote the 95% significance level relative to red noise.

ENSO phase does not influence either the ENSO cycle nor the skewness of SST strongly in our modelling approach.

5.5 *Conclusions and discussion*

The purpose of this investigation was to quantify the role of nonlinearities in the atmospheric components of the ENSO cycle. This was studied in a reduced model containing the most important dynamics of the ENSO cycle, the components of which are fitted separately to observations. The linear starting point describes the ENSO cycle reasonably well. One of the most obvious problems in this model is the absence of nonlinearities. The most distinct is the skewness of SST: in reality El Niño events are in general stronger than La Niña events. Nonlinearities in atmospheric responses and in the driving noise terms with characteristics close to observed atmospheric nonlinearities are added.
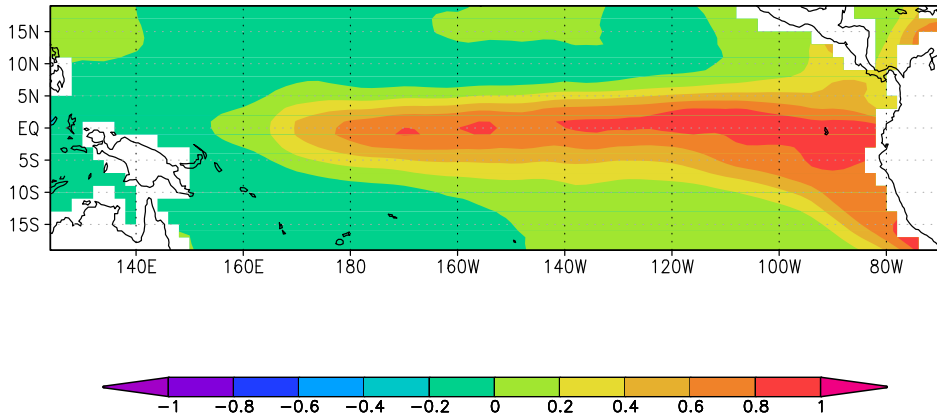
Fig. 5.7: First EOF of the ICM SST with linear atmosphere and 'full sd noise' which is ENSO-phase independent (*lin/full-sd/fix*-experiment).

Adding the fitted nonlinearities in the atmosphere, the output of the ICM indicates that the nonlinear mean response of wind stress to SST in the ENSO region has a dominant influence on the nonlinearities in SST in the ENSO cycle. However, the use of spatial noise fields with standard deviation, spatial decorrelation and temporal decorrelation similar to observed ('full sd noise') is necessary for a better description of characteristics like the first EOF and spectrum. With this description of the noise fields the first EOF is no longer too far to the central Pacific but located more in the east Pacific, as consistent with observations. The effects of using ENSO phase dependent (multiplicative) noise are relatively small. The skewness of the full noise fields (i.e. westerly wind events rather than symmetric or easterly ones) also has a minor effect.

In the investigation of the influence of atmospheric noise like WWEs on the nonlinearities in the ENSO cycle a distinction can be made between different aspects of WWEs. These can be expanded into mean, variance and skewness. In most studies where multiplicative noise is used in addition to stochastic noise (e.g., Perez et al, 2005; Eisenman et al, 2005; Gebbie et al, 2007; Tziperman and Yu, 2007) the focus is on the ENSO-phase dependent variance of WWEs. In this study we show that the mean effect of WWEs is much more important for ENSO skewness than the variance. Furthermore, this study shows that both the skewness of noise fields (i.e. westerly wind events) and the multiplicative nature of the noise influence SST skewness less.

Kessler and Kleeman (2000) already showed that the wind stress similar to that of the Madden-Julian Oscillation develops a rectified SST anomaly, which in turn results in a positively skewed SST. The MJO patterns used by Kessler and Kleeman (2000) are idealized sinusoidal waves in x and t. In this study the result is more general than that of Kessler and Kleeman (2000), since asymmetric WWEs can occur as well and the amplitude of WWEs
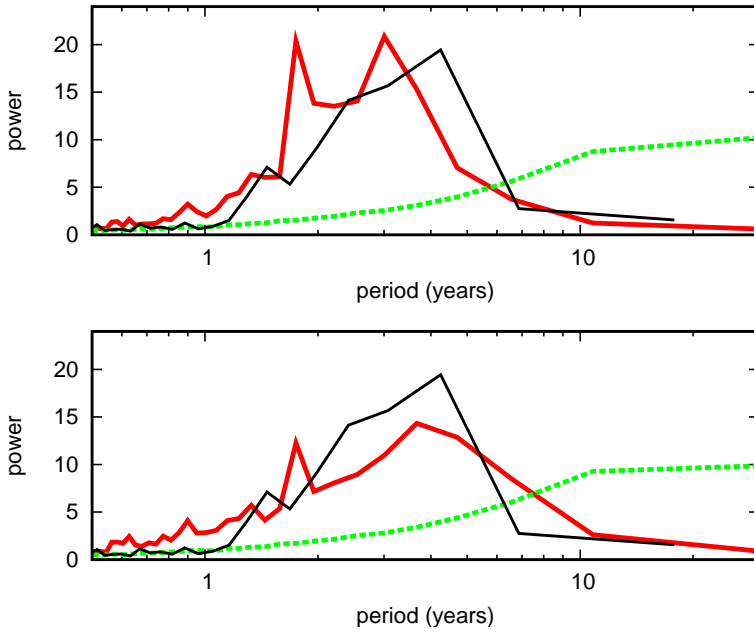
Fig. 5.8: Spectra of the ICM PC1 (red lines) with linear atmosphere (top) and nonlinear
atmosphere (bottom), both with 'full sd noise' which is ENSO-phase independent.
The significance level of the period is given by the green lines. Black lines show
the spectrum of the ERA40 re-analysis.
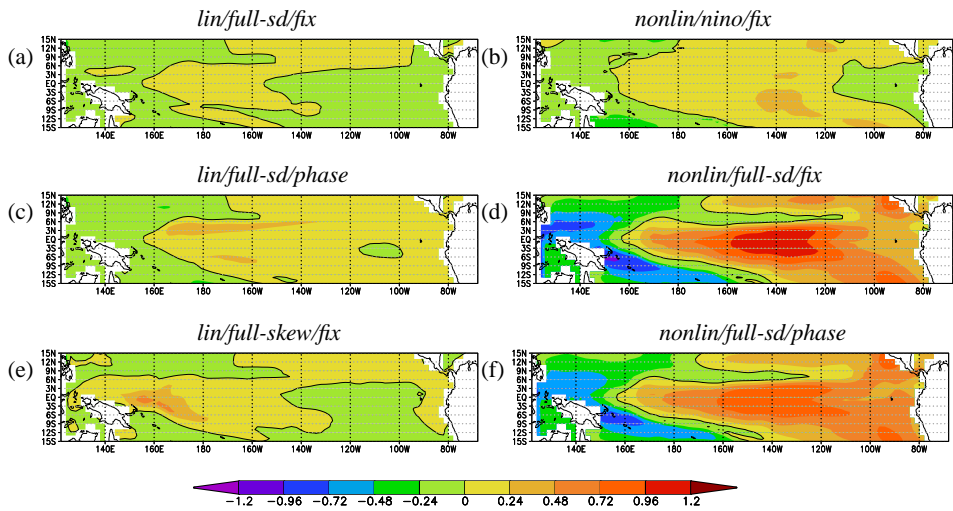
Fig. 5.9: Skewness of SST of the ICM for (a) linear atmosphere and fixed full noise standard deviation, (b) nonlinear atmosphere and noise on the SST indices, (c) linear atmosphere and full noise standard deviation dependent on the ENSO-phase, (d) nonlinear atmosphere and fixed full noise standard deviation, (e) linear atmosphere and full noise standard deviation and skewness dependent on the ENSO-phase and (f) nonlinear atmosphere and full noise standard deviation dependent on the ENSO-phase and bound on the thermocline(see Section 5.5).

can become larger. The main result is confirmed, i.e. the nonlinear relation between SST and wind stress is responsible for a skewed SST signal. This study furthermore shows that this is the most significant atmospheric contribution to SST skewness, more important than the contributions of the relation of amplitude and skewness of atmospheric noise to the background SST.

The atmospheric properties discussed so far have large implications for the modelled SST skewness. However, the skewness is still too strong in the central Pacific and too weak in the east Pacific. This is partly due to the ocean part of the ICM that is totally linear in the version of the ICM used so far. Note that so far no seasonal cycle is included in the ICM.

An improvement of the description of nonlinearities in the ocean part in the ENSO feedback will be needed. This study is concerned with the nonlinearities that arise from the atmosphere only. Preliminary results indicate that adding nonlinearities in the ocean model improves the skewness. Adding the restriction that the thermocline cannot outcrop above the sea surface improves the simulation of the skewness in both the central and east Pacific, see Figure 5.9f.

In addition, in the central Pacific, the relation between wind stress and local SST in observational data shows indications for nonlinearities. During El Niño the anomalous zonal ocean velocity u' is positive. At the same time, in general the zonal temperature gradient T'_x becomes less negative, so it has a positive anomaly. During La Niña these anomalies change sign. Thus, the second order anomalous term $u'T'_x$ tends to be positive during both warm and cold events. This results in an enhancement of La Niña and a weakening of El Niño, which in turn influences the skewness of SST in this region. The result is a shift towards lower skewness. In the east Pacific other nonlinearities in the ocean are important, see among others Zebiak and Cane (1987) and Jin et al (2003). We expect that the inclusion of the most important oceanic nonlinearities to extend the reduced model will give a good description of the complete ENSO cycle.

6. ATMOSPHERIC PROPERTIES OF ENSO: MODELS VERSUS OBSERVATIONS

Two important atmospheric features affecting ENSO are atmospheric noise and a nonlinear atmospheric response to SST (Chapter 5). In this article we investigate the roles of these atmospheric features in ENSO in observations and coupled Global Climate Models (GCMs).

We first quantify the most important linear couplings between the ocean and atmosphere. We then characterize atmospheric noise by its patterns of standard deviation and skewness and by spatial and temporal correlations. GCMs tend to simulate lower noise amplitudes than observations. Additionally we investigate the strength of a nonlinear response of wind stress to SST. Some GCMs are able to simulate a nonlinear response of wind stress to SST, although weaker than in observations. These models simulate the most realistic SST skewness.

The influence of the couplings and noise terms on ENSO are studied with an Intermediate Climate Model (ICM). With couplings and noise terms fitted to either observations or GCM output, the simulated climates of the ICM versions show differences in ENSO characteristics similar to differences in ENSO characteristics in the original data. In these model versions the skewness of noise is of minor influence on ENSO than the standard deviation of noise. Both the nonlinear response of wind stress to SST anomalies and the relation of noise to the background SST contribute to SST skewness. Although the ICM is not fully realistic, the results show that this is a promising route.

Overall, atmospheric noise with realistic standard deviation pattern and spatial correlations seems to be important for simulating an irregular ENSO. Both a nonlinear atmospheric response to SST and the dependence of noise on the background SST influence the El Niño/La Niña asymmetry.

6.1 Introduction

The El Niño – Southern Oscillation (ENSO) is one of the most important climate modes on interannual time scales (e.g., Guilyardi et al, 2009). This climate phenomenon has been extensively studied in both observations and models. The basic linear physics of ENSO is well understood, but more work is required on the physical mechanisms determining irregularities and asymmetries, e.g., El Niño events are in general larger than La Niña

events. For example, two candidate mechanisms for asymmetries and irregularities in ENSO that have been proposed are nonlinear internal dynamics and stochastic forcing.

Different types of nonlinear internal dynamics have been studied. Jin et al (2003) claim that nonlinear dynamical heating is an important nonlinearity in the eastern Pacific. In the Cane-Zebiak model of ENSO (Zebiak and Cane, 1987) a nonlinear coupling exists between sea surface temperature (SST) and the thermocline depth. Furthermore, the wind stress response to SST anomalies is not linear everywhere, and noise components in the wind that drive anomalies in the ocean can depend strongly on the background SST, like in the model of Kleeman et al (1995). Nonlinear analysis methods such as nonlinear principal component analysis have been used (e.g., An et al, 2005) to show that ENSO is a nonlinear cyclic phenomenon.

The role of atmospheric stochastic forcing has also been studied extensively. Blanke et al (1997) suggested that the addition of atmospheric noise increases ENSO irregularity and that the ocean is sensitive to the spatial coherence of noise fields. More recent studies focus on the interaction between ENSO and the atmospheric variability at shorter timescales such as the Madden-Julian Oscillation (MJO), and westerly wind events (WWEs) in both observations (e.g. Lengaigne et al, 2003; Vecchi et al, 2006; Kug et al, 2008) and coupled models (e.g. Lengaigne et al, 2004; Jin et al, 2007). For instance, Jin et al (2007) showed that the state-dependent noise can produce positive skewness of SST using a two-box model. Some studies prescribe noise with an idealized structure in models (Eisenman et al, 2005; Gebbie et al, 2007; Tziperman and Yu, 2007), others use Principal Component Analysis (Zavala-Garay et al, 2003; Perez et al, 2005; Zhang et al, 2008).

The latest generation of coupled climate models can produce a climate in which ENSO-like behavior is present, but improvements could still be made. Most climate models still do not capture for instance SST skewness: the fact that La Niña events occur more frequently but are weaker than El Niño events, see also Figure 6.9. Among the current generation of models even the most reliable coupled models show large differences (e.g., van Oldenborgh et al, 2005; Guilyardi, 2006). It is an open question to what extend linear or nonlinear feedbacks or noise terms are responsible for these differences.

Philip and van Oldenborgh (2009b) show that the nonlinear response of wind stress to SST anomalies largely influences ENSO in terms of SST skewness. Furthermore, the noise terms, defined as the wind stress residual of a (nonlinear) statistical atmosphere model, are described in terms of standard deviation, skewness, spatial correlations and temporal correlations. These noise terms do depend on the background SST. With an Intermediate Climate Model (ICM) for the Pacific Ocean in which feedbacks and noise terms are fitted to weekly observations this study shows that the spatial coherent field of noise in terms of standard deviation strongly influences SST variability. The noise skewness has only a minor influence. Furthermore, the nonlinear response of wind stress to SST anomalies affects SST skewness most, followed by the dependence of the noise standard deviation pattern on the background state.

As coupled global climate models (GCMs) still show large discrepancies with the observed ENSO we investigate the differences in these modelled processes and atmospheric noise terms compared to the observed ones as described in Philip and van Oldenborgh (2009b). This study examines a selection of five coupled GCMs that most realistically

simulate ENSO properties and linear feedbacks in the ENSO phenomenon, (see also van Oldenborgh et al (2005) and Section 6.2.3). We build linear, coupled ICM versions of these GCMs so that the dynamics are much easier to understand. With these ICM versions we are able to study the influence of additional noise properties or nonlinear terms on the characteristics of ENSO.

The question addressed in this chapter is: what are the most important similarities and dissimilarities in atmospheric properties between observations and GCMs influencing ENSO?

This question is answered in two steps, the methodology of which will be explained in detail in Section 6.2. In Section 6.3 we directly compare atmospheric noise terms of GCMs with atmospheric noise terms of observations. Section 6.4 compares nonlinearities in the description of the atmosphere of observations with GCMs. The influence of noise and nonlinear terms on ENSO is described in Section 6.5. Finally, conclusions are drawn in Section 6.6.

6.2 Method of investigation

We use the framework sketched in Figure 1.8 to describe ENSO. In this simplified model coupling strengths are fitted from observations and five GCMs. The atmospheric response to equatorial SST anomalies is described by a statistical atmosphere model. Here, we consider the atmospheric component that is dynamically most important, the zonal wind stress (τ_x) (Philander, 1990). Heat fluxes play a role as well, but are implemented as a damping term in the SST equation. A nonlinear atmospheric response is described with a second order term in the statistical atmosphere model. The noise is defined as the residual of the observed or GCM modelled wind stress minus the quantity described by the (nonlinear) statistical atmosphere. This noise is described by the first two non-zero statistical moments: standard deviation and skewness. This description does not include a dynamical structure in the noise terms. However, the ocean acts as a low pass filter. When the ocean model used in this study (see later) is forced with observed wind stress it shows similar SST characteristics compared to when the model is forced with noise characterized as above. Some GCMs have nonlinear aspects such that the ICM represents those GCMs less well than ERA40.

The other main couplings between zonal wind stress, SST and thermocline depth (Z_{20}) are fitted separately. The resulting set of coupling strengths describes all interactions in the conceptual ENSO model shown in Figure 1.8. Figure 1.8a shows the linear approximation, Figure 1.8b describes the nonlinear components that have been included in this study: the internal nonlinear response of wind stress to SST and the external noise terms. We only investigate nonlinearities between zonal wind stress and SST, omitting non-linearities in the ocean or related to other atmospheric processes like for instance heat fluxes (Sun et al, 2009).

In the next subsections we first describe how the coupling strengths and noise parameters were estimated. Then we explain how these were used to infer the influence of the atmospheric properties on ENSO.

6.2.1   Fitting the couplings and noise of ENSO

To start with, all linear and nonlinear couplings between τ_x, SST and Z_{20} and atmospheric noise terms as shown in Figure 1.8 are separately fitted to observations and GCM output. The coupling parameters of the linear model include a linear statistical atmosphere and a linear SST anomaly equation (investigated by van Oldenborgh et al (2005)) and a Kelvin wave speed. In this paper we extend the study with a description of the noise terms. Furthermore the characteristics of couplings fitted to GCMs will be compared in some more detail with the characteristics of the fitted couplings of observations.

The noise terms of both observations and GCMs are characterized by two-dimensional standard deviation and skewness patterns and spatial and temporal correlation. In addition to the linear feedbacks the nonlinear, second order response of wind stress to SST is investigated. Subsequently, the relation between noise and the background SST is characterized.

Once all components of the conceptual model are characterized for both observations and different GCMs, the terms of GCMs are compared to the observed characteristics. This shows to what extend the atmospheric noise and the nonlinear response of wind stress to SST anomalies of models correspond with the observed characteristics.

6.2.2   Influence of couplings and noise on ENSO

The influence of atmospheric noise and the nonlinear wind stress response to SST on ENSO is studied with an Intermediate Complexity Model (ICM). This ICM is based on the so called Gmodel (Burgers et al, 2002; Burgers and van Oldenborgh, 2003), see Chapter 2. The extended version of the Gmodel uses a more comprehensive conceptual model of ENSO than the original one (Figure 1.8b).

For a selection of five GCMs and for observations (see Section 6.2.3) the fitted components are coupled together, resulting in six versions of the extended Gmodel.

Simulations are performed with these six versions of the extended Gmodel. Nonlinearities and noise characteristics are added one by one. Using these tuned reduced models we estimate the influence of the similarities and dissimilarities of atmospheric noise and the nonlinear response of wind stress to SST described in Section 6.2.1.

6.2.3   Data

Observations (OBS) are approximated by two reanalysis datasets. For the statistical atmosphere and the noise terms, monthly ERA-40 data (Uppala et al, 2005) have been used. [Note that in Chapter 5 we use weekly data.] The ocean parameters are fitted to the monthly SODA 1.4.2/3 $0.5°$ ocean reanalysis dataset (Carton and Giese, 2008).

The set of GCMs we use in this study is a selection of five climate models that were available in the CMIP3-archive. The selection consists of GFDL_CM2.0 (GFDL2.0), GFDL_CM2.1 (GFDL2.1), ECHAM5/MPI-OM (ECHAM5), MIROC3_2(medres) (MIROC) and UKMO-Had-CM3 (HadCM3). Data of the available runs of the so-called 20c3m experiments are used, which simulate the climate of the 20th century. These models were found to have the most realistic description of the linear feedbacks defined in Figure 1.8a.

6.3   Noise properties and coupling strengths

The main components in the conceptual model (Figure 1.8) are: a statistical atmosphere model, atmospheric noise properties, an ocean model and an SST equation. Each of them will be fitted and discussed separately in the next four subsections.

6.3.1   Statistical atmosphere model

The atmosphere is described by a statistical atmosphere model, see Eq. 2.2. As basis for SST in this model we use n equal-sized boxes along the equator in $5°$ S–$5°$ N, $140°$ E–$80°$ W.

   The wind stress patterns of ERA-40 resemble a Gill response (Gill, 1980): for $n = 3$, the linear wind response to a positive SST anomaly in the central box is directed eastward in the West Pacific and westward in the East Pacific. Details such as the relative strengths of the equatorial responses and the off-equatorial structure differ from the Gill-type pattern. In the five GCMs the strength of the τ_x response to SST anomalies is in general weaker and the off-equatorial structures differ. A detailed description of all wind stress patterns is given by van Oldenborgh et al (2005).

   With this statistical representation of the atmosphere a wind stress pattern corresponds to an SST anomaly in one of the boxes, being insensitive to the SST anomalies in the other boxes. (Usually the SST anomalies are correlated.) In the GCM data, a zonal shift of the boxes would result in a zonal shift of the patterns $A_{1,i}(x,y)$. Curiously, this is not the case in the ERA-40 data, where for any index region the pattern always resembles a linear combination of the responses to the Niño3 and Niño4 indices. As it is unclear whether this is a model error or a lack of observational data we use the same three boxes as defined above throughout.

6.3.2   Noise properties of wind stress

In Eq. 2.2, the noise $\epsilon_1(x,y,t)$ is defined as the part of the wind stress anomaly that is not described by the statistical atmosphere model. Properties of this residue are calculated separately from the statistical atmosphere model. From Blanke et al (1997) we learn that noise amplitude and spatial coherence influence ENSO. Burgers and van Oldenborgh (2003) show that the time-correlation also strongly influences the amplitude of ENSO. The skewed nature of the zonal wind stress may have an effect on the ENSO skewness. Therefore the time-dependent noise fields are parameterized by the following statistical properties: standard deviation $\sigma(x,y)$, skewness $S(x,y)$, spatial correlation lengths $a_x(x,y)$ and $a_y(x,y)$ and temporal correlation $a_1(x,y)$.

   These statistical properties are related to the actual physical phenomenon as follows. The standard deviation is the amplitude of the monthly mean of the noise. Westerly wind noise is the sum of shorter time scale westerly wind events, such as storms, often associated with the MJO, or tropical cyclones. These occur on a background state of easterly trade winds plus ENSO response. Even on monthly time scales this translates into a positive skewness of the noise. The spatial correlation provides events to be physical rather than unphysical random noise. Finally, the noise is correlated in time due to other processes in

the equatorial Pacific. This accounts for the long lasting, larger scale anomalies (Burgers and van Oldenborgh, 2003; Cravatte et al, 2003).

For the ERA-40 reanalysis the noise standard deviation is shown in Figure 6.1 (left panels). Near the equator the noise standard deviation is highest in the West Pacific where temperatures are highest. The variance of the noise increases with latitude.

This structure is well captured by the five GCMs, but in general with a much lower amplitude on the equator and a higher amplitude off the equator (Figure 6.1). Compared to ERA-40, the standard deviation of the noise in the GFDL2.1 model is only 20% lower near the equator, and 40% stronger at higher latitudes. However, for GFDL2.0 and ECHAM5 the standard deviation is almost 40% lower near the equator and stronger at higher latitudes, 40% and 20% respectively. In the HadCM3 model the noise amplitude most notably differs from ERA-40 near the equator, with an underestimation of 40%. Finally, the atmospheric component of the MIROC model generates the least variability in zonal wind stress at the equator, with a standard deviation that is more than two times lower at the equator than that of ERA-40.

The skewness of the ERA-40 noise is shown in Figure 6.1 (right panels). In the warmer West Pacific strong, short time scale WWEs occur frequently. These cause the distribution of zonal wind stress to be positively skewed. The skewness reaches values up to 1.0 in this area. The GFDL2.0 model is very similar to ERA-40. Also, the noise of both the GFDL2.1 and ECHAM5 models is positively skewed in the West Pacific, although too strongly. The HadCM3 and MIROC models do not generate significant skewness in the noise. The latter two models therefore do not generate features which resemble the observed WWEs.

For ERA-40 the spatial correlation length (defined as the zonal or meridional width at a correlation of 1/e) varies very little from 36 degrees in longitude (a_x) and varies between 6 (between $10°$ N and $10°$ S) and 8 (higher latitudes) degrees in latitude ($a_y(y)$). For the GCMs the spatial correlation is slightly lower: $a_x = 24$ (20 for ECHAM5) and $a_y = 4$.

A good approximation of the time-correlation coefficient at lag one month $a_1(x, y)$ is given by a function that varies linearly along the equator and exponentially along the meridionals as

$$a_1(x, y) = 0.55 \frac{1 - (x - x_W)}{16(x_E - x_W)} e^{-|y|/12} \tag{6.1}$$

with x,y ranging between the boundaries of the domain x_E, x_W, y_S and y_N. This gives correlations around 0.45 near the equator and 0.1 near the northern and southern edges of the domain. The average autocorrelation of zonal wind stress averaged over the Niño34 region ($5°$ S: $5°$ N, $190°$ E: $240°$ E) is shown in Figure 6.2.

The temporal correlations of zonal wind stress noise in the GFDL2.0, GFDL2.1 and HadCM3 models are comparable to that of ERA-40. In the ECHAM5 and MIROC models the temporal correlation is almost zero.

6.3.3   Reduced gravity shallow water model

The response of thermocline anomalies Z'_{20} to zonal wind stress anomalies $\tau'_x(x, y, t)$ (see Figure 1.8a) is captured by the shallow water equations. The one free parameter of the reduced gravity ocean model that is used solve these equations is the Kelvin wave speed
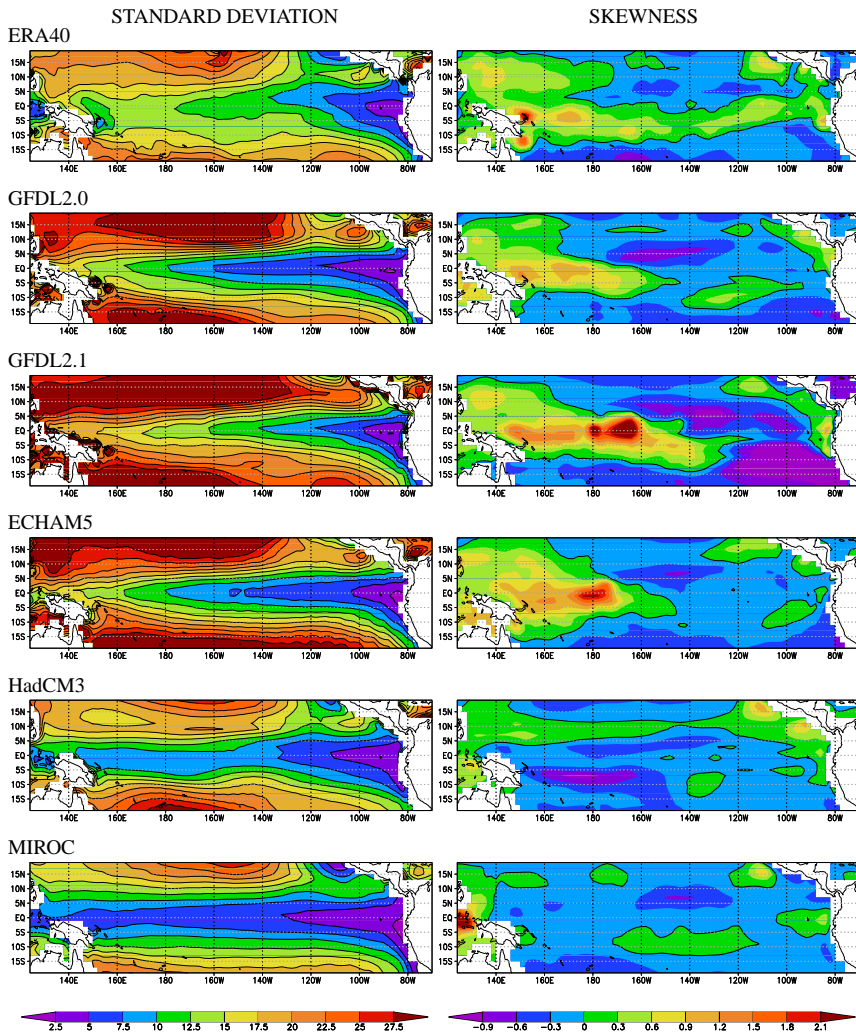
Fig. 6.1: Standard deviation $[10^{-3}\mathrm{Nm}^{-2}]$ (left) and skewness (right) of atmospheric noise. The top panels show noise characteristics for ERA-40 reanalysis data, the other panels show the characteristics of noise of GCM data. The lines in the skewness panels indicate zero-skewness.
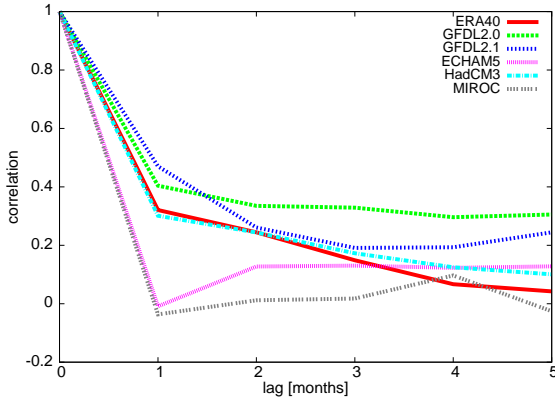
Fig. 6.2: Temporal auto-correlation of the zonal wind stress noise averaged over the Niño34 region. For three GCMs the time correlation coefficient at a lag of one month is comparable to that in ERA-40 reanalysis data. In the ECHAM5 and MIROC models this temporal correlation is almost zero.

(Burgers et al, 2002). This Kelvin wave speed is fitted to optimize ocean dynamics in the six un-coupled versions of the extended Gmodel. Values range between $1.9 \ \mathrm{ms}^{-1}$ for HadCM3 to $2.5 \ \mathrm{ms}^{-1}$ in the observations (see Table 6.1). All the models show a lower Kelvin wave speed, i.e., a smaller density gradient across the thermocline, than the observed value.

Tab. 6.1: Fitted shallow water Kelvin wave speed c.

Model	$c \ [\mathrm{ms}^{-1}]$
OBS	2.5
GFDL2.0	2.0
GFDL2.1	2.1
ECHAM5	2.0
HadCM3	1.9
MIROC	2.0

6.3.4 SST equation

The response of SST to $\tau'_x(x, y, t)$ and Z'_{20} (see Figure 1.8a) is described with a local linear SST anomaly equation, see Eq. 2.1.

The two-dimensional coupling parameters used for the six versions of the ICM are fitted from ERA-40/SODA data and from the five selected GCMs. The coupling parameters are

shown in Figure 6.3. For observed couplings the SST variability caused by thermocline anomalies (α) is strongest in the East Pacific where the thermocline is shallowest. The response of SST to wind stress anomalies (β) plays a role in SST variability in both the eastern and central Pacific. The absolute damping (γ) is strongest in the east Pacific, but compared to the other terms damping is very large in the West Pacific. For more details see also Philip and van Oldenborgh (2009b) or Chapter 5.

Although the GCMs were selected on having fairly realistic couplings along the equator, there are differences with the couplings derived from observations. Most models have SST variability caused by thermocline anomalies that is extended somewhat farther to the north in the East Pacific and to the west. For HadCM3 the strongest response is confined to the coast. The response simulated in the MIROC model is slightly smaller than observed. The fitted responses of SST to wind stress anomalies show only small differences. The most important differences are a weaker response in the central to western Pacific for GFDL2.1, a 10% stronger response for HadCM3 and a response for MIROC that is 20% weaker in the East Pacific and 20% stronger in the West Pacific. The modelled damping is in general about 25% weaker, with minor differences from the pattern of damping derived from reanalysis data.

6.4   Nonlinear extensions

In this chapter we consider two non-linear extensions to the atmospheric component discussed in the previous section: a second order term in the statistical atmosphere and the dependence of wind stress noise on the background SST (see Figure 1.8). We restrict the investigation in this study to non-linearities related to atmospheric noise and wind response to SST, elaborating on existing studies by e.g., Lengaigne et al (2004); Eisenman et al (2005); Vecchi et al (2006); Kug et al (2008); Gebbie et al (2007); Philip and van Oldenborgh (2009b). Non-linearities in the ocean model are not yet considered.

6.4.1   Statistical atmosphere model

The nonlinear response of wind stress to SST is represented by the second term of a Taylor expansion in the statistical atmosphere model, see Eq. 2.3. As the nature of the data allows for at most three boxes, in this study we chose to match the nonlinear boxes with those of the linear representation, with $m = 3$. Note that with the addition of the second order term in the statistical atmosphere model the first two non-zero statistical moments of the noise $\epsilon_2(x, y, t)$ also change slightly.

As the SST variability in the western box is small the patterns $B_1(x, y)$ are obscured by noise. The patterns $B_3(x, y)$ are very small compared to $B_2(x, y)$ in both observations and GCMs. Therefore in Figure 6.4 only the nonlinear responses of wind stress to SST in the central boxes of ERA-40 and the GCMs are shown.

For ERA-40 the maximum (eastward) second order wind stress response to SST anomalies is situated just east of the mean edge of the warm pool, here defined as the $28.5°$ C isotherm. The nonlinear response shows the effect of the change in background SST. During El Niño the convection zone is enlarged resulting in an enhanced positive zonal wind

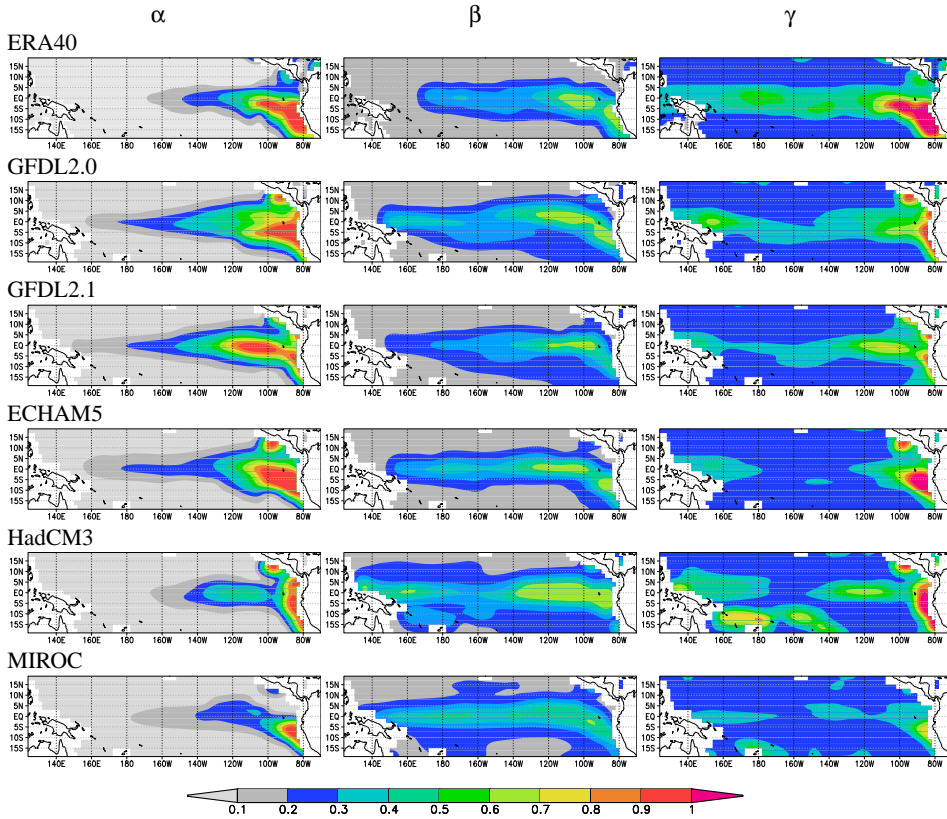*Fig. 6.3:* 2-dimensional parameters as described in the SST equation (Eq. 2.1), for ERA-40 (top panels) and GCM output. Left: α, the SST response to thermocline anomalies $[0.1 \text{Km}^{-1}\text{month}^{-1}]$. Center: β, the SST response to wind variability $[100 \text{KPa}^{-1}\text{month}^{-1}]$. Right: γ, the damping $[\text{month}^{-1}]$. Note that the top panels are identical to Figure 5.1

stress response to SST anomalies. This results in an enhancement of the westerly anomalies during El Niño. During La Niña the convection zone is reduced which leads up to reduce the negative response, again resulting in a net positive contribution (e.g., Philip and van Oldenborgh, 2009b). Kessler and Kleeman (2000) already showed this phenomenon of a rectified SST anomaly additional to the linear response in a much simpler model.

The negative response just north of the equator in the West Pacific shows the opposite effect. There El Niño causes an eastward wind stress response (van Oldenborgh et al, 2005), but this response is smaller than during near-neutral conditions as the distance to the edge of the warm pool increases. During a cold event, with the edge of the warm pool closer to that location, the westward wind stress response to SST is larger. Since during La Niña the response is negative the net effect is again positive. The negative response during both El Niño and La Niña gives rise to the negative non-linear term.

The GFDL2.0, GFDL2.1 and ECHAM5 models do show this effect of convective activity in the patterns. Both the magnitude and the shift of the pattern of the wind stress responses affect the difference between of positive and negative SST anomalies. The patterns are more sensitive to the exact location of the boxes than in ERA-40. Since in these models the edge of the warm pool is too far westward, the nonlinear response of wind to SST is also further westward. This is a major shift, where the nonlinear negative wind response almost falls outside the region considered here. One can also recognize the fact that SSTs are more symmetric around the equator in these patterns. However, only GFDL2.1 exhibits a response with strength similar to ERA-40. For GFDL2.0 the maximum response is twice as weak and for ECHAM5 the response is even more than twice as weak. HadCM3 shows almost no positive nonlinear response. The positive response for MIROC is north of the equator. Note that GFDL2.0 and HadCM3 also show the negative responses off the equator.

6.4.2 The relationship between noise properties and background SST

In the description of noise $\epsilon_1(x, y, t)$ or $\epsilon_2(x, y, t)$ in terms of standard deviation $\sigma(x, y)$ and skewness $S(x, y)$, the noise does not depend on the background SST. A simple method for obtaining an SST dependency is to split the noise timeseries into three equally likely categories where background SST conditions of the central box are warm, neutral or cold respectively. The standard deviation and skewness are then calculated for noise in each category separately.

Results for ERA-40 are shown in Figures 6.5 and 6.6 (top panels). Changes are described with respect to the neutral phase, and only significant changes are discussed. For instance, Kug et al (2009) already suggested that state-dependent noise is directly induced by the low-frequency wind anomaly, which is caused by SST associated with ENSO. Indeed, during the El Niño phase the amplitude $\sigma(x, y)$ of the noise is up to 65% stronger in the West Pacific. During La Niña the difference in amplitude is much smaller. This small change indicates up to 25% larger noise amplitudes in the central to western Pacific during La Niña compared to the neutral phase. This is contrary to what we expect from lower temperatures. The skewness of the noise indicates that westerlies are spread out over a larger area just south of the equator during El Niño. The positive skewness during cold conditions is much lower and more confined to the West Pacific.
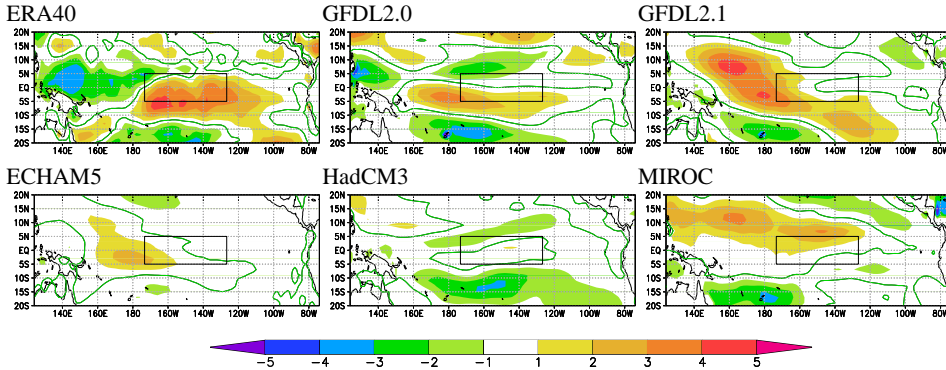
Fig. 6.4: Nonlinear responses of wind stress to SST $[10^{-3}\mathrm{Nm}^{-2}\mathrm{K}^{-2}]$ in the central boxes of
ERA-40 and the five GCMs. Positive numbers indicate an eastward wind anomaly.
In ERA-40 and in the models that do show a positive nonlinear response near the
equator, the response is close to the (modelled) edge of the warm pool.

Differences in GCM noise are described in the light of ERA-40 results. The changes
in noise amplitudes (Figure 6.5) of the warm phase from GFDL2.0, GFDL2.1 and ECHAM5
resemble the differences seen in ERA-40, although for GFDL2.1 the change is larger, namely
100%. Differences in the noise amplitude of HadCM3 and MIROC are much smaller. For the
cold phase, GFDL2.0, GFDL2.1 and HadCM3 show a small increase in noise amplitude of
about 20%, similar to observations. For GFDL2.0, GFDL2.1 and ECHAM5 westerlies indeed
extend further to the east during El Niño and are more confined to the West Pacific during
La Niña (Figure 6.6). However, the skewness is highest for warm conditions in all three
GCMs. The difference in skewness of HadCM3 and MIROC noise is not considered, since in
these models the noise shows no significant skewness to begin with.

6.5   Reconstruction of the ENSO phenomenon by the ICM

So far, all couplings and the noise shown in Figure 1.8 have been fitted to observations
and GCMs. We compared these properties of observations with properties of the GCMs.
We now want to validate the approach and check that the linear reduced models capture
the main characteristics of ENSO. This is achieved by tuning our ICM using the diagnostics
corresponding to each of the five GCMs or ERA-40/SODA data.

First, linear versions of the reduced model are built and examined for the ability to cap-
ture the most important ENSO properties as manifested in the original GCM or reanalysis
data. Next, atmospheric nonlinearities are added in order to investigate their influence on
ENSO. These nonlinearities include a realistic representation of the skewness of the noise,
the nonlinear response of the statistical atmosphere and state-dependent noise character-
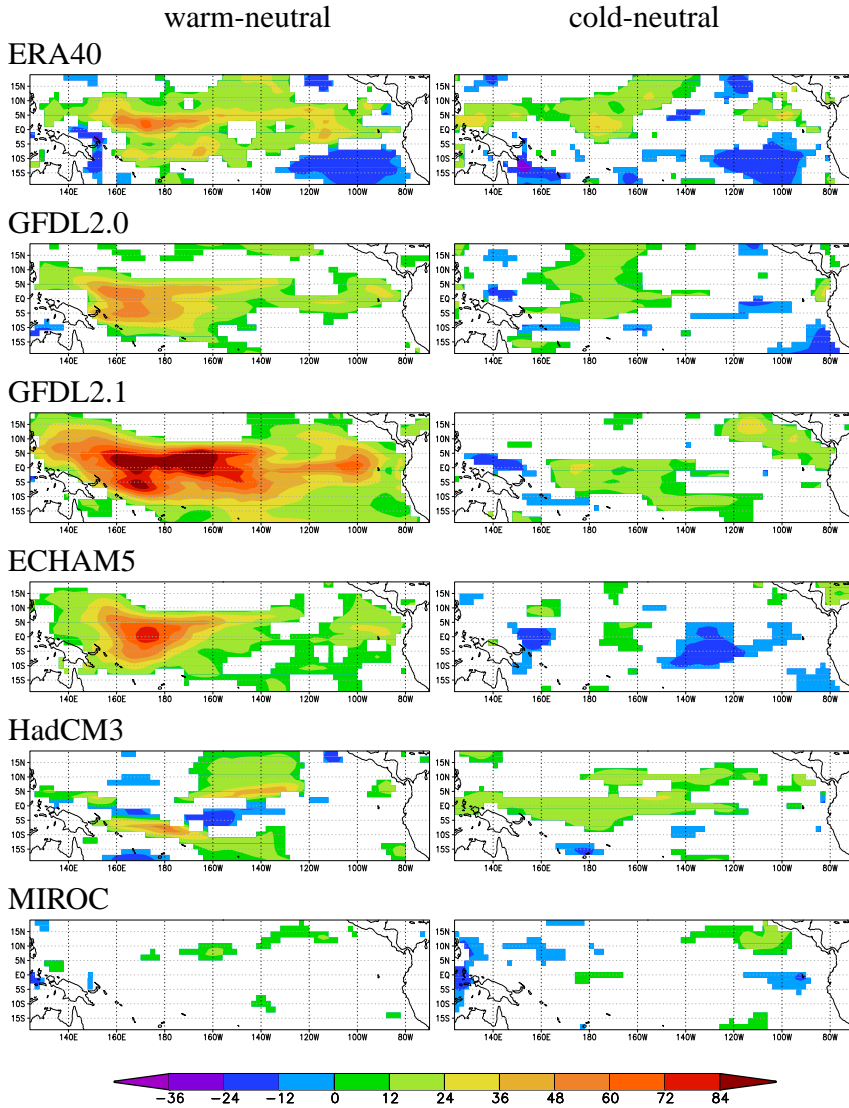
Fig. 6.5: State-dependent atmospheric noise standard deviation in ERA-40 and GCMs. Percentage of change in noise in the warm phase with respect to the neutral phase (left) and in the cold phase with respect to the neutral phase (right). Non-significant changes are masked out.

Fig. 6.6: State-dependent atmospheric noise skewness in ERA-40 and GCMs during the warm phase (left), the neutral phase (center) and cold phase (right). Only significant changes are mentioned in the text. The changes in HadCM3 and MIROC noise skewness are not significant.
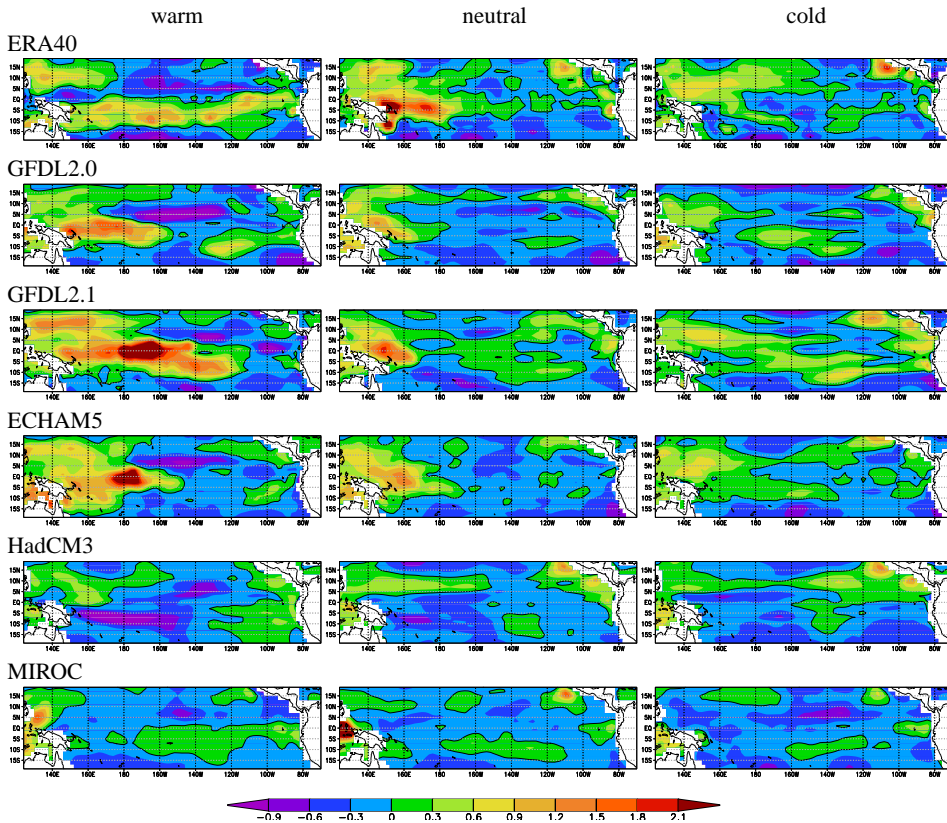
istics. For each combination of parameter settings the ICM is run for 400 years, with a spin-up time of 10 years.

Several ENSO characteristics will be discussed. These include the first EOF of SST anomalies (EOF1), the spectrum of the corresponding principal component (spectrum), the amplitude, defined by the maximum standard deviation of the SST in the East Pacific (off the coast), and the skewness of SST. The EOF1, amplitude and SST skewness have small random error margins in the ICM runs. With the decorrelaton scale of SST of 6 months, errors in amplitude A and skewness S become $0.03A$ and 0.09 respectively. The width of the spectra are robust, but single peaks cannot be interpreted in terms of dynamics.

Some constraints have been implemented in the ICM runs. The thermocline is forced not to outcrop above the surface. Furthermore, since the response to the western box in the nonlinear statistical atmosphere is not discernible from sampling noise, this 'signal' is included in the noise characteristics. The quadratic term of the statistical atmosphere is the only nonlinear term in the central Pacific, and in the ICMs this term is never compensated by nonlinear damping terms. Therefore for each model we cut off the nonlinear statistical atmosphere term at an SST anomaly index of $\pm 2K$, which corresponds to a fairly strong El Niño/La Niña. Without this restriction the ICM results would sometimes diverge because of the fixed positions of the patterns $A_{2,i}(x,y)$ and $B_2(x,y)$ in the statistical atmosphere that strengthen the positive feedback. The results are not very sensitive to the cut off level. Finally, the equilibria of the different reduced models are not necessarily reached for the same mean SST. The mean state of the models might differ. As the Gmodel is an anomaly model, we iteratively adjusted the input climatology until the output climatology was close to zero (less than $0.15\,K$). This did not substantially influence the ENSO characteristics.

The implementation of zonal wind stress noise generation with these prescribed standard deviation, skewness and spatial and temporal correlation lengths is described in detail in Section 2.6.

6.5.1   ENSO in the linear reduced model

The SST anomaly equation, Kelvin wave speed, linear statistical atmosphere model and specified noise characteristics are implemented in the Gmodel framework. Without tuning any parameters to optimize the simulation of ENSO, i.e., only using the coupling strengths and Kelvin wave speed that are adjusted separately, all six fitted reduced models turn out to simulate a climate which captures the main characteristics of ENSO.

In the observations, the main factor contributing to a realistic first EOF appears to be a correct characterization of the standard deviation of the noise, with realistic spatial correlations (Philip and van Oldenborgh, 2009b). The skewness of the noise has only minor influence on ENSO. Therefore we now discuss only ICM experiments with noise described solely by the standard deviation, spatially and temporally correlated. A more detailed discussion of the ICM fitted to weekly ERA-40 reanalysis data can be found in Chapter 5.

The first EOF of SST of the OBS-ICM experiment stretches about as far to the West Pacific as in the reanalysis data, and the meridional extend is smaller than in the reanalysis data (see Figure 6.7). The width of the spectra (at 50% of the peak value) show a

large similarity, with periods between 2-7 years for ERA-40 and 1-5 years for the OBS-ICM (Figure 6.8). The amplitude of 0.8 K is slightly lower than the amplitude of the ERA-40 reanalysis (Table 6.3).

Like the OBS-ICM, the GCM-fitted ICMs are found to be relatively insensitive to the noise skewness. For the thermocline feedback, the typical scale of an oceanic Kelvin wave is a few weeks and a few thousands of kilometers. In the contexts of (variants of) the recharge oscillator, which describes the slower components of ENSO, these scales are even longer and larger. Within these scales, the ocean just integrates the momentum transferred to it by the atmosphere. The effect of state-dependent noise can therefore be larger than the effect of skewed noise. Therefore we made no distinction between ICM runs with and without realistically skewed noise.

Results of the EOFs for the GCM-ICMs can be found in Figure 6.7. The first EOFs of the ICM show common biases with respect to the original data: the pattern is narrower, and does not extend as far westwards. However, the different ICM versions also have features that correspond to the original reanalysis or GCM. The systematic narrowing is due to the approach we use here: the SST-equation is fitted on dynamics close to the equator and is less reliable further off-equator.

The first EOFs of the ICM runs of GFDL2.1, HadCM3 and MIROC are in reasonable agreement with the corresponding GCM EOFs, although the meridional extend in the MIROC-ICM and to a lesser extend extreme also in the GFDL2.1-ICM is clearly too narrow. The conspicuous maximum in EOF1 in HadCM3 in the central Pacific and the far extension of EOF1 to the West Pacific in MIROC are most likely related to the strong response of SST to wind stress anomalies in the central to West Pacific. The first EOFs of GFDL2.0 and ECHAM5 in the ICM runs extend too far to the East Pacific compared to the GCMs. Spatial correlation coefficients between the GCM EOFs and the ICM EOFs are listed in Table 6.2.

The spectra (Figure 6.8) show several striking similarities between the ICMs and the GCMs. In most models the width of the spectra are almost equally broad. Note that for the ECHAM5, GFDL2.0, HadCM3 and MIROC models the width of the spectra are similar. The spectrum of the GFDL2.1 ICM is more confined than in the GCM run: 2-4 years versus 2-6 years. The overall correlation between width of the spectra of the reanalysis data and GCMs and their corresponding ICM run is 0.9.

Table 6.3 shows the SST amplitudes. The ECHAM5-ICM amplitude is much lower than expected, whereas the HadCM3-ICM amplitude is higher than expected. The MIROC-ICM amplitude is also very low, but this is in line with the low amplitude in the GCM. For MIROC this is most likely related to the atmospheric noise, which has a much too low amplitude and no temporal correlation.

The Kelvin wave speed in the ICMs could be changed in order to match the ENSO amplitudes in the ICM runs much better with the original ENSO amplitudes. A change in the Kelvin wave speed would also shift the peak value of the ENSO spectrum. We decided to fit the Kelvin wave speed for the best ocean dynamics and not for the best ENSO amplitude or period. We did not tune this Kelvin wave speed afterwards. Furthermore, with a 1.5 layer ocean model our ICM consists of only one Kelvin wave speed. It was beyond the scope of this article to study the influence of Kelvin waves corresponding to higher order
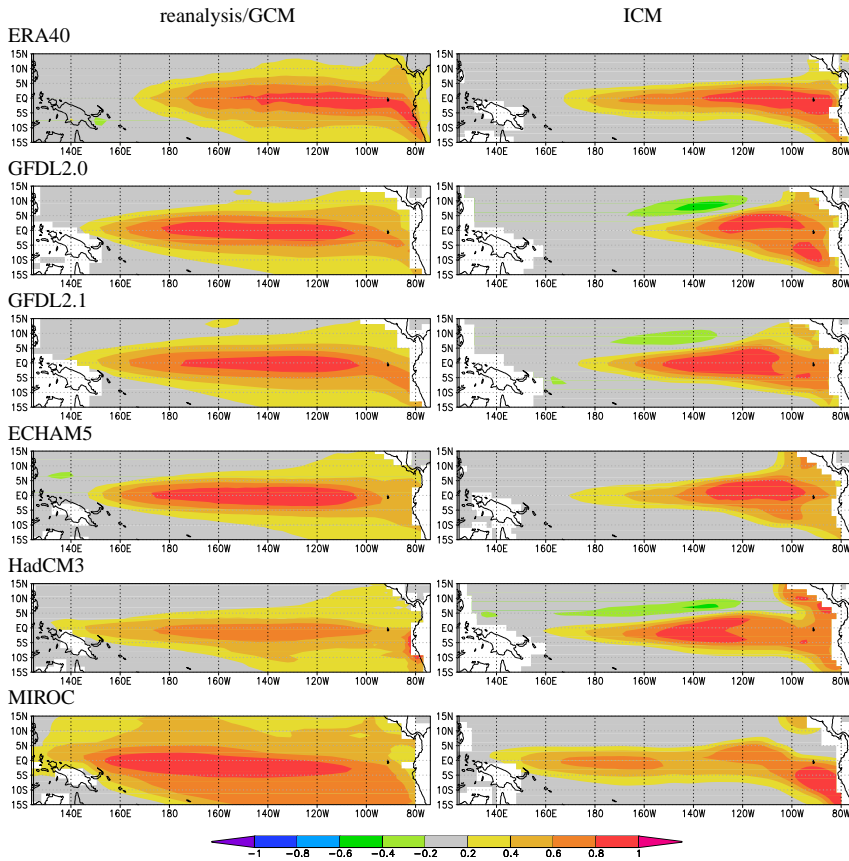
Fig. 6.7: First EOF of SST anomalies of reanalysis/GCMs (left) and corresponding ICMs (right). Spatial correlation coefficients between the original and ICM EOFs are listed in Table 6.2.
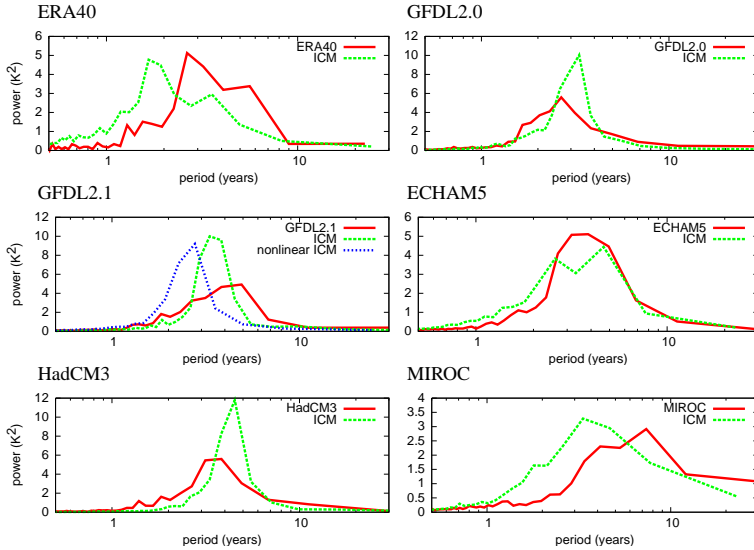
Fig. 6.8: Spectra of the principal components of the first EOFs of reanalysis/GCMs and corresponding linear ICM runs. The spectra for the nonlinear ICM runs are not shown as they almost overlay the spectra of the linear ICM runs, making the pictures difficult to read, except for GFDL2.1 where we also include a spectra using the nonlinear statistical atmosphere.

vertical modes.

In general, taking the common biases into account, there is a good agreement between the first EOFs and spectra of the GCMs and their corresponding ICM after fitting only linear coupling strengths. The SSTs of ICM versions do manifest outliers like the broad power spectrum and low amplitude of MIROC SST variability and the isolated maximum of the first EOF in the central Pacific in HadCM3 SST. The extent to which the ICM SST properties agree with the GCM SST properties is model dependent. Details of SST variability in the coastal zone of South America are not simulated correctly. This is partly the result of a low model resolution and a relatively simple description of the atmosphere. Also, ocean nonlinearities are disregarded.

Overall, we conclude that the linear ICM versions reproduce the characteristics accurately enough to use them for further study: all fitted ICMs turn out to simulate the main properties of ENSO. The investigation of the influence of atmospheric properties on these model versions could improve the performance of the models.

Tab. 6.2: Spatial correlation coefficients (15° S: 15° N, 140° E: 280° E) of the first EOFs of reanalysis data and GCMs and their corresponding ICM run.

data	correlation
ERA-40	0.9
GFDL2.0	0.5
GFDL2.1	0.8
ECHAM5	0.8
HadCM3	0.7
MIROC	0.7

Tab. 6.3: Measure for the ENSO amplitude as defined by the maximum standard deviation (sd) [K] in the East Pacific for reanalysis data and GCMs and their corresponding ICM run.

data	reanalysis/GCM	ICM
ERA-40	1.2	0.8
GFDL2.0	2.0	1.4
GFDL2.1	2.0	2.1
ECHAM5	1.9	0.6
HadCM3	1.5	2.2
MIROC	0.8	0.5

6.5.2   The influence of nonlinearities on ENSO

The second order term of the statistical atmosphere model and the relation between noise and the background SST have been added to the linear ICM. Their influence has been investigated separately and in combination. Just like the linear model versions, all fitted ICMs turn out to simulate the main properties of ENSO. Except for the GFDL2.1-ICM spectrum (see Figure 6.8), the first EOFs, spectra and amplitude in all ICM runs turn out to be relatively insensitive to the modifications. Therefore in this section only the modelled SST skewness will be elaborated upon.

In the OBS experiments, the largest changes in the ICM runs are seen after adding the combination of the nonlinear response of wind stress to SST and the relation of noise to background SST. This is in contrast to results in Chapter 5 in which weekly rather than monthly data are used. There the influence of the nonlinear statistical atmosphere has a larger influence on SST skewness than the relation of noise to the background SST. This can be attributed to the fact that we did not take the longer time scale of 6-8 weeks in the weekly noise data into account. Figure 6.9 shows the skewness of SST anomalies of reanalysis and GCM data, of the ICMs with a linear atmosphere ('linear ICM') and of the ICMs with both nonlinearities added ('nonlinear ICM'). The results of the ICMs in which the nonlinearities have been added separately are not shown, they are only discussed below. The focus is

on the most conspicuous effects. Only changes that are significant are mentioned in the text. Note that in the linear ICMs the SST can already be skewed due to the non-uniform mean thermocline depth; the East Pacific SSTs are most affected by the constraint that the thermocline can not outcrop above the sea surface. Relaxing this criterion gives a poorer resemblance to the observed SST skewness. Relative differences between SST skewness of the different ICM runs remains the same.

The SST output of the linear OBS-ICM run is not considerably skewed. ICM runs with skewed noise show values similar to runs where noise has zero skewness. Both the run with the dependence of noise to the background SST and the run with nonlinear wind response to SST are slightly positively skewed in the central and western Pacific with values up to 0.4, and slightly negatively skewed in the West Pacific. In the latter run the pattern shows the effect of the negative second order wind stress response to SST. The combination of the two nonlinearities is almost a linear combination, with positive skewness up to 0.8. For the Niño34 timeseries this means that the ten largest warm events have a mean anomaly of 1.5 K and the ten largest cold events only reach -1.0 K.

Results for the GCMs are shown in Figure 6.9. As there is a large diversity of responses the experiments are discussed per model. This diversity stems mainly from the large differences in fitted non-linearities in the GCMs.

In the GFDL2.0-ICM the negative off-equatorial second order wind stress response to SST (Figure 6.4) is reflected in corresponding areas of negative skewness in both the GCM and the nonlinear ICM. The difference between the positive SST skewness of the linear GFDL2.0 ICM and the ICM with nonlinear statistical atmosphere is smaller than expected from the nonlinear response of wind stress to SST. However, differences between other GFDL2.0-ICM runs are even smaller. The positive SST skewness of 0.5 in the eastern Pacific in the ICM is only slightly lower than the GCM skewness, but the negative skewness in the West Pacific is not captured by the ICM.

For GFDL2.1 the SST skewness of the linear ICM is exceptionally high, and the pattern agrees with the GCM skewness pattern. This implies that the interaction of the thermocline with the surface is an important factor causing skewness in this model. After adding only the second order term in the statistical atmosphere the skewness is somewhat lower. This model is the only one that shows a shift in the spectrum towards shorter periods with this additional term (indicated by the extra line in Figure 6.8). Using the state-dependency of the noise results in a much larger SST skewness. A closer inspection of the statistical atmosphere shows that a damping term is left aside in the ICM analysis for this specific model, influencing especially the nonlinear ICM, see also Section 6.5.3. Note that the ICM SST also shows the negative SST skewness in the West Pacific.

For the ECHAM5 SST skewness equally large influences are found for the nonlinear response of wind stress to SST and the dependence of noise on the background SST. The combination of the terms gives the highest SST skewnesses, but it is relatively low compared to observations and to the original GCM. The ICM does not capture the negative skewness in the West Pacific.

The HadCM3-ICM runs display much larger SST skewnesses than the GCM SSTs. The negative skewness bands of the nonlinear atmosphere are clearly seen in both the nonlinear ICM and the GCM.

For the MIROC-ICM runs the largest differences are found after adding the nonlinear response of wind stress to SST. The off-equatorial wind stress pattern results in a small positive SST skewness in the central to western equatorial Pacific.

6.5.3 Discussion

The ICM is build from the parameters that are fitted from the SST equation, the statistical atmosphere model, the Kelvin wave speed in the ocean and atmospheric noise. The ICM runs without tuning any of these parameters afterwards and without the addition of extra coupling parameters between the ocean and atmosphere models. We did use some restrictions to prevent the system to blow up due to the lack of damping on the nonlinearities. The ICM runs show common biases which we did not want to remove by tuning. Taking these common biases into account, there is a reasonable agreement between the differences between the GCMs and corresponding ICMs.

In most ICM runs the region of maximum SST skewness is located more towards the west than in the original GCM. While an improvement, the inclusion of atmospheric nonlinearities is only a first step towards building fully realistic reduced models. A full implementation will also have to consider nonlinearities in the ocean model. These tend to reduce the skewness in the central Pacific (Philip and van Oldenborgh, 2009b), and increase it in the eastern Pacific (e.g., Jin et al, 2003).

The ENSO of the GFDL2.1-ICM is clearly too regular in comparison with the original GCM. Moreover, this is the only ICM in which the period changes when adding the nonlinear statistical atmosphere term. Presumably this is due to a damping term that is missing in the ICM and one suggestion is an extra damping term in the statistical atmosphere model. When temperatures in the Niño34 region exceed $28°$ C in the GCM the zonal temperature gradient west of $170°$ E changes sign. As a result, west of $170°$ E the wind response to SST anomalies then reduces almost linearly, contrary to the general increase of the wind response to larger SST anomalies. The definition of the statistical atmosphere model used so far is thus no longer valid. This need for an additional damping term is only found for GFDL2.1.

Both the state-dependency of atmospheric noise and the second order term in the statistical atmosphere of HadCM3 are small. Nevertheless, the nonlinear statistical atmosphere significantly influences the SST skewness. This is due to the relatively large amplitude of the nonlinear wind response to SST anomalies in the eastern box compared to the central box (not shown).

6.6 Conclusions

This chapter tries to show the most important nonlinear characteristics in atmospheric properties in observations and GCMs influencing ENSO. We focus on the properties of the wind stress noise and the (nonlinear) zonal wind response to equatorial SST anomalies. The noise is defined as the wind stress residual of the statistical atmosphere model. Conclusions about this are drawn in two stages. In the first subsection we compare the strength of the couplings in the ENSO feedback loops and the properties of the noise in GCMs to reanalysis
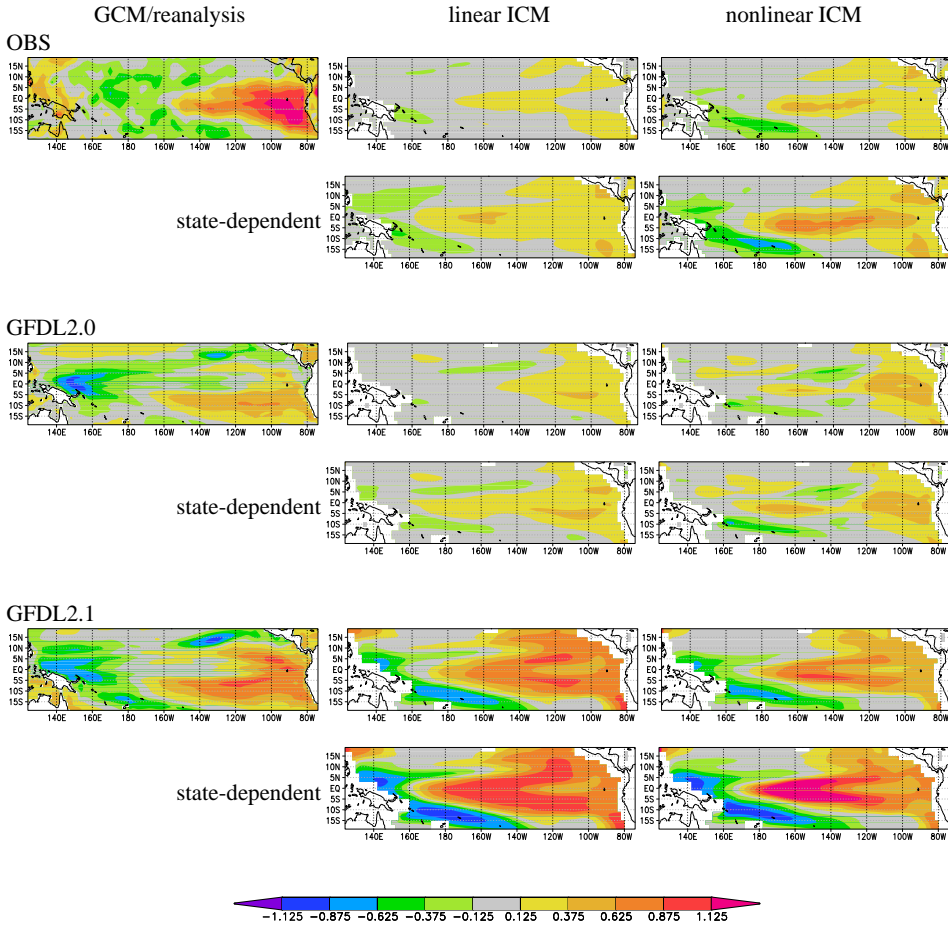
Fig. 6.9: Skewness of SST anomalies of reanalysis/GCMs and four corresponding ICM runs. In the column 'linear ICM' the linear statistical atmosphere is used. In the column 'nonlinear ICM' the nonlinear response of wind stress to SST anomalies is used as well. For each model in the lower two panels the state-dependency of the amplitude of atmospheric noise is included. In each ICM run the thermocline is constrained not to outcrop above the sea surface.

GCM/reanalysis   linear ICM   nonlinear ICM

ECHAM5

state-dependent

HadCM3

state-dependent

MIROC

state-dependent

$$-1.125 \quad -0.875 \quad -0.625 \quad -0.375 \quad -0.125 \quad 0.125 \quad 0.375 \quad 0.625 \quad 0.875 \quad 1.125$$

Fig. 6.9: continued.

data. In the second subsection we consider the influence of the coupling strengths and noise on ENSO.

6.6.1   Direct comparison of GCMs with observations

For a selection of five GCMs with the most realistic main ENSO feedbacks, noise terms and the dependence of noise on the background SST have been characterized and compared to the ERA-40 reanalysis. Subsequently, the nonlinear response of zonal wind stress to SST anomalies has been characterized.

The amplitude of zonal wind stress noise near the equator (i.e, wind stress anomalies unrelated to equatorial SST) is in general lower in GCMs than in the ERA-40 reanalysis. The difference ranges between 20% lower (GFDL2.1) to a factor 2 lower (MIROC). Furthermore, the lagged autocorrelation of the monthly noise fields near the equator is almost zero in the ECHAM5 and MIROC models, in contrast to the observed value of 0.4 at lag one month. However, the pattern of lowest standard deviation in the equatorial East Pacific and higher in the equatorial West Pacific is captured. Also, spatial correlation lengths of noise fields are comparable to observed values. So, models need stronger, coherent subseasonal variability (see also e.g. Slingo et al, 1996; Lin et al, 2006).

Low standard deviations and temporal correlations of the wind stress noise influence the ENSO amplitude. Comparing the GCMs to each other, the MIROC model has indeed by far the lowest ENSO amplitude. As the other coupling strengths of ENSO deviate less from observations, the low variability and temporal coherence of the westerly wind in the western and central Pacific seem the most important factors explaining the low ENSO amplitude in this model.

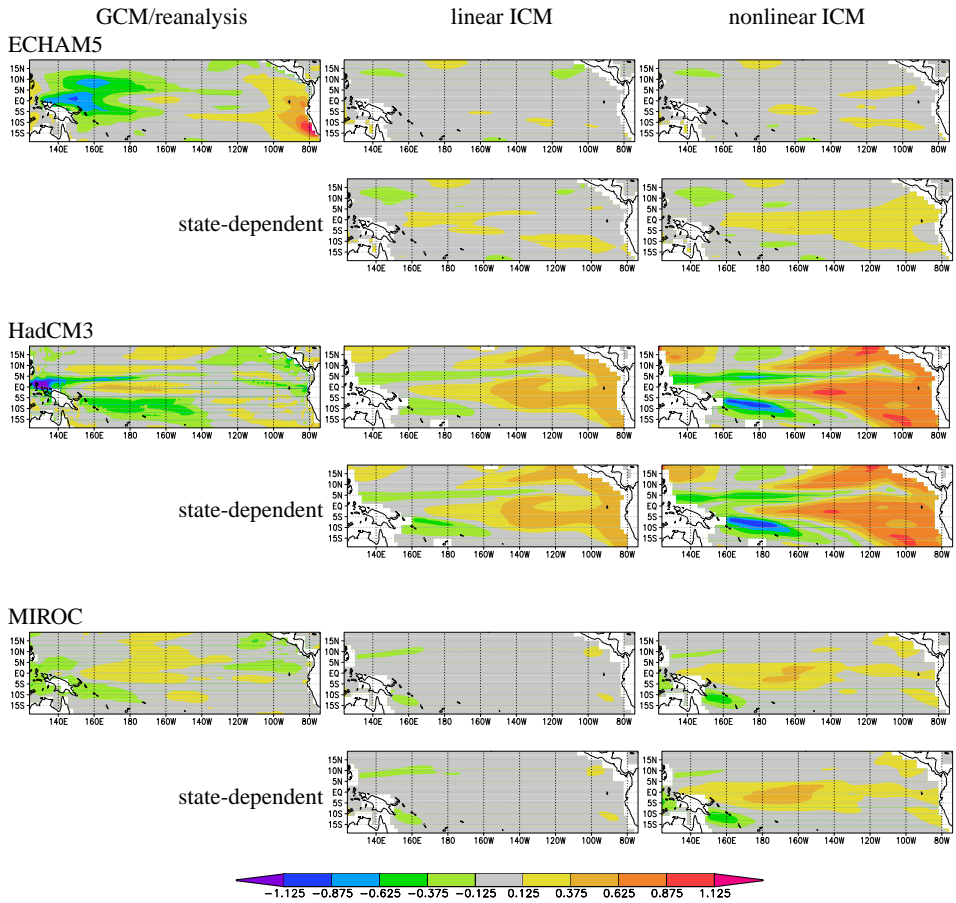SST skewness is influenced by two other characteristics of the noise fields. First, the skewness of the noise fields of reanalysis data is characterized by a positive values in the West Pacific (stronger westerly anomalies than easterly anomalies). Only three GCMs show comparable noise skewnesses. Second, the noise depends on the background state. In reanalysis data the noise amplitude is larger when SST anomalies are positive than during neutral SST conditions and the positive skewness extends further to the east. The GCMs do simulate this dependence of noise on the background SST, but only the GFDL2.0, GFDL2.1 and ECHAM models show differences of comparable size.

Reanalysis data indicate that SST anomalies in the central Pacific result in an eastward second order wind stress response near the edge of the warm pool. In the GFDL2.0, GFDL2.1 and ECHAM5 models we find a similar response, with maxima at locations corresponding to the edges of the modelled warm pools. HadCM3 shows no indications for an eastward nonlinear response for both El Niño and La Niña, and in MIROC the eastward response is only north of the equator. Off-equatorial bands of westward wind stress responses to SST anomalies in the central Pacific are seen in reanalysis data. GFDL2.0, HadCM3 and to a lesser extend also GFDL2.1 and MIROC show similar off-equatorial bands.

Previous findings stressed the importance of the non-linear atmospheric response to the skewness of SST. Indeed, the simplified models that represent this response most realistically also have the most realistic SST skewness. Results from the GFDL2.1 model show a nonlinear response to SST with strength roughly equal to the strength in the reanalysis

data. In the same model, the SST skewness pattern resembles the observed SST skewness pattern quite well. The nonlinear responses of GFDL2.0 and ECHAM5 wind stress to SST are weaker, and so is their calculated SST skewness. The wind stress patterns of HadCM3 and MIROC are very different from the patterns in reanalysis data, and these GCMs do not simulate the observed SST skewness at all. The nonlinear response of wind stress to SST is therefore thought to be directly related to SST skewness.

Overall, the standard deviation and time-correlation of the noise are in general underestimated. Three models simulate noise skewness and the dependence of noise on the background SST with strengths comparable to those in ERA-40 reanalysis data. The three models with the most realistic nonlinear response of wind stress to SST appear to simulate the best SST skewness.

6.6.2 *Comparison of ENSO in GCMs with observations using reduced models*

To study the impact of the coupling strengths and noise properties on ENSO, the fitted parameters are used to make six versions of an ICM, corresponding to the observations and the five GCMs under study. These reduced models can simulate the main properties of ENSO in observations and GCMs. The first step includes the direct feedbacks and noise characteristics. Later, the nonlinear response of wind stress to SST and the relation of noise to the background SST are added to these linear ICM versions.

Analyses of the SST output of the linear ICMs show that, taking into account the common systematic biases, the differences in the first EOFs are approximated reasonably well. The width of the spectra of the corresponding principal components are reproduced well by the reduced models, although the position of the peak is sometimes shifted. These ENSO properties do not change significantly after adding either the nonlinear response of wind stress to SST or the relation of noise to the background SST.

The observed ENSO amplitude is slightly stronger than in the runs of the ICM fitted to observations. The GCM and corresponding ICM amplitudes are correlated, although the correspondence is not perfect. In the MIROC model low noise standard deviations and temporal correlation can indeed be seen in the corresponding ICM run. The ECHAM5 model is an exception: it is yet unexplained why the modelled ENSO amplitude in the GCM is three times higher than in the ICM. One factor that influences the correspondence between GCM and ICM ENSO amplitudes is the Kelvin wave speed. The Kelvin wave speed is fitted for the best ocean dynamics and not for the best ENSO amplitude. Other possible factors influencing the ENSO amplitude have not yet been investigated in detail.

The ICMs reproduce the skewness in the reanalysis and GCMs fairly well. However, the skewness maps are in general not exactly the same, as the feedbacks characterized so far in the ICMs do not represent the full complexity of the system.

The ICM SST skewness is influenced by both the nonlinear response of wind stress to SST and the dependence of noise on the background SST. For monthly reanalysis data the impacts of both nonlinearities are about equally large and are nearly additive. In the GCMs the relative strengths of these two nonlinearities differ.

The wind stress noise itself is also nonlinear: westerly wind anomalies are larger than easterly ones. However, this has only a minor influence on SST skewness in the ICM exper-

iments.

Overall, we have built reduced models with linear feedbacks, atmospheric noise terms and a nonlinear response of wind stress to SST fitted to observations and GCMs. The linear ICMs capture ENSO characteristics like the first EOF and spectrum of the corresponding time series quite well. In both observations and GCMs, the influence of the skewness of noise has a smaller influence on ENSO than the standard deviation of the noise. For monthly observations both the nonlinear response of wind stress to SST anomalies and the relation of noise to the background SST contribute to SST skewness. GCMs that simulate a nonlinear response of wind stress to SST anomalies in general agree on this, although the relation of noise to the background SST is relatively more important in the climate models.

With this analysis a step forward has been made in building a realistic reduced model that describes the observations and GCMs in the equatorial Pacific region. However, this ICM is not yet fully evolved. There are still terms to be added in order to refine the ICMs. Further investigation per model is needed in order to refine the results. This will result in better understanding of the dynamics and in improvements in models and model predictions.

The results show that the five GCMs contain very different nonlinearities in their atmospheric components. How these relate to the model formulation could be studied systematically using a perturbed-physics ensemble such as the one described in Murphy et al (2004) and Toniazzo et al (2008).

7. THE ROLE OF ATMOSPHERE AND OCEAN PHYSICAL PROCESSES IN ENSO

We examine the behaviour of the El Niño – Southern Oscillation (ENSO) in an ensemble of global climate model simulations with perturbations to parameters in the atmosphere and ocean components respectively. The influence of the uncertainty in these parametrisations on ENSO are investigated systematically. The ensemble exhibits a range of different ENSO behaviour in terms of the amplitude and spatial structure of the SST variability. The nature of the individual feedbacks that operate within the ENSO system are diagnosed using an Intermediate Complexity Model (ICM), which has been used previously to examine the diverse ENSO behaviour of the CMIP3 multi-model ensemble. Unlike in that case, the ENSO in these perturbed physics experiments is not principally controlled by variations in the mean climate state. Rather the parameter perturbations influence the ENSO characteristics by modifying the coupling feedbacks within the cycle. The associated feedbacks that contribute most to the ensemble variations are the response of SST to local wind variability and damping, followed by the response of SST to thermocline anomalies and the response of the zonal wind stress to those SST anomalies. Atmospheric noise amplitudes and oceanic processes play a relatively minor role.

7.1   Introduction

Coupled numerical models (GCMs) now form the core of efforts to predict natural climate variability and forced climate change on time scales of seasons, decades and centuries. They also form the basis of a large number of studies, which seek to understand the mechanisms for those variations in climate. The El Niño – Southern Oscillation (ENSO) presents a considerable challenge for numerical models as the different physical (and biogeochemical) processes that need to act together to produce an oscillation are diverse; ranging from large to small-scale oceanic dynamics, atmospheric dynamics, cloud processes, surface fluxes etc.

There have been some notable advances in recent years in the ability of models to simulate ENSO. AchutaRao and Sperber (2006) track the ENSO-ability of models during two development cycles and note that the majority of the models in the most recent collection now has the ability to spontaneously produce an oscillation that has characteristics that

---

resemble those that are observed in the real-world ENSO. Numerous studies (e.g., van Oldenborgh et al, 2005; Guilyardi, 2006) however note that there is still a wide range of model ability in terms of the basic characteristics, including amplitude, period, phase locking to the annual cycle etc. Recent efforts have sought understanding of those basic characteristics in terms of the physical feedbacks that are involved in ENSO, see Chapter 3 and 6. Such diagnostics and metrics (Guilyardi et al, 2009) are currently being employed in efforts to reduce model 'errors' with a view to correcting and improving models or in assigning relative skill of different models in probabilistic projections.

It is useful to separate model errors that affect the ability to simulate ENSO into two types. The first type includes errors or biases in the mean climate state; both ocean and atmosphere errors as well as errors that are in some way coupled, including errors in the seasonal-cycle, are ubiquitous. Typical biases include the simulation of a cold tongue that is too cold and too extensive and the simulation of a South Pacific Convergence Zone that is too zonally oriented (Lin, 2007): the so-called 'double-ITCZ' problem. Other errors have also been described (e.g., Guilyardi, 2006). Mean-state errors develop quickly during model simulations and hence are often subject to much directed effort to reduce them.

The second type of potential model error is associated with inaccuracies in the physical processes involved in ENSO. For example, errors in the strength of the Bjerknes feedback whereby anomalies in sea surface temperatures (SSTs) force variations in the atmospheric winds and circulation that tend to reinforce those SST anomalies (a positive feedback). Such feedback processes are increasingly the focus of GCM ENSO studies in the literature (e.g., Philip and van Oldenborgh, 2006, 2009b; Lloyd et al, 2009).

The difficulty in separating model errors in this way is that they are clearly linked. Mean-state errors, for example, produce errors in the mean distribution of clouds, which may then affect the pattern and strength of surface-flux damping of ENSO SST anomalies. Likewise, errors in the surface-flux feedback may lead, non-linearly, to errors in mean-state SSTs. Our ability to understand ENSO errors in models and ultimately improve the baseline simulation of ENSO is complicated by such interactions.

Here we partly circumvent this problem by examining the simulation of ENSO in a set of model experiments with perturbations to key atmospheric and oceanic parameters. In these so-called 'perturbed physics' experiments, the mean climate state and annual cycle is, to a large extend, controlled by imposing flux adjustment terms which tie the model SSTs and salinities close to observed values. While the elimination of flux adjustment terms has been seen as a breakthrough in climate modelling (e.g. Gordon et al, 2000), non-flux-adjusted models suffer from biases in the mean state and seasonal cycle (Guilyardi, 2006).

In this case the flux adjustments serve to minimise the mean-state errors and allow us to examine the physical processes involved in ENSO in some detail. As coupled models are being improved, it is expected that mean-state errors will continue to reduce, which eventually enables the improvement of the realism of physical feedbacks in models in a more straightforward way (i.e. without the complication of errors in the mean state). This chapter anticipates such a situation.

We adopt the same approach as used in Chapter 2 and Chapter 6 in which an 'Intermediate Complexity Model' (ICM) is fitted to different GCMs to examine the role of both linear feedback loops and the non-linear role of atmospheric noise. The ICM can qualitatively re-

produce the basic characteristics of the ENSO behaviour in the individual CMIP3 GCMs when the parameters of the model are fitted to the GCM output. The different feedbacks are shown in Figure 1.8 and described in more detail in Section 7.3.

In a diverse multi-model ensemble, it is difficult to investigate the influence of each part of the ENSO feedback loop separately, as all components differ from each other. The fitted ICM is numerically stable as long as both the atmosphere and the ocean are fitted to the same GCM. The ICM is not necessarily numerically stable when using atmosphere parameters of one GCM and ocean parameters of another GCM. The variations in ENSO feedbacks are too large to put parts of the feedback loop from different models together. This problem is much less acute in the case of the perturbed physics ensemble examined here. Coupling of the ocean of one ensemble member with the atmosphere of another member often gives more consistent ICM runs than performing the same exercise with the parameters fitted from two very different GCMs. This proves to be a useful tool in understanding the behaviour of the different perturbed physics GCMs.

The approach is complementary to Toniazzo et al (2008) who test the variation of ENSO characteristics in a very similar model ensemble in which parameters in the atmosphere are perturbed. They compare subsets of the ensemble with low and high ENSO variability respectively. The assumption of Toniazzo et al (2008) that a stronger thermocline feedback would logically result in an SST anomaly propagation that is more eastward was not found in the perturbed parameter ensemble examined in Toniazzo et al (2008). Furthermore they only find a weak negative relation between ENSO strength and wind response to SST.

Here we quantify the influence of different coupling and atmospheric noise parameters of ENSO separately. We examine an updated version of the perturbed parameter ensemble used by Toniazzo et al (2008). The influence of the different parts of the ENSO feedback loop is tested in the context of the ICM. This enables us to choose parts of the ENSO feedback loop, individually fit them to different model runs and test the impact relative to a reference run. In the reference ICM we mutually exchange fit parameters from different perturbed physics GCM ensemble members. In this way the influence of each parameter can be quantified separately. The objective is to quantify the importance of different parts in the linear ENSO feedback loop on variations in ENSO.

The HadCM3 atmospheric parameter perturbed ensemble is presented in Section 7.2. The different parts of the feedback loop are described in Section 7.3. In Section 7.4 ENSO characteristics of the HadCM3 atmospheric parameter perturbed ensemble are briefly discussed. The terms of the conceptual model are fitted to the data in Section 7.5. The relations between these terms and ENSO characteristics are investigated in Section 7.6. Section 7.7 presents conclusions.

7.2 Perturbed physics GCM experiments

The 'perturbed physics approach' was developed in response to the call for better quantification of uncertainties in climate projections (see Chapter 14 of the IPCC Third Assessment Report, e.g., Moore et al, 2001). The basic approach involves a single model structure in which perturbations are applied to the values of a range of presumably uncertain parameters; the determination of the range of the parameters is based on discussions with col-

leagues involved in parameterisation development and/or surveys of the climate modelling literature. In some cases, different variants of physical schemes may be also be switched on or off. Also parameters in those alternative schemes are varied. Any experiment that is routinely performed with single models can be produced in 'ensemble mode' subject to constraints on computer time. A significant amount of perturbed physics experimentation has been done with HadCM3 and variants, starting with the work of Murphy et al (2004) and Stainforth et al (2005) and continuing with, for example, Piani et al (2005); Webb et al (2006); Knutti et al (2006); Collins et al (2006a); Harris et al (2006); Collins (2007); Sanderson and Piani (2007); Sanderson et al (2008); Rougier et al (2008). Nevertheless, other modelling centres are also investigating the approach using GCMs (e.g., Annan et al, 2005; Niehörster et al, 2006) and more simplified models (e.g., Schneider von Deimling et al, 2006) with a view to both understanding the behaviour of their models and to quantifying uncertainties in predictions.

Here we make use of perturbed physics ensembles produced with the version of HadCM3 in which a fully dynamical ocean and atmosphere are dynamically coupled. HadCM3 has the advantage that the model is structurally capable of simulating key aspects of ENSO as has been noted in a number of studies (Collins et al, 2001; AchutaRao and Sperber, 2006; K. AchutaRao, 2002; van Oldenborgh et al, 2005; Toniazzo, 2006a; Guilyardi, 2006). In our experiments, two ensembles are used of 16 members each. In one ensemble (hereafter ATM-ensemble, members 1-16), perturbations are only applied to parameters in the atmosphere component of the model, the ocean parameters being held fixed at their standard settings. In the second (hereafter OCN-ensemble, members 17-32), perturbations are only applied to parameters in the ocean component of the model, the atmosphere parameters being held fixed at their standard settings. The run with standard model parameter settings is denoted STAM. STAM, ATM and OCN thus comprise a total of 33 members. The 16 sets of atmosphere-parameter settings are chosen in order to sample a range of atmosphere feedbacks under climate change, to span a range of parameter values and to maximise the chance of getting model versions that have time-mean climates that are as close as possible to observations for a number of observed climate fields. The algorithm for choosing the ATM-ensemble parameters is described in Webb et al (2006). In the case of perturbations to the ocean parameters (OCN-ensemble) a slightly different approach is taken. For this ensemble, Latin-hypercube sampling of parameters that control horizontal mixing of heat and momentum, the vertical diffusivity of heat, isopycnal mixing, mixed layer processes and water type is performed. Despite this difference in sampling strategy, it will be demonstrated that both atmospheric and oceanic ENSO-processes are sufficiently perturbed to produce a wide range of different ENSO behaviour that can be diagnosed using the ICM approach. Collins (2009) discusses the experimental setup and aspects of global-model evaluation and feedbacks in some detail.

It should be noted that the experiments used here are an updated version of those used in Collins et al (2006a) and Toniazzo et al (2008) in which also ENSO characteristics are examined. In those ensemble experiments, significant SST and sea-ice biases arise in the North Atlantic and Artic oceans because of the particular implementation of flux-adjustments during the spin-up phase. Monthly-mean flux adjustments were employed to (i) prevent model drift that would result from perturbations to the parameters that lead to

top-of-atmosphere net flux imbalances, and (ii) to improve the credibility of the simulations in simulating regional climate change and feedbacks. The spin-up technique used in the experiments examined here is similar to that described in Collins et al (2006a) except that a less vigorous salinity relaxation is employed during the Haney-forced phase (in which SSTs and surface salinities are relaxed toward a seasonally-varying climatology - see Collins et al (2006a)). This is found to significantly alleviate the problem of SST and sea-ice biases found in the Collins et al (2006a) ensemble. It is unlikely that errors in simulated North Atlantic and Arctic climate would affect ENSO variability directly, hence comparisons with the findings of the Toniazzo et al (2008) study are possible.

7.3   Method: the Intermediate Complexity Model

The separate contributions of the main components that contribute to the characteristics of ENSO are shown schematically in Figure 1.8. In this conceptual model of ENSO, the main interactions are separated. These are the influence of wind stress on thermocline depth, the impact of SST anomalies on wind stress and the dependence of SST on both thermocline depth and on wind stress. External atmospheric noise also influences ENSO. We include only linear feedbacks and the standard deviation and spatial- and temporal correlations of the atmospheric noise term.

The terms shown in Figure 1.8 are represented in the ICM using statistical relationships derived from either observations or GCM output. They can be changed independently from each other or in combination in order to study the influence of the different components separately on ENSO.

7.3.1   Basic structure and experiments with the ICM

The equatorial Pacific ICM is based on the so-called Gmodel, see Chapter 2. In this chapter the length of each ICM run is 400 years, ensuring that the differences in ENSO characteristics due to significantly different coupling strengths are statistically significant.

Each of the 33 ensemble members of the perturbed parameter ensemble is characterised by a unique set of coupling parameter fields and noise characteristics. For each member, these terms are implemented in the ICM resulting in 33 unique versions. Sensitivity tests are also performed in which parameters are mutually exchanged between different ensemble members. This enables us to study the influence of the terms separately, assuming the effects add linearly.

7.3.2   SST-equation

The linear local SST anomaly equation is used to parameterise SST variability, see Eq. 2.1. Figure 7.1 shows the two-dimensional patterns for the STAM member. All terms in the SST-equation are important in the East Pacific near the coast of S. America. Away from this coastal region, the response of SST to thermocline anomalies (α) is largest in the central to eastern Pacific, the main region of SST anomalies in the model. In the West Pacific, both the response of SST to wind stress anomalies (β) and the damping on SST (γ) play an
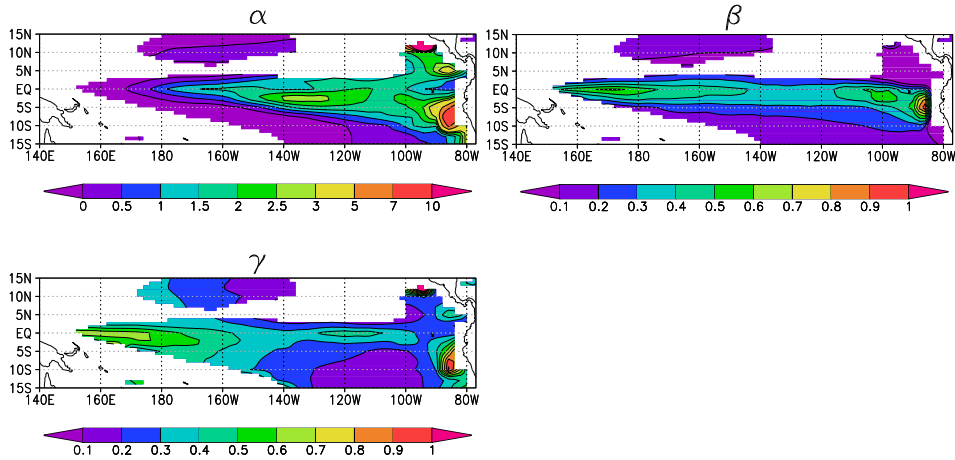
Fig. 7.1: Response of SST to thermocline anomalies, α [$0.1 \mathrm{Km}^{-1}\mathrm{month}^{-1}$] (top left) and to wind stress anomalies, β [$100 \mathrm{KPa}^{-1}\mathrm{month}^{-1}$] (top right) and the damping time on SST, γ [month^{-1}] for the STAM member. Only areas in which the SST-equation (Eq. 2.1) describes more than 40% of the SST variability are shaded. Note the nonlinear scale in the response of SST to thermocline anomalies.

important role. These patterns of responses are consistent with those fitted to observations as seen in Figure 5.1. Relative to observations, α is slightly stronger in the central Pacific, β is stronger in the West Pacific and γ is stronger in the West Pacific.

For the members of both the ATM- and OCN-ensembles, the spatial patterns of α, β and γ are qualitatively similar to the STAM member but the magnitudes are different. For this reason it is appropriate to compare the ensemble members by averaging the values of the parameters in boxes distributed on longitude and centred on the equator (see section 7.5).

7.3.3 Statistical atmosphere model for zonal wind stress

Another important term in the ENSO feedback loop is the response of the zonal wind stress to SST. This sensitivity can be fitted with a linear statistical atmosphere model, see Eq. 2.2 Based on testing a number of different configurations, the responses of zonal wind stress to SST anomalies is best resolved in three boxes in the Pacific Ocean. Using more and smaller boxes gives rise to excessive noise in the response patterns and instabilities in the ICM.

Figure 7.2 shows the zonal wind stress response patterns for the STAM member using the three highlighted SST boxes. The wind stress response is always convergent towards the positive SST anomalies. This is consistent with a heating anomaly on top of a background temperature gradient and background wind (Clarke, 1994). The wind response west of the anomaly is stronger than the response east of the anomaly and the response to an SST anomaly in the east Pacific is weaker than that in the central West Pacific. The latter is
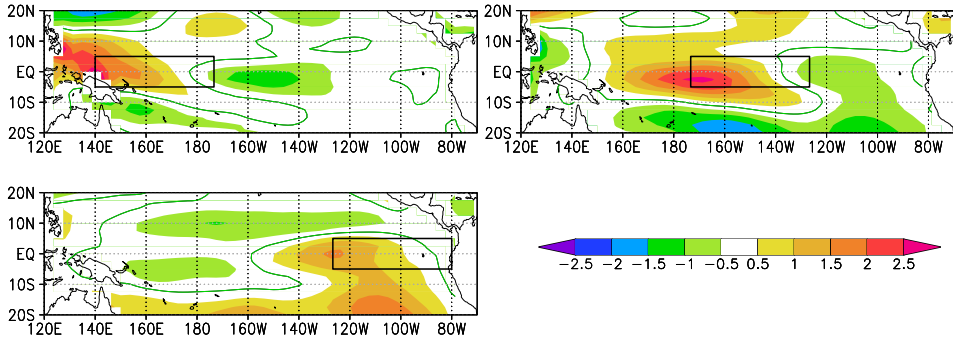
Fig. 7.2: The sensitivity of zonal wind stress anomalies to SST anomalies (term A in Eq. 2.2) of the STAM member $[10^{-3}\text{Nm}^{-2}\text{K}^{-1}]$. The response is calculated using the three SST boxes highlighted on each figure panel. Orange-red colours correspond to eastward wind stress response to a positive SST anomaly in the indicated box, green-blue colours correspond to negative (westward) anomalies.

due to the warmer background SST in the West Pacific relative to the East Pacific, which provides higher evaporation, more convection and consequently a stronger wind stress response to SST anomalies. The patterns and strength of the wind stress responses to the SST anomalies in the STAM member are in reasonable agreement with that of observations, see also Figures 3.2 and 3.3. Relative to observations, the wind stress response to an SST anomaly in box 1 is more a Gill-type pattern. The other two responses are comparable.

As in the case of the SST-equation parameters α, β and γ, the spatial patterns of A_i for the perturbed members of ATM- and OCN-ensemble are very similar to those for the STAM member shown in Figure 7.2.

7.3.4   Atmospheric noise properties

In the ICM used in this thesis ENSO is stable and driven by external atmospheric noise. In Chapter 6 we show that a physically consistent characterisation of this noise term is necessary. Therefore we describe the noise term with a two-dimensional pattern of noise amplitude and with a spatial and temporal autocorrelation.

Figure 7.3 shows the basin-wide amplitude of atmospheric noise for the STAM member. The noise amplitude is lowest in the eastern equatorial region where the background SST is lowest. The pattern resembles that calculated from observational data, but the amplitude is up to 40% lower near the equator compared to observations (Philip and van Oldenborgh, 2009a).

In order to quantify the noise characteristics in each ensemble member, spatial and temporal correlation coefficients are estimated from 25 equally distributed locations between $30°$ S-$30°$ N, $120°$ E-$90°$ W, divided in 5 locations zonally by 5 locations meridionally. This
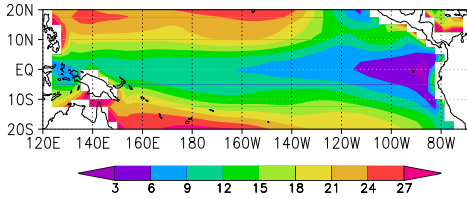
Fig. 7.3: Atmospheric noise standard deviation in $[10^{-3}\mathrm{Nm}^{-2}]$ of the STAM member.

number of locations is enough to cover the whole basin with sufficient resolution. The distance at which the spatial correlation is less than 0.36 is calculated to be 24 degrees zonally and 4 degrees meridionally. A good approximation of the time-correlation coefficient at a lag of one month $a_1(x,y)$ is given by a function that varies linearly along the equator and exponentially along the meridionals as $a_1(x,y) = 0.5(1+x/N_x)/\exp(\frac{1}{8}|y-2-\frac{1}{2}N_y|)$ with x,y ranging from 1 to N_x and 1 to N_y respectively and N_x=84, N_y=30. Minimum values are set to 0.15 and maximum values, just north of the equator in the West Pacific, are cut off at 0.4.

Again, the spatial patterns of atmospheric noise for the perturbed members of the ATM- and OCN-ensemble are very similar to those for the STAM member. However, as we see below, there are differences in the amplitudes of the patterns.

7.3.5   Ocean component of the ICM

The ocean component of the ICM uses a 1.5-layer ocean model with ocean wave dynamics described by the gravest baroclinic mode. The Kelvin wave speed is fitted to the ocean dynamical fields in the region $5°$ S-$3°$ N, $150°$ E-$110°$ E, i.e., in the region where the correlation between the GCM thermocline amomalies and ICM thermocline anomalies is highest. In this region, the thermocline is relatively important in comparison to the wind stress response to SST and in comparison to the damping. The SST-equation explains a large fraction of the variance (>0.4) (see also Figure 7.1).

The value for the Kelvin wave speed that results in the best-fit ocean dynamics is determined from a forced version of the ICM. In this version the SST-equation parameters in the ICM are fitted to all ensemble members separately. The forcing is represented by the two-dimensional zonal wind stress anomaly timeseries of the respective ensemble members. Different Kelvin wave speeds between 2.0 ms^{-2} and 2.6 ms^{-2} are tested for the highest average correlation between the ICM-thermocline depth and the thermocline depth of each ensemble member. For the STAM member the Kelvin wave speed that corresponds to the highest average correlation has a value of 2.4 ms^{-2}. This is a realistic value compared to observations.

7.4   Characteristics of modelled ENSO in the ensembles

Firstly we examine a set of diagnostics of ENSO behaviour in the STAM and perturbed members of the ensemble. Commonly used diagnostics in the equatorial Pacific region relate to the ENSO amplitude, period and pattern. We define the ENSO pattern by the standard deviation of SST anomalies σ and the amplitude is quantified by the average of σ (denoted by $\langle \sigma \rangle$) over the region $5°$ S–$5°$ N, $160°$ E–$100°$ W. (As most models tend to represent the cold tongue and the region with largest variability too far into the West Pacific, we choose a region that is larger than the common Niño3 or Niño3.4 boxes.) The mean period $\bar{T}$ is defined from the timeseries of the box-averaged SST anomalies over the region. The power spectrum of this timeseries is bandpass filtered between 1-10 year to filter out subseasonal and multi-decadal variability and then averaged by $\bar{T} = \exp \langle \log(1/f) \rangle$, where the angular brackets denote the averaging with a weight proportional to the power at frequency f.

The ENSO characteristics of the perturbed parameter ensemble are listed in Table 7.1. These characteristics are in reasonable agreement with ENSO characteristics obtained from Reynolds SST observations (Reynolds et al, 2002). The amplitude of the STAM member ($0.86°$ C) is only slightly lower than that of observations ($0.93°$ C).The mean period of 4.3 years is somewhat longer than that of observations (3.8 years), although estimating the period of such a complex oscillation can be significantly affected by sampling noise. In common with other GCMs, the maximum variability is too far to the west, although the displacement in this flux-adjusted HadCM3 is not as extreme as in, for example, the non-flux-adjusted version of HadCM3. ENSO characteristics of the perturbed parameter ensemble vary around the ENSO characteristics of the STAM member.

The mean climate in the ensemble can be described by the main actors in the ENSO phenomenon: SST, wind stress and thermocline depth. Additionally we calculate the mean mixed layer depth (MLD), as we need this later when we describe SST-equation parameters. To compare the mean climate of the ensemble members with the STAM member we defined a set of indices, all between $5°$ S–$5°$ N. The mean SST in the eastern Pacific T_{east} is calculated between $127°$ W–$85°$ W (3rd box in Eq. 2.2). An SST gradient ΔT is defined as the difference in SST between $127°$ W–$85°$ W and $140°$ E–$172°$ W (3rd box minus 1st box in Eq. 2.2). The mean wind stress and MLD are calculated for $140°$ E–$150°$ W ($\tau_{x,\text{west}}$) and $150°$ W–$85°$ W ($\tau_{x,\text{east}}$), and the mean thermocline depth is defined for $180°$–$150°$ W (H_{central}) and $130°$ W–$85°$ W (H_{east}).

In general the differences in mean climate state between each perturbed member of the ensemble and the STAM are not large; much smaller than the differences between the 19 structurally-different CMIP3 models examined in van Oldenborgh et al (2005). Some small variations around the STAM member are evident: a difference in T_{east} with the STAM member ranging from $-0.5°$ C to $0.4°$ C, an SST gradient that is at most 3.2 K larger than in the STAM member and a spread in thermocline depth between 74m and 98m. The variation of the mean wind stress and of thermocline depth are correlated with variations in ΔT, especially in the East Pacific. This is understood in terms of the well known balance between the pressure gradient force and the wind stress. The gradient in SST sets up the mean wind stress and this in turn influences the east-west gradient in thermocline depth.

Despite the similarities between the mean climates of the ensemble members that are

Tab. 7.1: ENSO characteristics in the perturbed parameter ensemble. The top row shows the characteristics from observations (obs) (Reynolds v2 SST, Reynolds et al (2002)). The errormargin for the period is obtained from NCDC ERSST v3b data. In bold the STAM member. The amplitude $\langle\sigma\rangle$ is defined as the mean SST-standard deviation σ [$^\circ$ C] over 5° S–5° N, 160° E–100° W. The mean period [years] is calculated from the timeseries of the average σ over this box. For the ENSO pattern the longitude at which the σ reaches a maximum $\sigma_{\max}$ in this box is given, together with a second maximum if this is approximately equally high. The term 'broad' describes the describes the fact that the amplitude has no clear maximum but is zonally rather broad. Members 1-16 are part of the ATM-ensemble, members 17-32 describe the OCN-ensemble.

ATM	$\langle\sigma\rangle$	period	$\sigma_{\max}$ lon$_1$	lon$_2$	OCN	$\langle\sigma\rangle$	period	$\sigma_{\max}$ lon$_1$	lon$_2$
obs	0.93±0.13	3.4±0.3	255						
0	**0.86**	**4.3**	**180**						
1	1.16	4.8	195	251	17	1.18	4.1	224	
2	1.04	4.2	191		18	0.88	5.0	194	
3	0.89	4.5	188		19	0.88	5.5	232	
4	0.93	3.8	180	229	20	0.99	4.1	194	244
5	1.14	3.5	240		21	0.86	4.2	198	
6	0.74	3.6	180	248	22	0.92	4.3	194	
7	0.57	4.2	154		23	1.13	4.9	232	
8	0.67	4.1	184	248	24	0.88	4.3	202	
9	0.67	4.1	169		25	1.00	4.1	232	broad
10	0.83	3.9	176		26	0.99	4.7	188	
11	0.60	4.1	158		27	1.22	4.8	218	
12	0.86	4.4	191		28	1.07	4.8	210	
13	0.56	3.7	180	251	29	1.06	4.2	202	226
14	0.79	4.0	183		30	0.92	3.8	232	
15	0.61	3.8	244		31	1.01	4.7	210	
16	0.80	4.2	180	244	32	0.99	4.0	210	

imposed by the use of flux-adjustments, there are some subtle differences between individual members, which may impact the ENSO variability. The strongest correlation between the mean climate and ENSO characteristics is a relatively large correlation of -0.83 between T_{east} and the ENSO amplitude for the ATM-ensemble. However, for the OCN-ensemble this correlation is only -0.39. We next examine the coupling characteristics in the ensemble members and their dependence on these subtle variations in the mean.

7.5   ENSO coupling strength in the ensemble

7.5.1   Description of the SST-equation parameters

The two-dimensional responses of SST to wind stress anomalies and thermocline anomalies and the damping coefficients are fitted to all the ensemble members. As noted above, whereas such patterns vary considerably between structurally different coupled GCMs (van Oldenborgh et al, 2005), the patterns are relatively similar across the ATM-ensemble and OCN-ensemble. Therefore it is possible to define indices for the amplitudes of the patterns that are used to quantify the differences in responses and damping terms. We can then check the dependence of the fitted parameters on the mean state.

To compare mean values of the responses and damping terms we average two regions where these terms are most important (see also Figure 7.1). For all East Pacific terms, the east region is 5° S–5° N, 150° W–85° W. For the response to wind stress anomalies and damping, the western-most region is defined as 5° S–5° N, 140° E–150° W. For the SST response to thermocline anomalies, the western-most region is defined as 5° S–5° N, 180° –150° W.

The values are listed in Table 7.2 and figure 7.4 shows a selection of the most important relations between these terms and the mean climate. From previous studies (e.g., Fedorov and Philander, 2001; Philip and van Oldenborgh, 2006) we might expect that α, (the response of SST to thermocline anomalies) will depend on the mean thermocline depth. Figure 7.4a shows that there is no such relation in the ATM-ensemble in either the east or the west. However, there is a relation between mean SST (T_{east}) and α on both sides of the basin (Figure 7.4b). Taking into account the fact that there is no high correlation between mean thermocline depth and T_{east}, this relation must be explained by involving the vertical temperature gradient. In case the mean SST is higher and the thermocline is equally deep the vertical temperature gradient is larger. This results in a stronger influence of thermocline anomalies on SST. In the OCN-ensemble we find a correlation of -0.76 between α and the mean thermocline depth in the East Pacific. The difference in this correlation between the ATM- and OCN-ensembles can be explained by the fact that α depends on both the vertical gradient and the thermocline depth. The standard deviation in mean SST is 0.25 ° C across the ATM-ensemble members and 0.16 ° C across the OCN-ensemble members. The standard deviation in mean thermocline depth is 2.9m in the ATM-ensemble and 7.4m in the OCN-ensemble. Perturbing ocean-model parameters apparently leads to more differences in mean thermocline depth than perturbing atmosphere-model parameters. We find the highest correlations between α and mean SST in the ATM-ensemble and between α and mean thermocline depth in the OCN-ensemble.
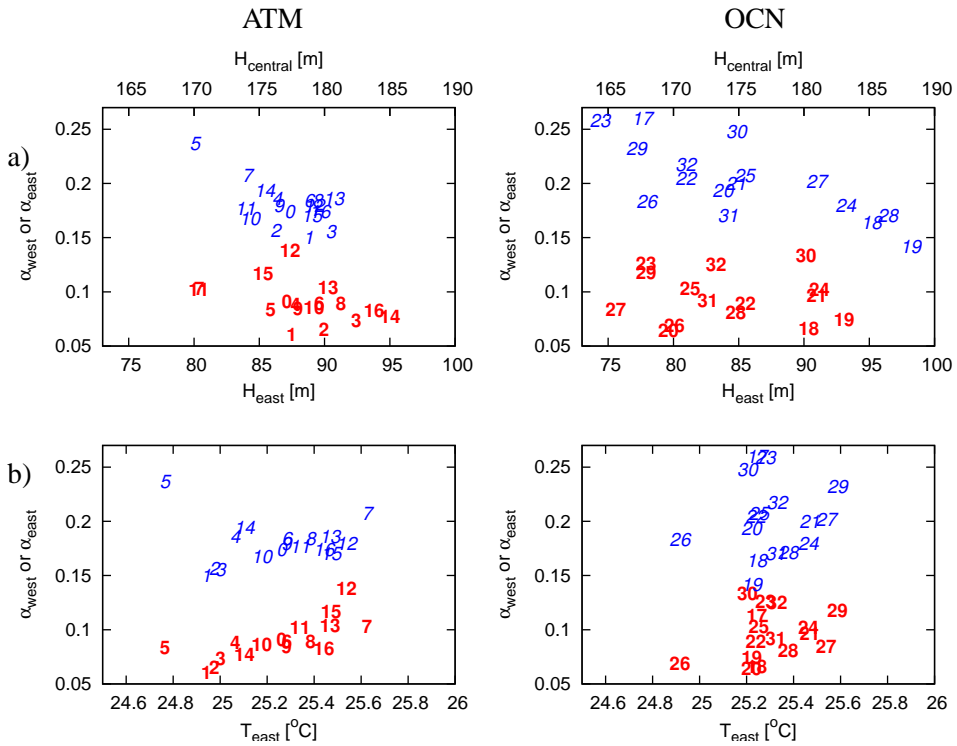
Fig. 7.4: Fitted SST-equation parameters as in Eq. 2.1 and Figure 7.1 for all members, indicated by the numbers. Red are the values for the West Pacific, blue for the East Pacific. The left column shows the ATM ensemble, the right column shows the OCN ensemble. a) Response of SST to thermocline anomalies, α [$0.1\mathrm{Km}^{-1}\mathrm{month}^{-1}$] versus mean thermocline depth. The labels for H_{central} are plotted on top of the figures. b) α versus mean East Pacific temperature.

ATM

OCN

Fig. 7.4: continued: c) wind stress anomalies, β $[100\mathrm{KPa}^{-1}\mathrm{month}^{-1}]$ versus mean mixed layer depth. d) damping time on SST, γ $[\mathrm{month}^{-1}]$ versus mean East Pacific temperature.

From Figure 7.4c we find a correlation of -0.72 between the response of SST to wind stress anomalies (β) and the mixed layer depth (MLD) in the OCN-ensemble. This is similar to what w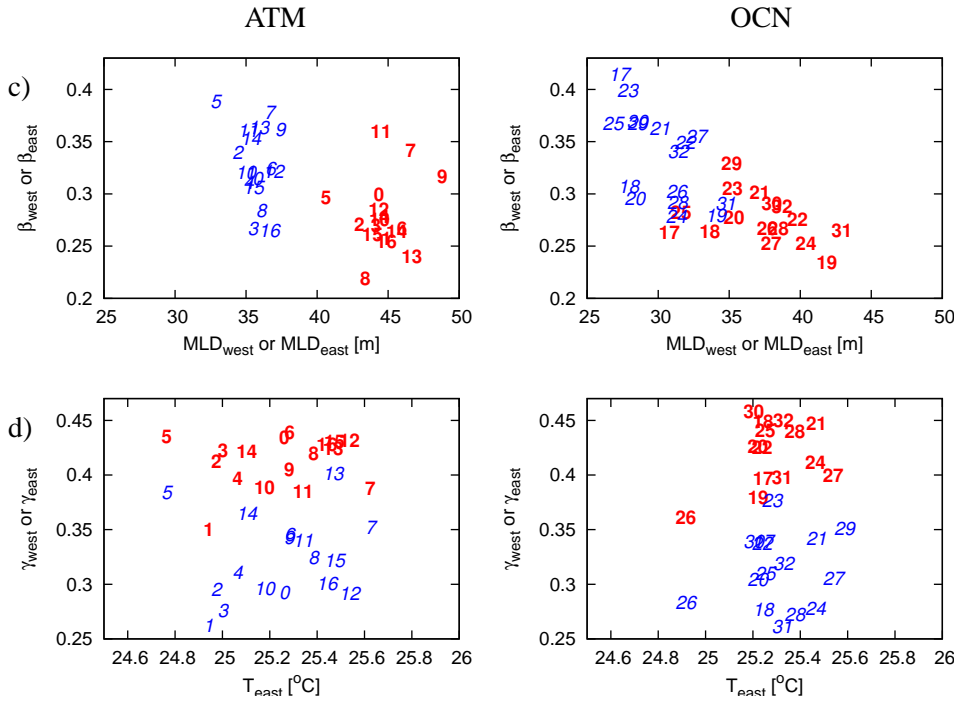as found in the climate change scenario experiments (Philip and van Oldenborgh, 2006) where a shallower mixed layer depth results in a stronger response of SST to wind stress anomalies. A thinner mixed layer reacts more strongly to a wind anomaly than a thicker mixed layer. In the ATM-ensemble we see no significant correlation between the response of SST to wind stress anomalies and the mixed layer depth (recall that each member of the ATM ensemble uses the same ocean parameters). However, in the ATM-ensemble other parameters that influence β, e.g. processes which affect surface heat fluxes, are perturbed.

Finally, for higher mean SST we expected that clouds extend more to the east, resulting in stronger damping on SST. However, we do not find a relation between damping on SST and T_{east} (see Figure 7.4d), indicating that other terms influence the damping term. It should be noted that for the HadCM3 model, clouds and latent heat flux are equally important for the damping term (Philip and van Oldenborgh, 2006).

Summarizing, we find some correlations between coupling parameters and the mean climate. This only applies when parameter perturbations affect only one of the main terms contributing to that coupling parameter.

7.5.2   Description of the statistical atmosphere model parameters

From Eq. 2.2, the wind stress response to SST anomalies in three boxes along the equator is fitted for all the ensemble members. Again, the agreement between the spatial patterns is much higher than in the CMIP3 ensemble shown in van Oldenborgh et al (2005) but the strength and meridional width do vary.

Differences between the models are described on the basis of four diagnostics. The first three are the amplitudes of the wind stress responses west of the three boxes to SST anomalies within the three boxes. The last one is the meridional width of the wind stress response west of the central box to an SST anomaly within this central box. The amplitudes of the wind stress responses are defined as averages over (5° S–10° N, 130° E–170° E), (5° S–5° N, 160° E–150° W) and (5° S–3° N, 150° W–100° W) for the three boxes respectively. These values are listed in Table 7.2. The meridional width of the wind stress response to an SST anomaly in the central box is defined by the meridional locations at which the domain-wide, zonally averaged wind stress response is zero (or, in some cases, reaches a minimum).

We might expect a warmer background temperature to provide higher evaporation and consequently a stronger wind stress response to SST anomalies (A_i in Eq. 2.2). The results of the ATM and OCN perturbed parameter ensemble show that there is no significant relation between background SST and wind stress response to SST anomalies at all, see Figure 7.5a. Nevertheless, by perturbing parameters in the atmosphere-component of the model it is possible to induce different levels of wind-stress response; a wider spread is evident in ATM when compared to the standard-atmosphere OCN ensemble. The perturbed parameters influence convective processes, for example, which may affect the sensitivity of evaporation to SST anomalies.

Kirtman (1997), Zelle et al (2005) and Capotondi et al (2006) showed that the period
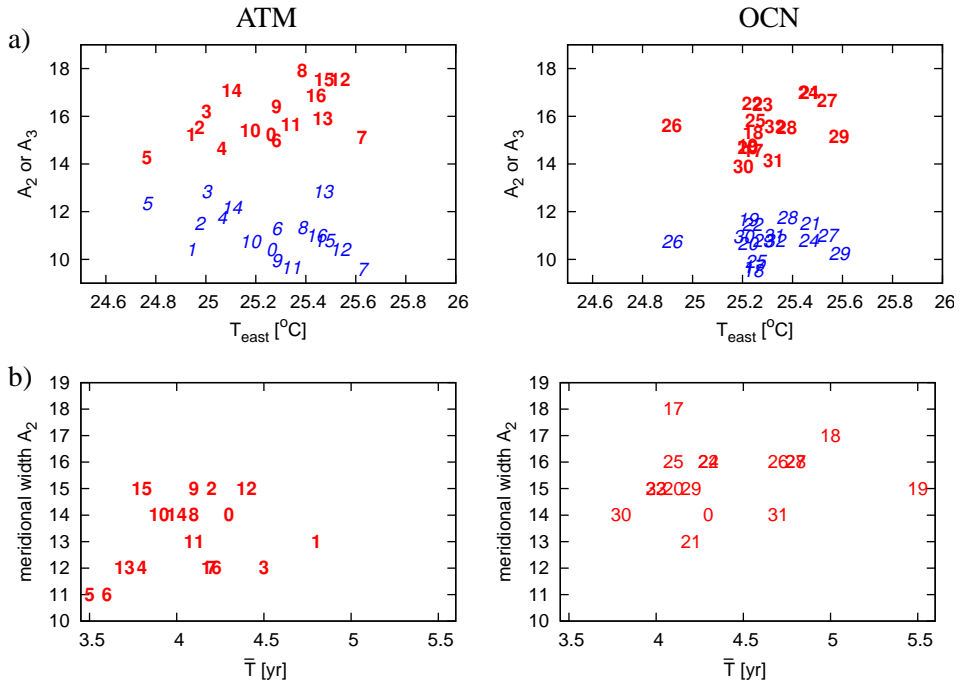
Fig. 7.5: a) Statistical atmosphere box 2 and 3 in $[10^{-3}\mathrm{Nm}^{-2}\mathrm{K}^{-1}]$ vs SST for all members. Box 1 is not shown as this box shows no correlation with T_{east} at all. Red are the western mean values (box2), blue the eastern ones (box3). The left column shows the ATM ensemble, the right column shows the OCN ensemble. b) Meridional width of the response of wind stress to SST [degrees] in the central Pacific versus the mean period [years].

of ENSO depends on the meridional width of the wind stress response to SST. Figure 7.5b shows that there indeed exists a weak relation within the perturbed parameter ensemble (correlation 0.45).

7.5.3 Description of the atmospheric noise properties

The wind stress noise, as defined in Section 7.3.4, has an amplitude and a spatial- and temporal-autocorrelation structure. The noise standard deviation pattern is similar for all the members of the ATM and OCN ensembles, with higher amplitudes in the East Pacific relative to the West Pacific (see Figure 7.3 for the STAM member). Variations are described below on the basis of average values over the regions $5°$ S–$5°$ N, $140°$ E–$190°$ E and $5°$ S–$5°$ N, $190°$ W–$85°$ E.

The standard deviation of the noise is the noise-characteristic that varies most between the ensemble members. The spatial- and temporal-autocorrelation coefficients appeared to be relatively similar in each case. For the implementation of the noise field in the ICM (see later) it is thus possible to use one single set of autocorrelation coefficients to describe all ensemble members (see Philip and van Oldenborgh, 2009b). We therefore focus on the analysis of the standard deviation of the noise. These values are listed in Table 7.2.

It can be seen from Table 7.2 and Figure 7.6 that members 7 and 11 (ATM-ensemble) have very low noise levels. In both the West and East modest negative correlations, of -0.48 and -0.68, are found between mean SST and noise amplitude in the ATM-ensemble respectively. In contrast, these correlations are positive in the OCN-ensemble, with values of 0.55 and 0.45 respectively, although the spread in the noise is much smaller in OCN than in ATM. Perturbing atmosphere-model parameters results in a much wider variation of noise amplitudes, as might be expected, although the change of the sign of the correlation between noise amplitude and mean SST was not expected.

We expect that for higher noise levels the ENSO amplitude, $\langle \sigma \rangle$, becomes larger. Figure 7.6 confirms this positive correlation between noise and ENSO amplitude. For the ATM-ensemble in the East Pacific the correlation is 0.78. For the OCN-ensemble there is no strong correlation, as the variation in noise is relatively low.

7.5.4   Description of the gravest baroclinic mode

A gravest mode equatorial Kelvin wave speed of 2.4 m/s results in the best agreement between the ocean dynamics in the reference ICM and corresponding GCM STAM member (Section 7.3.5). For the other ensemble members most fitted values are somewhat lower (Table 7.2). A minimum value of 2.1 m/s is fitted for members 7, 11, 13 and 15. As we see below, this ICM parameter has little influence on the behaviour of ENSO amplitude and pattern and can be held constant when using the ICM to reproduce the variability in SST amplitude and pattern of the GCM experiments.

7.5.5   Summary of fitted ICM model parameters

Parameter perturbations lead to variations in SST, wind and thermocline couplings, noise amplitude and damping on SST. In general, the variations in fitted ocean-parameters are larger in the OCN-ensemble and the variations in fitted atmosphere-parameters are larger in the ATM-ensemble. This is what we expect from the design of the perturbed parameter ensemble. In some cases these variations enhance each other in the influence on ENSO characteristics. E.g., a stronger noise amplitude and weaker damping tend to result in higher SST variability. In some specific members, both atmospheric noise and wind stress response to SST anomalies are weaker while SST responses to thermocline anomalies and wind stress anomalies are stronger and damping is weaker. This means that in these members the influence of the atmosphere is much smaller. Finally, we do not find simple correlations between the fitted components in the feedback loop and some of the main ENSO characteristics listed in Table 7.1. However, this might be the effect of compensating ENSO feedbacks, which masks the ultimate effect on the ENSO characteristics.
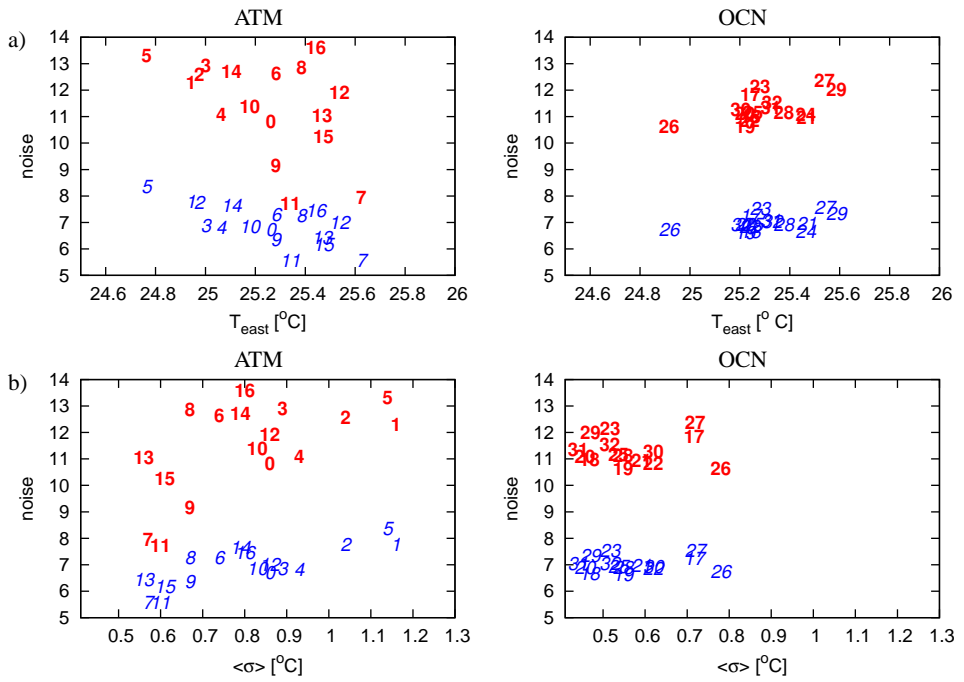
Fig. 7.6: a) Atmospheric noise amplitude in $[10^{-3}\mathrm{Nm}^{-2}]$ vs SST T_{east} and b) vs SST standard deviation (ENSO amplitude) for all members. Red are the western mean values, blue the eastern ones.

Tab. 7.2: Feedback parameters in % of change in the ATM-ensemble relative to the STAM member. The reference mean values of the parameters of the STAM member are also listed, with the values for the Kelvin wave speed c_{oc} in [m/s], α in [0.1Km^{-1}month^{-1}], β in [100KPa^{-1}month^{-1}], γ in [month^{-1}], the statistical atmosphere in [10^{-3}Nm^{-2}K^{-1}] and the atmospheric noise in [10^{-3}Nm^{-2}].

ATM	c_{oc}	α_{west}	α_{east}	β_{west}	β_{east}	γ_{west}	γ_{east}	A_1	A_2	A_3	ϵ_{west}	ϵ_{east}
0	2.4	0.0911	0.174	0.299	0.315	0.434	0.293	13.2	15.2	10.4	10.8	6.72
1	−4.2	−32	−13	−14	4.2	−18	−9.8	−17	9.9	2.5	14	16
2	−4.2	−28	−9.0	−7.8	9.1	−4.7	1.5	4.9	6.8	12	17	14
3	−4.2	−19	−10	−11	−15	−2.9	−5.4	103	9.2	25	20	1.9
4	−4.2	−4.1	6.3	−3.2	−0.27	−8.3	6.1	17	−5.1	15	2.7	0.18
5	−4.2	−9.7	37	0.89	24	0.83	31	−7.8	−4.1	25	23	22
6	−4.2	−4.4	5.1	−12	3.6	1.6	18	101	−5.4	11	17	7.6
7	−13	12	21	23	23	−9.2	21	22	−5.4	−7.7	−27	−18
8	−13	−4.5	5.3	−27	−8.4	−3.1	11	60	20	10	20	9.6
9	−8.3	−7.4	3.3	8.3	18	−4.3	17	−17	2.3	−8.0	−16	−6.7
10	−4.2	−6.2	−2.8	−9.1	2.8	−9.8	1.1	−6.2	−1.8	6.8	4.9	0.72
11	−13	11	4.2	30	18	−9.2	17	0.11	5.4	−10	−29	−18
12	4.2	49	4.3	−5.3	34	−0.033	−0.022	−1.7	11	1.1	11	3.6
13	−13	12	8.5	−20	19	−0.67	39	58	7.2	26	2.3	−4.5
14	−4.2	−16	12	12	12	−0.78	25	39	15	20	18	12
15	−13	28	−1.6	−13	−1.2	0.39	11	23	22	3.2	−4.7	−8.3
16	−4.2	−11	0.31	−16	−15	−1.1	2.7	98	4.3	10	27	10

7.6   Influence of feedback strengths on ENSO properties

To investigate the effect of the variations of parameters across the ensembles on ENSO features and feedbacks, we run the ICM versions. Since the patterns of the components that are fitted in Section 7.5 are relatively similar, we can substitute the coupling strengths from one model version with those from another. This results in ICM versions that are fitted to a combination of, for example, the STAM member and one other perturbed physics member. This allows the isolation of specific features emerging from the simulations. We first investigate the most important ENSO characteristics of the ICM runs and compare them to the original GCM runs. Furthermore, we separate the contribution of each of the components to the ENSO properties into four categories. The first group includes the parameters of the SST-equation (Eq.2.1), which include the responses of SST to wind and thermocline depth variability and damping. The second group describes the statistical atmosphere, with three boxes along the equator. Thirdly, we study the influence of the atmospheric noise. Finally, the influence of the Kelvin wave speed is investigated. For clearness and readability we will mainly show results of the ATM-ensemble. However, we use both the ATM- and OCN-ensembles to draw conclusions.

7.6.1   Verification of the ICM runs

First, the ICM runs in which the whole feedback loop is fitted to one single ensemble member are investigated. For convenience we call this type of ICM experiment a 'full-run'. Most ICM versions corresponding to ATM-ensemble members run well, except for the members 7, 9 and 11, in which the integration is numerically unstable. These are the models with very low SST standard deviation, a low noise amplitude and SST variability that is located too far in the West Pacific. It is possible to achieve numerical stability in these runs by adding an extra coupling term $\mu = 0.82$ (members 7, 11) or $\mu = 0.95$ (member 9) between the ocean and atmosphere, such that in Eq. 2.2 $A_i(x,y)$ is replaced by $A'_i(x,y) = \mu A_i(x,y)$. This allows us to show some qualitative results. However, as the coupling parameter changes the ICM runs and there is very little ENSO variability in both the HadCM3 and ICM runs we will not use these runs for a quantitative comparison. In the OCN-ensemble, the full-runs of members 17 and 26 need an extra coupling parameter of $\mu = 0.90$ and $\mu = 0.95$ respectively for the same reason.

Figure 7.7 shows the SST standard deviation patterns of the ICM full-runs and the original GCM ensemble members. We note that, as found in previous studies, the ICM does not simulate off-equatorial SST variability well as it is only a conceptual model of ENSO.

Close to the equator, the SST variability simulated with the ICM is slightly lower than the original GCM SST variability. Although not all SST standard deviation patterns of the ICM runs resemble the patterns calculated from GCM output, there are some remarkable similarities. For instance, in members STAM, 10, 12 and 16 the maximum is located in the central to West Pacific, in member 5 the maximum is further to the East Pacific, and in member 6 there are two clear maxima in both the east and the west.

In order to quantify the resemblance we consider the maximum of SST standard deviation and the corresponding location (Figure 7.8). With the exception of members 7, 9 and

11 (noted above), there is a clear relation between the locations of the maximum SST standard deviation of the ATM-full-runs. For the ATM- and OCN-full-runs together this becomes 0.88. Except for members 13, which has an unrealistic low SST variability, and 14, which is a clear outlier, the correlation between the maximum SST variability of the GCM runs and ICM runs is also reasonably good, although the ICM ensemble displays systematically lower values than the GCMs and the data are not distributed along a 1:1 line. For member 13 the problem is similar to that of members 7, 9 and 11: the ICM is not able to capture the unrealistically low ENSO variability. The exceptionally high ENSO amplitude for the ICM run of member 14 is due to the statistical atmosphere (see next section).

We note here that there is no correlation between GCM ENSO period and the corresponding fitted ICM ENSO period in these experiments (figure not shown). This reveals a weakness in the ICM approach which needs to be addressed in future research. The ICM ENSO period is principally determined by the phase speed of the gravest baroclinic Kelvin wave, which, as we note above, has little spread when computed from the GCM experiments. Another factor influencing the period is the meridional width of the wind stress response to SST variability. Nevertheless, there is a modest spread in ENSO period from the GCM ensemble experiments. The ENSO period has also been hard to reproduce in many other studies. We omit discussion of the period of ENSO in what follows.

Overall, the ICM runs capture the amplitude and spatial ENSO characteristics reasonably well. This is sufficient to use them as a basis to better understand the influence of the parameter perturbations on ENSO by investigating the relative contribution of the different couplings on ENSO characteristics.

7.6.2   Contribution of feedback strengths to ENSO

Having established that ENSO properties are only weakly correlated with the mean state in this ensemble, we proceed to investigate the direct effects on ENSO of the various couplings defined in Figure 1.8. Note again that in the CMIP3 ensemble, these two effects were inextricably intertwined. Due to the flux-corrected mean state of the perturbed physics ensemble we have a reasonably clean isolation of the direct effects. For instance, we can investigate the influence of the set of SST-equation parameters of the ATM-ensemble on ENSO by running the ICM with parameters fitted to the STAM member and then varying the parameters in one of the components in the feedback loop. In Figure 7.9 we show SST standard deviation patterns σ of a selection of six ensemble members that illustrates this investigation. For each member the upper three panels show the σ of the ICM runs in which either the set of SST-equation parameters or the statistical atmosphere parameters or the atmospheric noise are changed. (For member 11 the extra coupling of μ is used in all runs.) With this method we disentangle the influence of the different components of the feedback loop on ENSO amplitude and pattern. The fourth panel shows again the σ of the ICM full-run in which all components are fitted to one GCM ensemble member. The three intermediate panels are compared to the reference ICM and the full-run ICM.

Runs in which only the Kelvin wave speed is changed are not shown, as the change in σ is mainly seen in the amplitude and period and not in the pattern, and the differences between the ICM versions are not large. Using a Kelvin wave speed of 2.3 m/s instead of
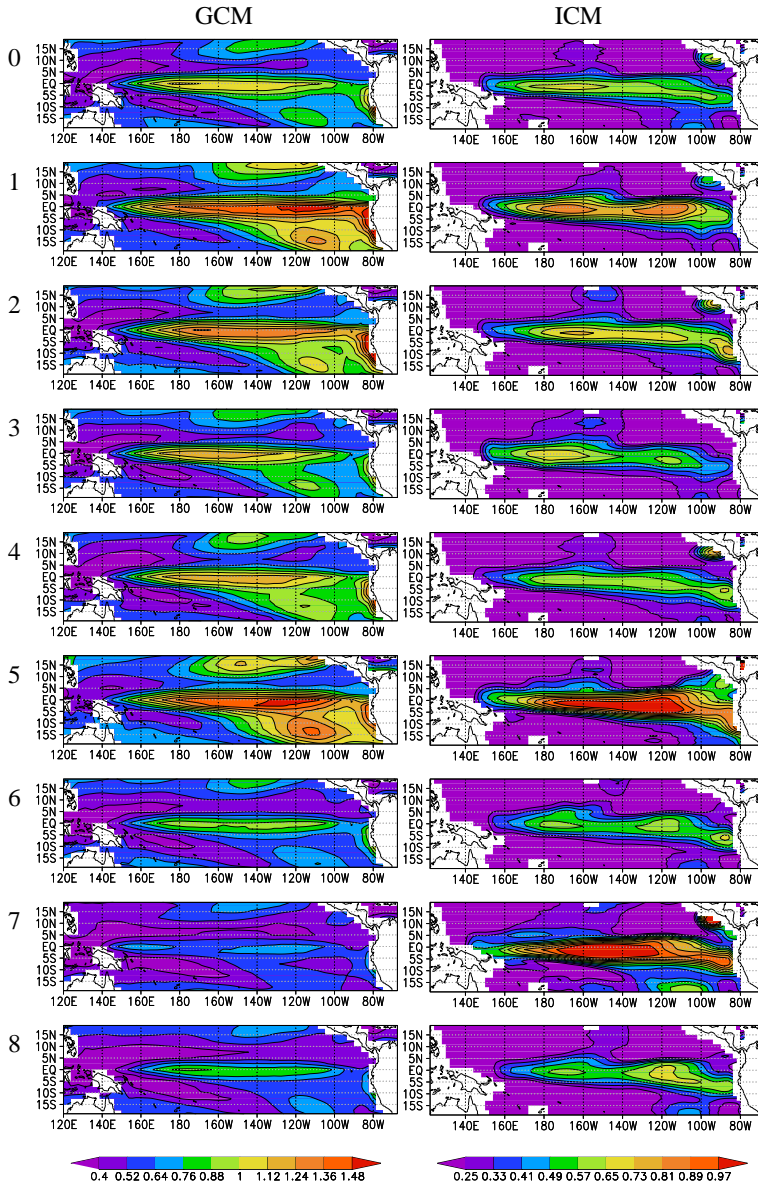
Fig. 7.7: Pattern of SST standard deviation for GCM ensemble members (left) and corresponding full ICM runs (right): STAM-member and ATM-members 1-9. Note the factor of 2/3 difference in scale.
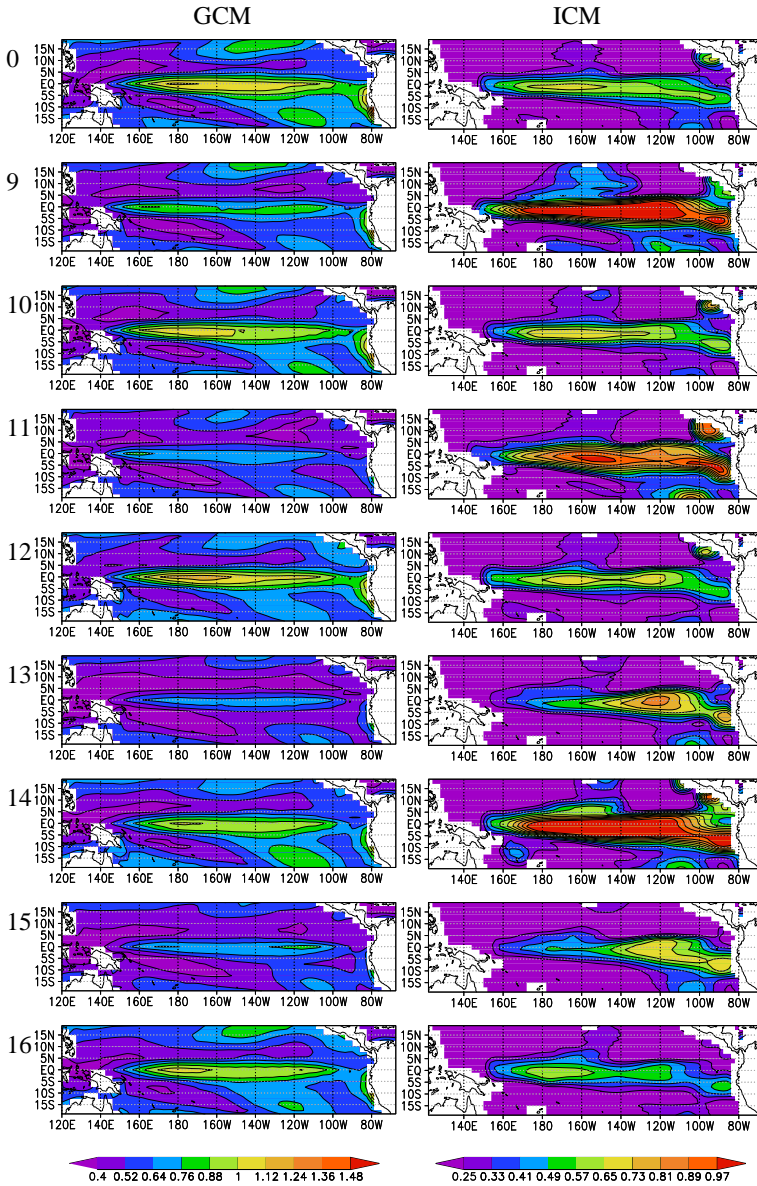
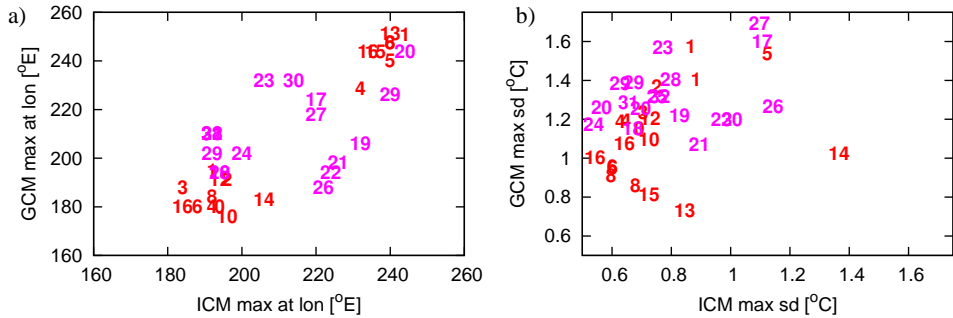Fig. 7.7: continued: STAM-member and ATM-members 9-16.

Fig. 7.8: a) Location of maximum SST standard deviation in degrees E. If two locations exist in both GCM and ICM run, both are plotted. b) Amplitude at the location of maximum SST standard deviation of GCM ensemble members vs corresponding ICM runs. In red the ATM-full-runs and in pink the OCN-full-runs.

the standard value of 2.4 m/s results in an amplitude that is only 0.03 K higher than the reference amplitude of 0.50 K.

Figure 7.9 shows that the different SST variability results from a combination of changes. In most cases the different components of the feedback loop add almost linearly. The SST variability, $\langle \sigma \rangle$, of GCM ensemble member 2 is larger than in the STAM member, while the pattern is relatively similar. In the ICM this is reproduced correctly. A lower $\langle \sigma \rangle$ would be expected based on the values of the statistical-atmosphere parameters, but this is counteracted by the higher $\langle \sigma \rangle$ resulting from higher atmospheric noise.

In member 5 the GCM SST variability is located further to the east than in the standard member (which is more like in reality). From the ICM runs we learn that this is caused mainly by the SST-equation parameters. The two distinct maxima seen in SST variability in member 6 are mainly caused by the values of the statistical-atmosphere parameters.

Considering the pattern of variability in GCM member 11, we see that the responses described by the SST-equation are responsible for the SST variability being located much too far in the West Pacific in the GCM (see also Figure 7.7). In this ensemble member the damping of SST anomalies γ is extraordinarily low. Further investigation shows that this is mainly due to a very low latent heat flux sensitivity to SST variations.
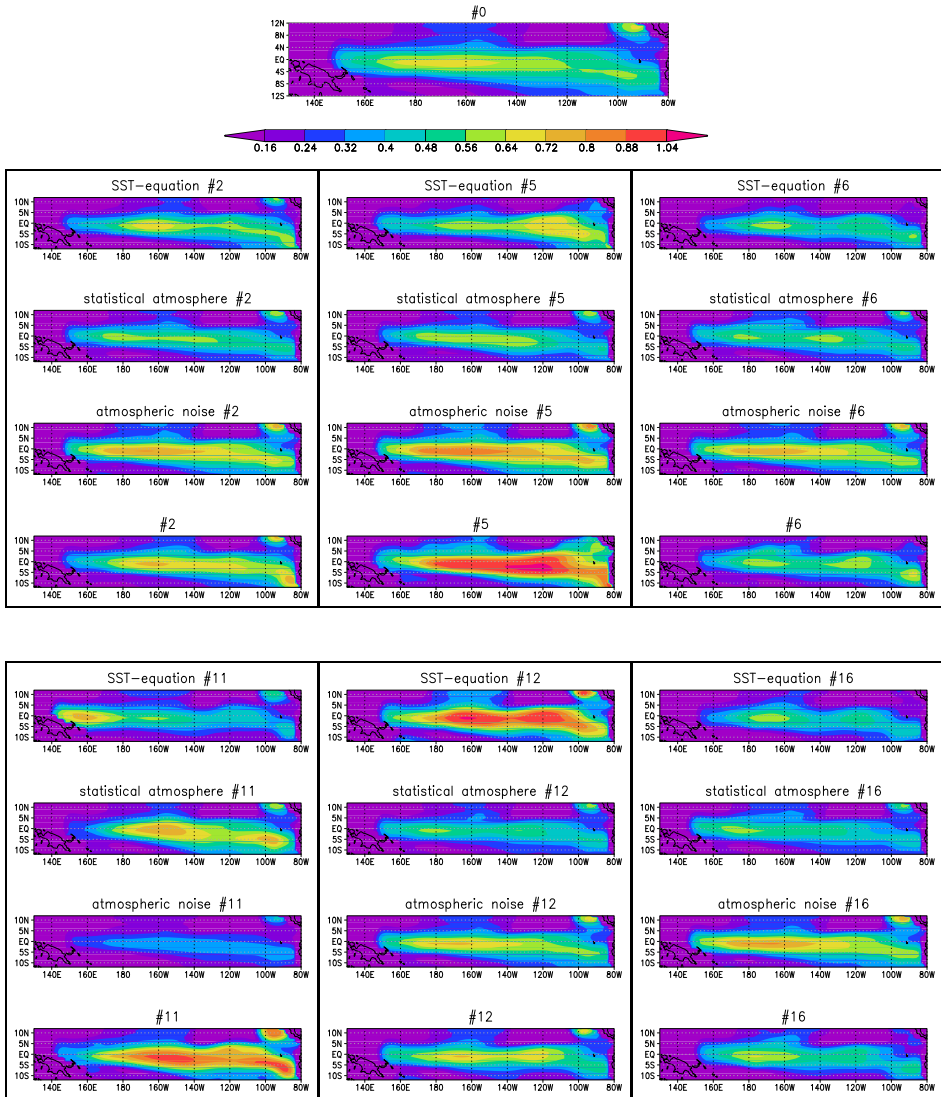
Fig. 7.9: Caption on next page.

Fig. 7.9: SST standard deviation σ [K] for a selection of ICM fits to the GCM ensemble members but isolating the influence of different components of the ICM. Top: σ for the STAM member 0 and colorbar. In each of the panels for members 2, 5, 6, 11, 12 and 16, from top to bottom we show σ in a ICM run with only the SST-equation parameters from the perturbed member, but with the other ICM parameters held fixed at the standard values; σ in a ICM run with statistical-atmosphere parameters from that member and all other ICM parameters held fixed at the standard values; σ in a ICM run with atmospheric noise parameters from that member and all other ICM parameters held fixed at the standard values and σ from the full-runs (reproducing the fields in figure 9). Note that 11 uses an extra coupling $\mu = 0.82$. The influence of the Kelvin wave speed is not shown as it only results in a change in amplitude. See also text.

The SST variability in member 12 suggests that this member is almost similar to the STAM member. However, this is a combination of much higher SST variability from the responses described by the SST-equation, compensated by much lower SST variability caused by a weaker atmospheric response to SST anomalies. Finally, the lower SST variability in member 16 is the result of both changes in the ocean and the atmosphere, which is not entirely repaired by the higher noise level. It seems that there is some compensation between the different feedback loops such that the range of possible ENSO behaviour is reduced.

The behaviour of members 7, 9 and 11 is rather exceptional. Compared to the STAM member, these members have both weaker noise and weaker or similar wind stress response to SST anomalies. Moreover, the ocean parameters α and β are larger and the damping is weaker in the West Pacific and stronger in the East Pacific. This results in much lower SST variability, with maximum SST variability far in the West Pacific. This SST variability is no longer directly related to El Niño. As our conceptual model is based on ENSO dynamics, we suspect that our approach is not valid for these three members.

The ICM full-runs of the GCM OCN-ensemble member 17 and 26 are numerically unstable. For member 17, we can attribute this to the SST-equation parameters. Combining SST-equation parameters of the STAM member with all other parameters of member 17 results in a stable ICM-version. We could potentially add a nonlinear damping term that counterbalances the high responses of SST to thermocline and wind stress variability in the East Pacific in this member. In member 26, T_{east} is very low compared to the rest of the OCN-ensemble. We do not think that this is caused by the numerical instability of the ICM. Replacing an arbitrary part of the feedback loop of the full-run with member 26 by the parameters of the STAM-member results in a stable ICM.

Overall, we conclude that the SST-equation parameters and atmosphere response to SST anomalies affect both the ENSO amplitude and the pattern of variability. The noise amplitude (without significantly modifying the noise pattern) has a small influence on the ENSO amplitude and period.

We can quantify the influence of the different components in the feedback cycle on ENSO by studying different groups; in each group of ICM-runs only one set of coupling parameters is varied. Table 7.3 shows the influence of each group of coupling strengths in the ENSO feedback loop; the SST-equation parameters, the statistical atmosphere parameters, the atmospheric noise ampitude and the Kelvin wave speed. Besides the total influence of the whole SST equation, we also quantify the influence of the thermcline coupling α, the direct wind coupling β and the damping γ in Eq. 2.1 separately. We ignore nonlinear interactions between the components of the feedback loop, but in Figure 7.9 we show that this is a reasonable estimate.

To determine the influence of the set of SST-equations on ENSO, we substitute the set of SST-equation parameters with the sets of parameters derived from the 16 ATM-ensemble members. We calculate the average amplitude of the SST variability, $\langle \sigma \rangle$ of these 16 ICM runs and subtract $\langle \sigma \rangle_{STAM}$, which gives us 16 numbers giving a distribution around the $\langle \sigma \rangle$ of the STAM-ICM. The width (standard deviation) of this distribution is a measure of the variation in ENSO amplitude accomplished by changing only one component in the feedback loop. This measure is given as a percentage of the width of the equivalent distribution of $\langle \sigma \rangle$ that is obtained when the full perturbations are used in the ICM ensemble. We

perform a similar analysis in the OCN-ensemble. In principle the results depend strongly on the (subjective) choice of perturbed parameters in the ensemble. In practice, however, the results for the ATM and OCN ensembles are very well comparable, which implies that the results are quite general. Results are summarised in table 7.3. The influence of the components on the SST variability pattern is given qualitatively.

In the perturbed physics ensembles studied here, the changes in Kelvin wave speed do not influence ENSO amplitude and pattern very much. Surprisingly, neither does the variation in noise amplitude, in spite of the good correlations found in the CMIP3 ensemble between noise amplitude and ENSO amplitude (Philip and van Oldenborgh, 2009a). The spread of properties of the atmospheric response and SST equation explain most of the spread of the ensembles.

The influence of the three SST-equation parameters separately is larger than the combined variation, which means that variations in SST-equation parameters counteract each other. The largest variability in ENSO amplitude $\langle\sigma\rangle$ is obtained by the variations in the damping γ. In the OCN ensemble this is equal to the influence of variations in the direct wind coupling β. In both ensembles the variability in the response of SST to thermocline anomalies (α) has a smaller influence.

Comparing the influence of parameter perturbations on ENSO amplitude between the ATM and OCN ensemble we conclude that the influence of the variability in SST response to thermocline variations α is largest in the OCN ensemble. This is what we expect from perturbing ocean parameters. Secondly, the zonal wind feedback β depends strongly on the ocean mixed layer depth, resulting in a larger influence this parameter β on ENSO in the OCN ensemble. Thirdly, atmospheric parameter perturbations lead to a larger influence of variations in the statistical atmosphere on SST in the ATM ensemble than in the OCN ensemble.

To investigate the processes behind the large variability of the damping term γ we separated out the latent and short-wave (cloud) feedback components. ATM ensembles members with strong SW radiation feedback have reduced SST variability in the West Pacific. The strength of this feedback varies by a more than a factor two in the ATM ensemble and seems an important factor in determining the westward extend of SST variability. As expected, the OCN ensemble has a much smaller spread of feedback strengths. The models with high SST variability in the West Pacific have a stronger contribution from latent heat flux damping.

We conclude that the ocean and atmosphere parameters affect both the ENSO amplitude and the pattern of variability. For the amplitude, the influence of the SST-equation parameters is approximately equivalent to the influence of the parameters that control the statistical atmosphere. However, the influence of damping of SST anomalies γ and the response of SST to wind stress variability on SST β are larger than the combined parameter settings. For the spatial pattern, the influence of the SST-equation parameters is greater. The role of the atmospheric noise amplitude and ocean dynamics on the spread of ENSO amplitude and spatial structure is relatively smaller.

Tab. 7.3: Influence of different components in the feedback loop on ENSO amplitude and pattern in the ICM when varying the parameters in different ICM components based on the values fitted from the GCM experiments. Values are calculated as the spread in the amplitude, expressed as a percentage change from the STAM-member accomplished by varying one of the components in the feedback loop separately. Absolute values for the amplitude $\langle\sigma\rangle$ for the STAM member are given in the top row. For the pattern, we qualitatively assess the influence of the components as ranged from very little influence (0) to largest influence (++). For the SST-equation parameters a the total contribution is listed as well as the influence of the three parameters separately.

	parameter	$\langle\sigma\rangle$	pattern
	reference	**0.50**	
ATM	SST-equation	20	++
	α	*12*	+
	β	*24*	++
	γ	*44*	++
	statistical atmosphere	28	+
	atmospheric noise	10	0
	Kelvin wave speed	8	0
OCN	SST-equation	19	++
	α	*23*	+
	β	*36*	++
	γ	*36*	++
	statistical atmosphere	19	+
	atmospheric noise	4	0
	Kelvin wave speed	4	0

7.7   Conclusions

We have quantified the role of various components in the ENSO feedback loop on the amplitude and pattern of ENSO variability. In most multi-model studies these couplings affect both the mean state and the couplings, making it difficult to separate the influences. Here, we used two flux-corrected perturbed physics ensembles to negate the effects of mean state changes to first order. This allows us to study the effects of the parameter changes on the ENSO cycle directly.

The two ensembles are variants of the HadCM3 climate model with perturbations to either the parameters of the atmosphere model (ATM-ensemble) or perturbations to ocean parameters (OCN-ensemble). Both ocean-atmosphere couplings and atmospheric noise terms are directly impacted by the parameter perturbations, the noise terms more so in the case of the ATM-ensemble. The spread in ENSO characteristics does not show one-to-one relations with the spread in the mean climate variables, as might be expected from imposing

flux adjustments in the ensemble runs, which tend to produce mean climates which are, to leading order, similar in each member. Rather the parameter perturbations affect ENSO coupling strengths directly, independently from the mean climate.

An Intermediate Complexity Model (ICM) in which the main ENSO feedbacks are fitted to one GCM ensemble member or to a combination of ensemble members is employed to illuminate the GCM behaviour. The ICM successfully reproduces the behaviour of 28 out of 33 ensemble members. The influence of four different components of ENSO is studied one by one. These components include SST-equation parameters, covering the response of SST on thermocline anomalies and wind stress anomalies and damping on SST, the response of wind stress on SST anomalies, a gravest baroclinic Kelvin wave speed in the ocean and the amplitude of atmospheric noise. The SST-equation parameters influence the pattern and amplitude of SST variability most, followed by the response of wind stress on SST anomalies. The influence of the SST-equation parameters separately is larger than the influence of the combination of parameters, which means that they counteract each other. The influence of the amplitude of atmospheric noise and the Kelvin wave speed on the ENSO pattern is much smaller. However, both factors do contribute to the ENSO amplitude. We observe that coupling strengths between the ocean and atmosphere tend to counteract each other, thereby reducing the potential range of variability in ENSO characteristics that might have been realised without this compensating feedback.

We can speculate on the mechanisms leading to the difference in coupling parameters in the GCM ensemble. Atmospheric parameter perturbation influences the ocean as well. The variations in α, the SST response to thermocline variations, are due to changes in the the shallow ocean stratification that is influenced by atmospheric model parameters. These also affect the SST response to zonal wind stress anomalies, the mean wind stress β through the mean wind stress and the mixed layer depth. Finally, cloud and atmospheric boundary layer parametrisations strongly affect the damping of SST anomalies through latent heat flux and cloud formation, especially in the western Pacific.

The oceanic parameter perturbation influences the atmosphere via the SST, which is affected by changes in ocean surface currents, ocean mixed layer depth and temperature. Via this pathway oceanic parameter settings impact atmospheric coupling parameters in the ENSO feedback cycle, such as the response of wind stress to SST anomalies, atmospheric noise characteristics and cloud feedbacks. Due to the indirect pathway, the variation in this response is smaller in the OCN ensemble than in the ATM ensemble.

We conclude that variations in the mechanisms affecting SST influence ENSO characteristics most. These mechanisms include couplings with the thermocline and wind stress and damping. Variations in these mechanisms can be related to uncertainties in both oceanic and atmospheric model parameters. Perturbing oceanic physics causes the largest spread in oceanic responses. However, as the above mentioned mechanisms play a role on the boundary of the atmosphere and the ocean, the spread in atmospheric responses via the indirect pathway should be taken into account as well.

In this chapter perturbations to atmospheric and oceanic physics cause a spread in ENSO characteristics that can directly be related to the spread in ocean-atmosphere coupling strengths. This is somewhat different from previous work on multi-model studies and climate change scenarios. In multi-model studies both mean climates and ocean-

atmosphere coupling strengths differ (Guilyardi, 2006; van Oldenborgh et al, 2005; Merryfield, 2006), which makes it difficult to discuss the effect of physical parameters separately. In climate change scenario studies model parameters other than those related to climate change are not varied (Philip and van Oldenborgh, 2006). Nevertheless, Collins (2009) does show that climate change induced changes in mean climate in the HadCM3 perturbed parameter ensemble do result in increases in the amplitude and frequency of ENSO.

The main conclusion is that independent of the mean state, the largest uncertainties in the modelled amplitude and pattern of ENSO are in the sensitivity of SST to local wind in the central Pacific and damping of SST anomalies. The wind stress response to SST anomalies also plays a major role. The influence of the sensitivity of SST to thermocline depth in the eastern Pacific on ENSO is slightly smaller. Variations in modelled weather noise properties and Kelvin wave speed do not contribute much to the model uncertainty of ENSO properties.

8. DISCUSSION

Increasing our understanding of ENSO is important for making progress in climate prediction and assessing the effects of global change on ENSO. The negative impacts of ENSO on regional and global scales have been reduced through better planning based on seasonal forecasts. However, better models are still needed for ENSO forecasts and for projections of ENSO into a future climate. The aim of this thesis is to improve our understanding of El Niño and of the differences between the models that are used to describe characteristics of El Niño.

Our understanding of the physical processes responsible for the ENSO cycle is mainly based on observations. Nowadays, real-time measurements of, among others, surface winds, sea surface temperature and subsurface temperature are taken and stored in a central database (McPhaden et al, 1998). The Tropical Atmosphere-Ocean (TAO) array of moored buoys in the Pacific, a surface drifting buoy program, an island and coastal tide gauge network, an observing ship network and satellite missions contribute to this database.

Observations form the basis of most models. Observational data are used by many model studies, ranging from case studies (e.g., McPhaden, 2004; Boulanger et al, 2001; Lengaigne et al, 2003; Vecchi et al, 2006) to multi-model studies (e.g., Guilyardi, 2006; Capotondi et al, 2006).

Observations can be used to explore ENSO characteristics. Before we can use models for studying ENSO we first have to explore ENSO characteristics in observations. Besides, we need to investigate mechanisms acting on ENSO both in observations and simplified models, as simple models allow easier interpretation of the complex system. Only then we are able to discuss ENSO and its characteristics in more advanced climate models.

Different types of ENSO 'modes', coupling strengths and ENSO mechanisms have been investigated in observations and models. The first type of normal modes (stationary oscillation solutions) of simplified models of ENSO were presented from studies by Philander et al (1984) and Hirst (1986). In a model with SST proportional to thermocline depth and a so-called Gill atmospheric model they found eastward propagating SST anomalies. A mechanism for westward propagating SST anomalies (involving zonal advection of an east-west SST gradient) was noted by Gill (1985). Hirst (1986, 1988) obtained both eastward and westward propagating modes, analysing an idealised SST equation in a modified linear shallow water model. More recently, Fedorov and Philander (2001) defined a local mode with zonal advection and a remote mode with vertical thermocline movements, and they related the response of these modes on changes in the mean climatic state of the Pacific ocean. The direction of phase propagation was quantified by Trenberth and

Stepaniak (2001). They described the Trans Nino Index (TNI): the lag of the zonal SST gradient between Niño12 in the East Pacific and Niño4 in the West Pacific with the Niño3 index. Guilyardi (2006) used this TNI to verify which models are in a thermocline-mode with eastward propagating SST anomalies, in an SST-mode with westward propagating SST anomalies, or in a hybrid mode including both propagation directions.

We would like to use models to forecast ENSO and make projections into a future climate. However, there are still missing pieces in our understanding of the various ENSO mechanisms. Moreover there are systematic differences between observations and models that need to be quantified, and mutual differences between models that need to be understood. We ask several questions involving these differences:

- Which ocean-atmosphere coupling mechanisms governing ENSO can be traced in observations and models?

- Considering El Niño, can we select a subset of models that perform better than others?

- Do models agree about El Niño in a future climate?

- What possible mechanisms cause the asymmetry between El Niño and La Niña?

- Are models good enough to represent the asymmetry between El Niño and La Niña?

- Which mechanisms that are not primarily linked to the mean climate contribute most to ENSO?

The answers to these research questions are summarized in Section 8.1. Section 8.2 discusses the new aspects of this thesis. Finally, Section 8.3 gives some recommendations for future research.

8.1 Summary of key findings

- Which ocean-atmosphere coupling mechanisms governing ENSO can be traced in observations and models?

In Chapter 3 the mechanisms governing El Niño have been traced in observations and in a set of 19 coupled global climate models (GCMs). We used a conceptual model that describes the relations between subsystems that play a role in ENSO using local linear regressions. These mechanisms include a wind response to SST variability, the responses of SST to thermocline and wind stress variability and damping on SST.

- Considering El Niño, can we select a subset of models that perform better than others?

Furthermore, in Chapter 3 we also selected a subset of models that perform better than other ones. Six GCMs have been categorised as having the most realistic balance of feedback mechanisms compared to observations. In four of these models the interannual mode also resembles the observed ENSO both spatially and temporally. In the other 13 models at least one part in the feedback loop between the ocean and atmosphere behaves different from the observations. We selected a subset of best models based on the mechanisms that are important to describe El Niño.

- Do models agree about El Niño in a future climate?

Many studies have addressed ENSO in a changing climate. Different climate scenarios have been used, and both transient changing climate scenarios and stabilised climate scenarios have been investigated. These studies include investigations of single models (e.g., Timmermann, 2001; Wittenberg, 2002; Zelle et al, 2005; Toniazzo, 2006a) and of multi-model ensembles (e.g., Collins, 2004; Merryfield, 2006; Guilyardi, 2006). These studies indicate that models do not agree on the impact of climate change on ENSO. Sometimes the sign of a change is even not consistent between models.

To say something about ENSO in a changing climate, model projections into a future stable, warmer climate for a subset of models as defined above have been analyzed in Chapter 4. Although there are large changes in the mean state, the overall ENSO properties do not change much. This is due to the fact that the effects of the changes in the different ENSO relations tend to cancel. In all models, the signs of the response of particular ENSO mechanisms to a warmer climate are similar. However, the sign of the small net effect differs from model to model. We did not find an underlying physical reason for this cancellation.

- What possible mechanisms cause the asymmetry between El Niño and La Niña?

So far, we explained the differences in models by some linear couplings between the ocean and atmosphere. In general, however, El Niño is larger than La Niña. In other words, the distribution of SST anomalies in the East Pacific is positively skewed. We tested whether models are good enough to consider the nonlinearity between El Niño and La Niña by including nonlinear terms in our analysis and explicitly addressing skewed and state-dependent atmospheric noise properties.

Chapter 5 focuses on the role of atmospheric noise on ENSO properties, using observations. The linear couplings described above are complemented by a new (nonlinear) description of atmospheric noise properties and nonlinearities in the wind response to SST variability. The effect of these nonlinearities are studied with an Intermediate Complexity Model (ICM). ICMs have been used more often in literature to investigate climate phenomena like ENSO (e.g., van der Vaart et al, 2000; Fedorov and Philander, 2001; Toniazzo, 2006b). Often these studies use tuning parameters such that the ICM corresponds best to the original data. However, in this study the fitted couplings and noise properties are implemented directly in this ICM, and no further tuning is carried out.

The conclusion of Chapter 5 is that the description of atmospheric noise properties in terms of standard deviation patterns and realistic spatial and temporal correlations is sufficient for the excitation and simulation of ENSO in this ICM. The ENSO period and pattern of the ICM agree reasonably well with that found in observations. The skewness of SST anomalies has been evaluated after adding three additional terms: a nonlinearity in the response of the wind stress to SST anomalies, the state-dependence of atmospheric noise and the positively skewed nature of atmospheric noise (i.e., the occurrence of WWEs). The SST skewness in observations is most affected by a nonlinearity in the response of the wind stress to SST anomalies. This is followed by the state-dependence of atmospheric noise. The skewed nature of atmospheric noise has only a minor effect on SST skewness.

- Are models good enough to represent the asymmetry between El Niño and La Niña?

The next question that is answered in Chapter 6, is how well the subset of models agrees on these above findings. GCMs tend to simulate lower noise amplitudes than observations. Some GCMs show a nonlinear response of wind stress to SST, although weaker than in observations. These models simulate the most realistic SST skewness. We remark that the influence of state-dependent noise on the ENSO amplitude is smaller in the weekly data than in the monthly data. This can be attributed to the fact that we did not take the longer time scale of 6-8 weeks in the weekly noise data into account. Overall, in GCMs, both a nonlinear atmospheric response to SST and the dependence of noise on the background SST influence the El Niño/La Niña asymmetry.

In the above discussion many differences between models are shown. It is useful to separate model errors into two types. The first type includes errors or biases in the mean climate state; both ocean and atmosphere errors as well as errors which are in some way coupled, including errors in the forced seasonal-cycle, are ubiquitous. The second type of model error is associated with inaccuracies in the physical processes involved in the ENSO cycle. Studies such as that by Schneider von Deimling et al (2006), Niehörster et al (2006) and Toniazzo et al (2008) show that the model behaviour is very diverse if parameters in the ocean or atmosphere are varied.

The first type of model errors, errors or biases in the mean climate state, is discussed in the multi-model studies in the Chapters 3, 4, and 6. The second type of model errors, inaccuracies in the physical processes, is investigated in Chapter 7. The problem is addressed by examining the simulation of ENSO in a set of GCM experiments with perturbations to key atmospheric and oceanic parameters. In such an ensemble variations in the feedback cycle that are caused by GCM parameters are not principally controlled by variations in the mean climate state.

- Which mechanisms that are not primarily linked to the mean climate contribute most to ENSO?

In Chapter 7 we test the uncertainty of ENSO within a GCM using the same method as for the multi-model ensemble described above. Perturbations to atmospheric and oceanic physics cause a spread in ENSO characteristics that cannot directly be related to the spread of the mean climate. The perturbed physics causes a spread in ENSO feedback mechanisms, which in turn influences the basic ENSO characteristics. Feedbacks involved in the ICM response of SST to variations in wind stress and damping of SST anomalies provide the leading-order control on ENSO amplitude and spatial structure. This is followed by feedbacks in ICM response of wind stress to variations in SST anomalies and the variability in response of SST to thermocline depth anomalies. The atmospheric noise amplitude and ocean wave dynamics play only a minor role.

The multi-model studies and perturbed physics experiments studies together suggest that both types of errors contribute to the spread in ENSO mechanisms in climate models. Errors in ENSO will not disappear as soon as the mean climate is realistic; modellers should not forget the influence of the various physical processes. It is highly model dependent which part of the ENSO feedback loop and physical processes should be focused on in order to improve climate models.

8.2   New methods for exploring ENSO

Several new methods have been developed in this thesis. First, couplings between the ocean and atmosphere have been fitted systematically from a set of model data and compared to those fitted from observational data. Second, wind stress noise has been characterised by its standard deviation, skewness, and spatial- and temporal correlations. Third, some nonlinear atmospheric properties have been explored in order to test their influence on SST skewness. Finally, these couplings and noise characteristics have been implemented in an ICM. The global properties in this ICM are not tuned; the individual couplings are fitted to the observations or GCM results. With this ICM we have been able to study the influence of different parts in the ENSO feedback loop and in atmospheric noise properties on ENSO.

The ICM that is built from the fitted parameters is not yet fully evolved. However, the combination of the new methods described above leads to a promising route in exploring ENSO and its mechanisms. With this method the influence of separate parts in the feedback loop on ENSO can be studied. In addition, as models become better, they also become more complicated. With this method it becomes easier to disentangle different types of nonlinearities that influence ENSO in the GCMs. These nonlinearities can then be compared with nonlinearities fitted from observational data.

8.3   Recommendations for future research

The focus of this thesis is on linear couplings, atmospheric noise terms and nonlinearities that arise from the coupling between atmospheric noise and background SST. A second order response of wind stress to SST anomalies is considered as well. As a consequence, the ICM modelled SST skewness as well as other ENSO characteristics differ from the characteristics found in observational or GCM data. However, with this study we show that we capture the basic ENSO mechanisms in the linear feedbacks, and investigate the influence of some nonlinearities on ENSO properties. Improvements towards a more realistic reduced model will be subject of future investigations.

While an improvement, the inclusion of atmospheric nonlinearities is only a first step towards building fully realistic reduced models. An improvement of the ICM can be made in, for example, the ocean model. It has been shown that nonlinearities in the ocean model tend to reduce the skewness in the central Pacific (Philip and van Oldenborgh, 2009b), and increase it in the eastern Pacific (e.g., Jin et al, 2003). Another type of nonlinearities we ignore are the ones related to heat fluxes. An additional noise term could be introduced in the heat flux; westerly wind events are thought to introduce more clouds and consequently a more noisy signal. Furthermore, the seasonal cycle has been neglected throughout. For instance, Guilyardi (2006) and Lengaigne et al (2006) show that the seasonal cycle is important for the phase-locking of El Niño. The above mentioned types of terms and non-linearities have been investigated in many other studies. Implementing these terms in the ICM will most likely improve the simulations.

However, there are limitations to the benefits of an extended ICM. The strength of the research in this thesis is that we only use coupling terms that are fitted to the data. We assume that the terms fitted to observations are correct. As the ICM fitted to observations

shows no large problems, we think the representation of the couplings and noise terms is correct, although some second order terms are still missing. We expect that in a perfect model world terms fitted from GCM data are similar to that fitted from observational data. However, in the real model world some GCMs have nonlinear aspects such that the ICM represents those GCMs less well than observations.

On the one hand the ICM analysis itself can be improved to better understand the behaviour of ENSO. On the other hand, GCM climate modellers can also learn from this study. This method enables us to fit each GCM separately to find out which term is included in the GCM. We showed that the strengths of the linear coupling terms between the ocean and the atmosphere in GCMs are very diverse. Using only GCMs with the best strengths of the linear coupled atmosphere-ocean feedback loops we concluded that GCMs tend to simulate lower noise amplitudes than observations. Some GCMs are able to simulate a nonlinear response of wind stress to SST, although weaker than in observations. We recomment modellers to diagnose the weakness of their model with the ICM analysis described here.

This method provides the possibility to distinguish per model differences with observations rather quickly and easily. Using this method will give better insight in GCMs and seasonal forecast models, which will help modellers improving their models. This will facilitate better seasonal forecasts and climate projections.

BIBLIOGRAPHY

AchutaRao K, Sperber KR (2006) ENSO simulation in coupled ocean-atmosphere models: are the current models better? Climate Dyn 27(1):1–15, DOI 10.1007/s00382-006-0119-7

An SI, Hsieh WW, Jin FF (2005) A nonlinear analysis of the ENSO cycle and its interdecadal changes. J Climate 18:3229–3239

Annan JD, Hargreaves JC, Ohgaito R, Abe-Ouchi A, Emori S (2005) Efficiently constraining climate sensitivity with ensembles of paleoclimate simulations. Scientific on-line letters on the atmosphere 1:181–184

Behringer DW, Ji M, Leetmaa A (1998) An improved coupled model for ENSO prediction and implications for ocean initialization. Part I: The ocean data assimilation system. Mon Wea Rev 126:1013–1021

Berlage HP (1957) Fluctuations of the general atmospheric circulation of more than one year, their nature and prognostic value. No. 69 in Mededelingen en verhandelingen, KNMI, De Bilt, Netherlands

Bjerknes J (1966) A possible response of the atmospheric Hadley circulation to equatorial anomalies of ocean temperature. Tellus 18:820–829

Blanke B, Neelin JD, Gutzler D (1997) Estimating the effect of stochastic wind stress forcing on ENSO irregularity. J Climate 10:1473–1486

Bonekamp H, van Oldenborgh GJ, Burgers G (2001) Variational assimilation of TAO and XBT data in the HOPE OGCM, adjusting the surface fluxes in the tropical ocean. J Geophys Res C106:16,693–16,709

Boulanger JP, Durand E, Duvel JP, Menkes C, Delecluse P, Imbard M, Lengaigne M, G M, Masson S (2001) Role of non-linear ocean processes to westerly wind events : new implications for the 1997 El Niño onset. Geophys Res Lett 28:1603–1606

Burgers G, Balmaseda MA, Vossepoel FC, van Oldenborgh GJ, van Leeuwen PJ (2002) Balanced ocean-data assimilation near the equator. J Phys Oceanogr 32:2509–2529

Burgers G, Jin FF, van Oldenborgh GJ (2005) The simplest enso recharge oscillator. Geophys Res Lett 32:L13,706, DOI 10.1029/2005GL022951

Burgers GJH, van Oldenborgh GJ (2003) On the impact of local feedbacks in the Central Pacific on the ENSO cycle. J Climate 16:2396–2407

Cai W, Collier MA, Gordon HB, Waterman LJ (2003) Strong ENSO variability and a super-ENSO pair in the CSIRO coupled climate model. Mon Wea Rev 131:1189–1210

Cane M, Zebiak S (1985) A theory for El Niño and the Southern Oscillation. Science 228:1085 – 1087, DOI 10.1126/science.228.4703.1085

Capotondi A, Wittenberg A, Masina S (2006) Spatial and temporal structure of tropical Pacific interannual variability in 20th century coupled simulations. Ocean Modeling 15:274–298

Carton JA, Giese BS (2008) SODA: A reanalysis of ocean climate. MWR 139:2999–3017

Clarke AJ (1994) Why are surface equatorial ENSO winds anomalously westerly under anomalous large-scale convection? J Climate 7:1623–1627

Codron F, Vintzileos A, R S (2001) Influence of mean state changes on the structure of ENSO in a tropical coupled GCM. J Climate 14:730–742

Collins M (2000a) The El-Niño Southern Oscillation in the second Hadley Centre coupled model and its response to greenhouse warming. J Climate 13:1299–1312

Collins M (2000b) Uncertainties in the response of ENSO to greenhouse warming. Geophys Res Lett 27:3509–3513

Collins M (2004) El Niño- or La Niña-like climate change? Climate Dyn 24:89–104, DOI 10.1007/s00382-004-0478-x

Collins M (2007) Ensembles and probabilities: a new era in the prediction of climate change. Philosophical Transactions of the Royal Society A 365 (1857):1957–1970

Collins M (2009) An anthropogenic influence on El Niño. Nature Geoscience In review

Collins M, Tett SFB, Cooper C (2001) The internal climate variability of HadCM3, a version of the Hadley Centre coupled model without flux adjustments. Climate Dyn 17:61–81

Collins M, Booth B, Harris G, Murphy J, Sexton D, Webb M (2006a) Towards quantifying uncertainty in transient climate change. Climate Dyn 27 (2-3):127–147

Collins WD, Bitz CM, Blackmon MI, Bonan GB, Bretherton CS, Carton JA, Chang P, Doney SC, Hack JJ, Henderson TB, Kiehl JT, Large WG, McKenna DS, Santer BD, Smith RD (2006b) The Community Climate System Model: CCSM3. J Climate 19:2122–2143, DOI 10.1175/JCLI3761.1

Cravatte S, Picaut J, G E (2003) Second and first baroclinic Kelvin modes in the equatorial Pacific at intraseasonal timescales. JGR 108(C8):3266, DOI 10.1029/2002JC001511

Schneider von Deimling T, Held H, Ganopolski A, Rahmstorf S (2006) Climate sensitivity estimated from ensemble simulations of glacial climates. Climate Dyn 27:149–163, DOI 10.1007/s00382-006-0126-8

Delworth TL, Broccoli AJ, Rosati A, Stouffer RJ, Balaji V, Beesley JA, Cooke WF, Dixon KW, Dunne J, Dunne KA, Durachta JW, Findell KL, Ginoux P, Gnanadesikan A, Gordon CT, Griffies SM, Gudgel R, Harrison MJ, Held IM, Hemler RS, Horowitz LW, Klein SA, Knutson TR, Kushner PJ, Langenhorst AR, Lee HC, Lin SJ, Lu J, Malyshev SL, Milly PCD, Ramaswamy V, Russell J, Schwarzkopf MD, Shevliakova E, Sirutis JJ, Spelman MJ, Stern WF, Winton M, Wittenberg AT, Wyman B, Zeng F, Zhang R (2006) GFDL's CM2 global coupled climate models – Part 1: Formulation and simulation characteristics. J Climate 19:643–674, DOI 10.1175/JCLI3629.1

Dijkstra HA (2000) Nonlinear Physical Oceanography. Kluwer Academic Publishers, Dordrecht, the Netherlands

Eisenman I, Yu L, Tziperman E (2005) Westerly wind bursts: ENSO's tail rather than the dog? J Climate 18:5224–5238

Fedorov AV, Philander SG (2001) A stability analysis of tropical ocean-atmosphere interactions: bridging measurements and theory for El Niño. J Climate 14:3086–3101

Gebbie G, Eisenman I, Wittenberg A, Tziperman E (2007) Westerly wind burst modulation by sea surface temperature as an intrinsic part of ENSO dynamics. J Atmos Sci 64:3281–3295

Gill AE (1980) Some simple solutions for heat induced tropical circulation. Quart J Roy Meteor Soc 106:447–462

Gill AE (1982) Atmosphere–Ocean Dynamics. Academic Press, Orlando, 662 pp.

Gill AE (1985) Elements of coupled ocean-atmosphere models for the tropics, vol 40. Coupled Ocean-Atmosphere Models,Elsevier Oceanography Series, Elsevier, New York

Gordon C, Cooper C, Senior CA, Banks H, Gregory JM, Johns TC, Mitchell JFB, Wood RA (2000) The simulation of SST, sea ice extents and ocean heat transport in a version of the Hadley Centre coupled model without flux adjustments. Climate Dyn 16:147–168

Gordon HB, Rotstayn LD, McGregor JL, Dix MR, Kowalczyk EA, O'Farrell SP, Waterman LJ, Hirst AC, Wilson SG, Collier MA, Watterson IG, Elliott TI (2002) The CSIRO Mk3 climate system model. Tech. Rep. 60, CSIRO Atmospheric Research, Aspendale

Guilyardi E (2006) El Niño - mean state - seasonal cycle interactions in a multi-model ensemble. Climate Dyn 26:329–348

Guilyardi E, Gualdi S, Slingo J, Navarro A, Delecluse P, Cole J, Madec G, Roberts M, Latif M, Terray L (2004) Representing El Niño in coupled ocean-atmosphere GCMs: the dominant role of the atmosphere component. J Climate 17:4623–4629

Guilyardi E, Wittenberg A, Fedorov A, Collins M, Wang C, Capotondi A, van Oldenborgh GJ, Stockdale T (2009) Understanding El Niño in Ocean-Atmosphere General Circulation Models: progress and challenges. Bull Amer Met Soc 90:325–340, DOI 10.1175/2008BAMS2387.1

Harris G, Sexton D, Booth B, Collins M, Murphy J, Webb M (2006) Frequency distributions of transient regional climate change from perturbed physics ensembles of general circulation model simulations. Climate Dyn 27:357–375

Hirst AC (1986) Unstable and damped equatorial modes in simple coupled ocean-atmosphere model. J Atmos Sci 43:606–630

Hirst AC (1988) Slow instabilities in tropical ocean basin - global atmosphere models. J Atmos Sci 45:830–852

Ingleby B, Huddleston M (2007) Quality control of ocean temperature and salinity profiles - historical and real-time data. J Mar Sys 65:158–175

Jin FF (1997) An equatorial recharge paradigm for ENSO, part I: Conceptual model. J Atmos Sci 54:811–829

Jin FF, An SI, Timmermann A, Zhao J (2003) Strong El Niño events and nonlinear dynamical heating. Geophys Res Lett 30(3):1120, DOI 10.1029/2002GL016356

Jin FF, Lin L, Timmermann A, J Z (2007) Ensemble-mean dynamics of the ENSO recharge oscillator under state-dependent stochastic forcing. Geophys Res Lett 34:L03,807, DOI 10.1029/2006GL027372

Johns T, Durman C, Banks H, Roberts M, McLaren A, Ridley J, Senior C, Williams K, Jones A, Keen A, Rickard G, Cusack S, Joshi M, Ringer M, Dong B, Spencer H, Hill R, Gregory J, Pardaens A, Lowe J, Bodas-Salcedo A, Stark S, Searl Y (2004) HadGEM1 — model description and analysis of preliminary experiments for the IPCC Fourth Assessment Report. Tech. Rep. 55, U.K. Met Office, Exeter, U.K.

Jungclaus JH, Keenlyside N, Botzet M, Haak H, Luo JJ, Latif M, Marotzke J, Mikolajewicz U, Roeckner E (2006) Ocean circulation and tropical variability in the coupled model ECHAM5/MPI-OM. J Climate 19:3952–3972, DOI 10.1175/JCLI3827.1

K-1 model developers (2004) K-1 coupled model (MIROC) description. Tech. Rep. 1, Center for Climate System Research, University of Tokyo, www.ccsr.u-tokyo.ac.jp/kyosei/hasumi/MIROC/tech-repo.pdf

K AchutaRao KS (2002) Simulation of the el niõ southern oscillation: Results from the coupled model intercomparison project. Climate Dyn 19:191–209, DOI 10.1007/s00382-001-0221-9

Kaplan A, Cane MA, Kushnir Y, Clement AC, Blumenthal MB, Rajagopalan B (1998) Analyses of global sea surface temperature 1856–1991. J Geophys Res 103:18,567–18,589

Keenlyside N, Latif M, Botzet M, Jungclaus J, Schulzweida U (2005) A coupled method for initializing El Niño Southern Oscillation forecasts using sea surface temperature. Tellus A57:340–356, DOI 10.1111/j.1600-0870.2005.00107.x

Kessler W, Kleeman R (2000) Rectification of the Madden-Julian oscillation into the ENSO cycle. J Climate 13:3560–3575

Kessler WS (2002) Is ENSO a cycle or a series of events? Geophys Res Lett 29:2125–2128, DOI 10.1029/2002GL015924

Kim SJ, Flato GM, de Boer GJ, McFarlane NA (2002) A coupled climate model simulation of the last glacial maximum, part 1: transient multi-decadal response. Climate Dyn 19:515–537, DOI 10.1007/s00382-002-0243-y

Kirtman B (1997) Oceanic Rossby wave dynamics and the ENSO period in a coupled model. J Climate 10:1690–1704

Kleeman R, Moore A, Smith NR (1995) Assimilation of subsurface thermal data into a simple ocean model for the initialization of an intermediate tropical coupled ocean–atmosphere forecast model. Mon Wea Rev 123:3103–3114

Knutson TR, Manabe S, Gu D (1997) Simulated ENSO in a global coupled ocean-atmosphere model: Multidecadal amplitude modulation and CO_2 sensitivity. J Climate 10:42–63

Knutti R, Meehl GA, Allen MR, Stainforth DA (2006) Constraining climate sensitivity from the seasonal cycle in surface temperature. J Climate 19:4224–4233

Kug JS, Jin FF, Sooray KP, Kang IS (2008) State-dependent atmospheric noise associated with ENSO. Geophys Res Lett 35:L05,701, DOI 10.1029/2007GL032017

Kug JS, Sooray KP, Kim D, Kang IS, Jin FF, Takayabu YN, Kimoto M (2009) Simulation of state-dependent high-frequency atmospheric variability associated with ENSO. Climate Dyn 32(5), DOI 10.1007/s00382-008-0434-2

Lengaigne M, Boulanger JP, Menkes C, Madec G, Delecluse P, Guilyardi E, Slingo J (2003) The march 1997 westerly wind event and the onset of the 1997/98 El Niño: Understanding the role of the atmospheric response. J Climate 16:3330–3343

Lengaigne M, Guilyardi E, Boulanger JP, Menkes C, Delecluse P, Inness P, Cole J, Slingo J (2004) Triggering of El Niño by westerly wind events in a coupled general circulation model. Climate Dyn 23:601–620

Lengaigne M, Boulanger JP, Menkes C, Spencer H (2006) Influence of the seasonal cycle on the termination of El Niño events in a coupled general circulation model. J Climate 19:1850–1868, DOI 10.1175/JCLI3706.1

Li T, Philander S (1996) On the cnnual cycle of the Eastern Equatorial Pacific. J Climate 9:2986–2998, DOI 10.1175/1520-0442(1996)009⟨2986:OTACOT⟩2.0.CO;2

Lin JL (2007) The double-itcz problem in ipcc ar4 coupled gcms: Ocean-atmosphere feedback analysis. J Clim 20:4497–4525

Lin JLGK, Mapes B, Weickmann K, Sperber K, Lin W, Wheeler M, Schubert S, Genio AD, Donner L, Emori S, Gueremy JF, Hourdin F, Rasch P, Roeckner E, Scinocca J (2006) Tropical intraseasonal variability in 14 IPCC AR4 climate models. part i: Convective signals. J Climate 19:2665–2690, DOI 10.1175/JCLI3735.1

Liu Z, Vavrus S, He F, Wen N, Zhong Y (2005) Rethinking tropical ocean response to global warming: The enhanced equatorial warming. J Climate 18:4684–4700

Lloyd J, Guilyardi E, Weller H, Slingo J (2009) The role of atmosphere feedbacks during enso in the cmip3 models. Atmos Sci Letts Submitted

Lucarini L, Russell GL (2002) Comparison of mean climate trends in the northern hemisphere between National Centers for Environmental Prediction and two atmosphere-ocean model forced runs. J Geophys Res D15, DOI 10.1029/2001JD001247

Marti O, Braconnot P, Bellier J, Benshila R, Bony S, Brockmann P, Cadulle P, Caubel A, Denvil S, Dufresne JL, Fairhead L, Filiberti MA, Fichefet T, Friedlingstein P, Grandpeix JY, Hourdin F, Krinner G, Lévy C, Musat I, Talandier C (2005) The new IPSL climate system model: IPSL-CM4. Tech. rep., Institut Pierre Simon Laplace des Sciences de l'Environnement Global, IPSL, Case 101, 4 place Jussieu, Paris, France

McPhaden MJ (2004) Evolution of the 2002/03 el niño. BAMS 85:677–695, DOI 10.1175/BAMS-85-5-6776

McPhaden MJ, Busalacchi AJ, Cheney R, Donguy JR, Gage KS, Halpern D, Ji M, Julian P, Meyers G, Mitchum GT, Niiler PP, Picaut J, Reynolds RW, Smith N, Takeuchi K (1998) The Tropical Ocean Global Atmosphere (TOGA) observing system: a decade of progress. J Geophys Res 103:14,169–14,240

Meehl GA, Branstator GW, Washington WM (1993) Tropical Pacific interannual variability and CO_2 climate change. J Climate 6:42–63

Meehl GA, Gent PR, Arblaster JM, Otto-Bliesner BL, Brady EC, Craig A (2001) Factors that affect the amplitude of El Niño in global coupled climate models. Climate Dyn 17:515–526

Merryfield WJ (2006) Changes in ENSO under CO_2 doubling in the IPCC AR4 coupled climate models. J Climate 19:4009–4027, DOI 10.1175/JCLI3834.1

Monahan AH (2008) Probability distribution of sea surface wind stresses. Geophys Res Lett 35:L05,704, DOI doi:10.1029/2007GL032268

Moore B, Gates W, LJ M, Underdal A (2001) Advancing our understanding. In Climate Change 2001: The Scientific Basis. Contribution of Working Group I to the Third Assessment Report of the Intergovernmental Panel on Climate Change. Cambridge University Press, houghton, J.T. and Ding, Y. and Griggs, D.J. and Noguer, M. andvan der Linden, P.J. and Dai. X. and Maskell, K. and Johnson, C.A

Murphy JM, Sexton DMH, Barnett DN, Jones GS, Webb MJ, Collins M, Stainforth DA (2004) Quantification of modelling uncertainties in a large ensemble of climate change simulations. Nature 430:768–772

Neelin JD, Battisti DS, Hirst AC, Jin FF, Wakata Y, Yamagata T, Zebiak SE (1998) ENSO theory. J Geophys Res 103:14,261–14,290

Niehörster F, Spangehl T, Fast I, Cubasch U (2006) Quantification of model uncertainties: Parameter sensitivities of the coupled model ECHO-G with middle atmosphere, vol 8. EGU06-A-08526

van Oldenborgh GJ, Philip SY, Collins M (2005) El Niño in a changing climate: a multi-model study. Ocean Science 1:81–95

Otto-Bliesner B, Brady E (2001) Tropical Pacific variability in the NCAR Climate System Model. J Climate 14:3587–3607

Perez CL, Moore AM, Zavala-Garay J, Kleeman R (2005) A comparison of the influence of additive and multiplicative stochastic forcing on a coupled model of ENSO. J Climate 18:5066–5085

Philander SG (1990) El Niño, La Niña and the Southern Oscillation. Academic Press, San Diego, 293 pp.

Philander SGH, Yamagata T, Pacanowski RC (1984) Unstable air-sea interactions in the tropics. J Atmos Sci 41:604–613

Philip SY, van Oldenborgh GJ (2006) Shifts in ENSO coupling processes under global warming. Geophys Res Lett 33:L11,704, DOI 10.1029/2006GL026196

Philip SY, van Oldenborgh GJ (2009a) Atmospheric properties and ENSO: models versus observations. Climate Dyn Accepted

Philip SY, van Oldenborgh GJ (2009b) Significant atmospheric nonlinearities in the ENSO cycle. J Climate Accepted

Piani C, D J Frame DJ, Stainforth DA, Allen MR (2005) Constraints on climate change from a multi-thousand member ensemble of simulations. Geophys Res Lett 32:L23,825, DOI doi:10.1029/2005GL024452

Picaut J, Ioulalen M, Menkes C, Delcroix T, McPhaden MJ (1996) Mechanism of the zonal displacement of the Pacific warm pool: implications for ENSO. Science 274:1486–1489

Reynolds RW, Rayner NA, Smith TM, Stokes DC, Wang W (2002) An improved in situ and satellite SST analysis for climate. J Climate 15:1609–1625, DOI DOI:10.1175/1520-0442(2002)015⟨1609:AIISAS⟩2.0.CO;2

Rougier J, Sexton D, Murphy J, Stainforth D (2008) Analysing the climate sensitivity of the HadSM3 climate model using ensembles from different but related experiments. J Climate In press

Sanderson B, Knutti R, Aina T, Christensen C, Faull N, Frame D, Ingram W, Piani C, Stainforth D DA andStone, Allen M (2008) Constraints on model response to greenhouse gas forcing and the role of subgrid-scale processes. J Climate 21:2384–2400

Sanderson BM, Piani C (2007) Towards constraining climate sensitivity by linear analysis of feedback patterns in thousands of perturbed-physics gcm simulations. Climate Dyn 30:175–190

Schmidt GA, Ruedy R, Hansen JE, Aleinov I, Bell N, Bauer M, Bauer S, Cairns B, Canuto V, Cheng Y, Del Genio A, Faluvegi G, Friend AD, Hall TM, Hu Y, Kelley M, Kiang NY, Koch D, Lacis AA, Lerner J, Lo KK, Miller RL, Nazarenko L, Oinas V, Perlwitz J, Perlwitz J, Rind D, Romanou A, Russell GL, Sato M, Shindell DT, Stone PH, Sun S, Tausnev N, Thresher D, Yao MS (2006) Present day atmospheric simulations using GISS ModelE: Comparison to in-situ, satellite and reanalysis data. J Climate 19:153–192

Slingo JM, Sperber K, Boyle J, Ceron JP, Dix M, Dugas B, Ebisuzakiand W, Fyfe J, Gregory D, Gueremy JF, Hack J, Harzallah A, Inness P, Kitoh A, Lau WM, McAvaney B, Madden R, Matthews A, Palmer T, Park CK, Randall D, Renno N (1996) Intraseasonal oscillations in 15 atmospheric GCMs: results from an AMIP diagnostic subproject. Climate Dyn 12:325–357, DOI 10.1007/s003820050112

Stainforth DA, Aina T, Christensen M C Collins, Faull DJ N andFrame, Kettleborough JA, Knight S, Martin A, Murphy JM, Piani C, Sexton LA D Smith, Spicer RA, Thorpe AJ, Allen MR (2005) Uncertainty in predictions of the climate response to rising levels of greenhouse gases. Nature 433:403–406

Sun DZ, Yu Y, Zhang T (2009) Tropical water vapor and cloud feedbacks in climate models: A further assessment using coupled simulations. J Climate 22:1287–1304, DOI 10.1175/2008JCLI2267.1

Sura P, Newman M, Penland C, Sardeshmukh PD (2005) Multiplicative noise and non-gaussianity: A paradigm for atmospheric regimes? J Atmos Sci 62:1391–1409

Sura P, Newman M, Alexander MA (2006) Daily to decadal sea surface temperature variability driven by state-dependent stochastic heat fluxes. J Phys Oceanogr 36:1940–1958

Tett S (1995) Simulation of El-Niño/Southern Oscillation like variability in a global AOGCM and its response to CO_2 increase. J Climate 8(6):1473–1502

Timmermann A (2001) Changes of ENSO stability due to greenhouse warming. Geophys Res Lett 28:2061–2064

Timmermann A, Oberhuber J, Bacher A, Esch M, Latif M, Roeckner E (1999) Increased El-Niño frequency in a climate model forced by future greenhouse warming. Nature 398:694–696

Toniazzo T (2006a) Properties of the El Niño Southern Oscillation in different equilibrium climates with the HadCM3 model. J Climate 19:4854–4876, DOI 10.1175/JCLI3853.1

Toniazzo T (2006b) A study of the sensivity of ENSO to the mean climate. Advances in Geosciences 6:111–118

Toniazzo T, Collins M, Brown J (2008) The variation of ENSO characteristics associated with atmospheric parameter perturbations in a coupled model. Climate Dyn 30:643–656

Trenberth KE, Stepaniak DP (2001) Indices of El Niño evolution. J Climate 14:1697–1701, DOI 10.1175/1520-0442(2001)014⟨1697:LIOENO⟩2.0.CO;2

Tziperman E, Yu L (2007) Quantifying the dependence of westerly wind bursts on the large scale tropical Pacific SST. J Climate 20:2760–2768

Uppala SM, Kålberg PW, Simmons AJ, Andrae U, da Costa Bechtold V, Fiorino M, Gibson JK, Haseler J, Hernandez A, Kelly GA, Li X, Onogi K, Saarinen S, Sokka N, Allan RP, Anderson E, Arpe K, Balmaseda MA, Beljaars ACM, van den Berg L, Bidlot J, Borman N, Caires S, Dethof A, Dragosavac M, Fisher M, Fuentes M, Hagemann S, Hólm E, Hoskins BJ, Isaksen L, Janssen PAEM, Jenne R, McNally AP, Mahfouf JF, Mocrette JJ, Rayner NA, Saunders RW, Simon P, Sterl A, Trenberth KE, Untch A, Vasiljevic D, Viterbo P, Woollen J (2005) The ERA-40 re-analysis. Quart J Roy Meteor Soc 130:2961–3012, DOI 10.1256/qj.04.176

van der Vaart PCF (1998) Nonlinear tropical climate dynamics. PhD thesis, Universiteit Utrecht

van der Vaart PCF, Dijkstra HA, Jin FF (2000) The Pacific Cold Tongue and the ENSO mode: Unified theory within the Zebiak-Cane model. J Atmos Sci 57:967–988

Vecchi GA, Wittenberg AT, Rosati A (2006) Reassessing the role of stochastic forcing in the 1997-1998 El Niño. Geophys Res Lett 33, DOI 10.1029/2005GL024738

Volodin EM, Diansky NA (2004) El-Niño reproduction in coupled general circulation model of atmosphere and ocean. Russian meteorology and hydrology 12:5–14

Von Storch H, Zwiers F (2001) Statistical Analysis in Climate Research. Cambridge University Press, The Edinburgh Building, Cambridge CB2 2RU, UK, ISBN 0 521 45071 3 / 0 521 01230 9

Vossepoel F (1999) Sea-level data assimilation for estimating salinity variability in the tropical pacific. PhD thesis, Technische Universiteit Delft

Walker GT, Bliss EW (1932) World weather V. Mem Roy Meteor Soc 4:53–84

Washington WM, Weatherly JW, Meehl GA, Semtner AJ Jr, Bettge TW, Craig AP, Strand WG Jr, Arblaster J, Wayland VB, James R, Zhang Y (2000) Parallel climate model (PCM) control and transient simulations. Climate Dyn 16:755–774

Webb MJ, Senior CA, Sexton DMH, Ingram WJ, Williams KD, Ringer MA, McAvaney BJ, Colman R, Soden BJ, Gudgel R, Knutson T, Emori S, Ogura T, Tsushima Y, Andronova N, Li B, Musat I, Bony S, Taylor KE (2006) On the contribution of local feedback mechanisms to the range of climate sensitivity in two GCM ensembles. Climate Dyn 27:17–18

Wittenberg AT (2002) Enso response to altered climates. PhD thesis, Princeton University, 475pp. Available at http://www.gfdl.noaa.gov/ atw/research/thesis

Wittenberg AT, Rosati A, Lau NC, Ploshay J (2005) GFDL's CM2 global coupled climate models, part 3: Tropical Pacific Climate and ENSO. J Climate Accepted

Wyrtki K (1975) El Niño — the dynamic response of the equatorial Pacific Ocean to atmospheric forcing. J Phys Oceanogr 5:572–584

Yu B, Boer G (2002) The roles of radiation and dynamical processes in the El Niño-like response to global warming. Climate Dyn 19:539–554, DOI 10.1007/s00382-002-0244-x

Yu Y, Zhang X, Guo Y (2004) Global coupled ocean- atmosphere general circulation models in LASG/IAP. Adv Atmos Sci 21:444–455

Yukimoto S, Noda A (2002) Improvements of the Meteorological Research Institute Global Ocean-atmosphere Coupled GCM (MRI-CGCM2) and its climate sensitivity. Tech. Rep. 10, NIES, Japan

Zavala-Garay J, Moore AM, Perez CL, Kleeman R (2003) The response of a coupled model of ENSO to observed estimates of stochastic forcing. JCL 18:2441–2459

Zebiak SE, Cane MA (1987) A model of El Niño–Southern Oscillation. Mon Wea Rev 115:2262–2278

Zelle H, Appeldoorn G, Burgers G, Van Oldenborgh GJ (2004) On the relationship between sea surface temperature and thermocline depth in the eastern equatorial Pacific. J Phys Oceanogr 34:643–655

Zelle H, Van Oldenborgh GJ, Burgers G, Dijkstra HA (2005) El Niño and greenhouse warming: Results from ensemble simulations with the NCAR CCSM. J Climate 18:4683–4669

Zhang RH, Busalacchi AJ, DeWitt DG (2008) The roles of atmospheric stochastic forcing (SF)and oceanic entrainment temperature (Te) in decadal modulation of ENSO. J Climate 21:674–704, DOI 10.1175/2007JCLI1665.1

SAMENVATTING

De naam 'El Niño' of 'het jongetje' werd door Peruaanse vissers gebruikt voor een warme oceaanstroming. Deze warme stroming keerde elk jaar rond kerst terug. Voor de vissers betekende dit het begin van een slechtere periode met minder visvangst: vis leeft beter in kouder, voedselrijk water. Dit 'kerstkind' was dus geen welkome gast.

Tegenwoordig wordt de term El Niño algemener gebruikt om periodes aan te duiden waarin het oppervlaktewater in de centrale tot oostelijke equatoriale Stille Oceaan warmer dan normaal is. Ook in de huidige definitie vindt de piek van El Niño plaats rond kerst.

De fluctuaties in de oceaan gaan gepaard met veranderingen in de atmosfeer erboven. De fluctuaties in de atmosfeer worden vaak aangegeven in drukverschillen tussen de oostelijke en westelijke equatoriale Stille Oceaan, de zogenaamde Zuidelijke Oscillatie. De toestand van de oceaan en atmosfeer tezamen wordt beschreven met de term El Niño – Zuidelijke Oscillatie (ENSO).

Het fenomeen ENSO is de grootste klimaatschommeling op aarde met een frequentie tussen de één en 100 jaar. Hoewel het klimaatfenomeen El Niño zijn oorsprong heeft in de tropische Stille Oceaan, zijn de invloeden wereldwijd merkbaar. Via de atmosfeer boven de equatoriale Stille Oceaan en de circulatie in de atmosfeer wordt het weer over de hele aarde beïnvloed. Aangezien El Niño tot ongeveer een half jaar vooruit voorspelbaar is, geeft dit de mogelijkheid om het gemiddelde weer in deze gebieden op die termijn te voorspellen. Seizoensverwachtingen zijn dan ook voor een groot gedeelte op El Niño gebaseerd. Het is daarom belangrijk om inzicht te krijgen in ENSO en de ontwikkeling van El Niño.

Om El Niño te begrijpen, hebben we eerst kennis nodig van de gemiddelde toestand rond de equatoriale Stille Oceaan. De oceaan is opgebouwd uit een dunne laag warm water van ongeveer 100 meter dik bovenop 5 km koud water. De scheiding tussen het warme en koude water noemt men de thermoklien. De bovenste tientallen meters van de warme bovenlaag zijn goed gemengd door de wind. Dit wordt de menglaag genoemd. In de atmosfeer erboven waait voortdurend een wind langs de evenaar van oost naar west, de passaatwind. De drie variabelen die de belangrijkste rollen vertolken bij El Niño zijn: de thermoklien, de passaatwind en de temperatuur van het oceaanoppervlak (meestal aangeduid met SST, sea surface temperature). De thermoklien staat scheef omdat de passaatwind het warme oppervlaktewater naar het westen blaast, richting Indonesië. Door het opwellen van koud water is de temperatuur in het oosten, bij de kust van Zuid-Amerika, laag voor de tropen: zo'n 20 graden. Daarboven vormt zich een hogedrukgebied, terwijl boven het warme water in het westen een lagedrukgebied wordt gevormd. Het drukverschil in de atmosfeer versterkt weer de passaatwind. Normaal gesproken zijn deze drie factoren met elkaar in evenwicht.

Soms wordt het evenwicht tussen SST, wind en thermoklien verstoord, bijvoorbeeld door een westerstorm in het westen van de Stille Oceaan. Een deel van het warme water in het westen stroomt daardoor terug naar het oosten. Daar stijgt aan de oppervlakte de zeewatertemperatuur. Het drukverschil wordt kleiner en de passaatwind zwakt af, waardoor er nog meer warm water terug kan vloeien naar het oosten: El Niño is geboren. Het tegenovergestelde – met lagere zeewatertemperaturen in het oosten en een sterkere passaatwind – wordt La Niña genoemd.

El Niño wordt vaak met een aantal grootheden gekarakteriseerd. De eerste is een maat voor de sterkte van El Niño: de amplitude. Een tweede grootheid is de periode: hoe vaak komt een El Niño situatie gemiddeld voor. Ook de positie van de SST anomalie wordt vaak beschreven. Soms wordt met de zogenaamde scheefheid in SST anomalieën ook nog aangeduid dat de amplitude van El Niño over het algemeen groter is dan de amplitude van La Niña; men zegt dan dat de verdeling van SST anomalieën positief scheef is.

Er komen steeds betere klimaatmodellen die de circulatie in de oceanen en de atmosfeer beschrijven. Deze modellen worden onder andere gebruikt voor klimaatscenario's: simulaties van het huidige klimaat, maar ook simulaties van toekomstscenario's. Maar zijn deze modellen ook realistisch genoeg om El Niño en de fysica erachter te beschrijven? En, meer gedetailleerd, zijn modellen ook in staat om bijvoorbeeld het verschil in amplitude tussen El Niño en La Niña te modelleren?

In Hoofdstuk 2 wordt een methode uitgelegd waarmee we modellen met observaties kunnen vergelijken. Ten eerste moeten natuurlijk de amplitude, periode en positie van de temperatuurafwijking overeenkomen. Daarnaast moeten de koppelingsparameters tussen de verschillende aspecten van El Niño ongeveer even sterk zijn als in de waarnemingen. Deze koppelingsparameters worden hieronder eerst beschreven.

De temperatuur langs de evenaar in de oostelijke Stille Oceaan hangt sterk af van de diepte van de thermoklien: hoe dieper het koude water is, hoe warmer het oppervlak. In de centrale Stille Oceaan is een secundair mechanisme actief; hier hangt de zeewatertemperatuur van de lokale wind af, doordat daarmee water van het warme gebied in het westen naar de koude tong in het oosten of omgekeerd getransporteerd wordt. Tenslotte dempt een SST anomalie uit door een feedback in de wolken. Deze mechanismen worden beschreven met een lineaire SST-vergelijking.

Daarnaast wordt er aan de hand van data gekeken hoe de wind gemiddeld reageert op een afwijking van de temperatuur van het oceaanwater. Met een regressiemodel kunnen we representeren wat de respons van de wind over de hele tropische Stille Oceaan op een plaatselijke temperatuurafwijking is. Met de beperkte waarnemingsdataset die we hebben (ongeveer 50 jaar) kan de respons op een temperatuurafwijking in drie onafhankelijke gebieden nog uit elkaar gehaald worden. Ook een tweede orde respons op temperatuurafwijkingen kan worden beschreven, om een idee te krijgen van de invloed van niet-lineariteiten in de atmosfeer op SST scheefheid.

Ten derde wordt bepaald met welke snelheid informatie door de thermoklien wordt doorgegeven van west naar oost. Dit doorgeven van informatie gebeurt met zogenaamde Kelvin golven: warm water stroomt in de vorm van zwaartekrachtsgolven die door de thermoklien van west naar oost kunnen reizen. Daar kunnen ze een El Niño initiëren.

Als laatste wordt ruis in de atmosfeer bestudeerd. Onder ruis verstaan we alle wind die

niet beschreven kan worden met het regressiemodel wat hierboven beschreven is. Deze ruis drijft in ons conceptuele model de ENSO cyclus aan. Zo kan bijvoorbeeld een westerstorm een Kelvingolf initiëren en daarmee ENSO aandrijven. De amplitude van de ruis wordt bekeken, maar ook de scheefheid van de ruis: de mate waarin de amplitude van oostenwind anomalieën verschillen van de amplitude van westenwind anomalieën. Ten slotte wordt de afhankelijk van deze twee grootheden met de achtergrond SST beschreven, alweer om een idee te krijgen van de invloed van niet-lineariteiten in de atmosfeer op SST scheefheid.

Voor modeldata worden dezelfde vergelijkingen gebruikt. Een model wordt als 'goed genoeg' beschouwd als de parameters van de lineaire vergelijkingen ongeveer overeen ko- men met de parameters van observationele data. Alleen voor deze modellen worden dan een toekomstscenario beschouwd en niet-lineaire termen bekeken.

Ten slotte kunnen alle bovenstaande parameters in een gereduceerd model geïmple- menteerd worden. Met dit model kan de invloed van de gefitte parameters op ENSO bestu- deerd worden.

In hoofdstuk 3 worden 19 gekoppelde klimaatmodellen (GCM's) bestudeerd en verge- leken met observaties. Om te beginnen worden alleen de lineaire termen tussen de subsys- temen bestudeerd: de respons van de wind op SST anomalieën, de responsen van SST op variaties in thermokliendiepte en wind en uitdemping van SST anomalieën. Zes modellen vallen binnen de categorie met de meest realistische balans tussen de feedback mechanis- men. Vier van deze zes modellen laten een interjaarlijkse variabiliteit zien die sterk lijkt op die in observaties, zowel in plaats als in tijd. In de overige 13 modellen verschilt minstens een van de lussen van de ENSO feedback met die in observaties. Aan de hand hiervan selecteren we een groep met beste modellen waarmee we verder gaan werken.

Hoofdstuk 4 beschrijft de resultaten voor de geselecteerde modellen die gedraaid zijn in een toekomstscenario, met onder andere een hogere CO_2 concentratie in de atmosfeer en hogere temperaturen. Hoewel deze veranderingen vrij groot zijn, lijkt ENSO niet veel te veranderen. Het blijkt dat de deelprocessen wel veel veranderen, maar dat deze verande- ringen de neiging hebben elkaar op te heffen. Het resultaat hangt daarom sterk af van de details van de modellen, waardoor ze verschillen in het teken van de veranderingen.

In hoofdstuk 5 worden alleen observationele data bestudeerd. De lineaire koppelingen plus karakteristieken van de atmosferische ruis worden in een relatief eenvoudig ('geredu- ceerd') model geïmplementeerd. De beschrijving van de atmosferische ruis in amplitude en ruimtelijke- en temporele correlaties is voldoende om in het model een ENSO cyclus te initiëren. Het model blijkt redelijk goed in het representeren van de belangrijkste ENSO eigenschappen zonder dat er verdere aanpassingen nodig zijn. Daarna worden drie extra termen een voor een aan het model toegevoegd om de invloed op SST scheefheid te bestu- deren. Het blijkt dat de niet-lineaire respons van de wind op SST anomalieën de grootste invloed heeft op SST scheefheid. Daarna volgt de afhankelijkheid van de amplitude van de atmosferische ruis van de achtergrondtemperatuur: tijdens El Niño is er sterkere ruis dan tijdens La Niña. De scheefheid van de atmosferische ruis blijkt de minste invloed op SST scheefheid te hebben.

De GCM's worden getoetst aan de hand van de bovenstaande bevindingen in hoofdstuk 6. In de GCM's is de amplitude van de atmosferische ruis vaak lager dan die van observatio- nele data. Net als bij observaties is de representatie van de ruis in termen van amplitude en

ruimtelijke- en temporele correlaties weer belangrijk voor het simuleren van een onregelmatige ENSO cyclus. Verder simuleren een aantal modellen een niet-lineaire respons van de wind op SST anomalieën. Deze respons is meestal wel zwakker dan in observaties wordt gezien. De GCM's die dit het meest realistisch modelleren, simuleren over het algemeen de meest realistische SST scheefheid. Maar ook de afhankelijkheid van de atmosferische ruis van de achtergrondtemperatuur levert een belangrijke bijdrage aan de asymmetrie tussen El Niño en La Niño.

Onzekerheden komen voort uit modellen die onderling verschillen, maar elk model op zich heeft ook een onzekerheid. In hoofdstuk 7 wordt een zelfde analyse uitgevoerd als hierboven op een heel ensemble van experimenten met een enkel GCM. In dit GCM zijn fysisch realistische variaties in parameters in de oceaan en atmosfeer aangebracht. Aan de hand hiervan hebben we de onzekerheid binnen een model bepaald, in plaats van de verschillen tussen modellen. De onzekerheid binnen een model is niet direct gerelateerd aan het gemiddelde klimaat, zoals het geval is in de modellen die voor een toekomstscenario gedraaid zijn. De factoren die het meest bijdragen aan de basiskarakteristieken van ENSO zijn de respons van SST op variaties in wind en uitdemping van SST anomalieën, gevolgd door de respons van de wind op SST anomalieën, de respons van SST op variaties in thermokliendiepte. De amplitude van atmosferische ruis en de snelheid waarmee Kelvin golven door de thermoklien reizen spelen een kleinere rol.

Ten slotte worden in hoofdstuk 8 conclusies samengevat en resultaten bediscussieerd. In dit proefschrift is een nieuwe methode ontworpen om verschillende delen uit de ENSO cyclus te beschrijven. Dit zijn de respons van de wind op SST anomalieen, de respons van de SST op anomalieën in wind en thermokliendiepte en demping van SST anomalieën en de snelheid waarmee Kelvin golven door de thermoklien reizen. Daarnaast worden verschillende aspecten van de atmosferische ruis bekeken. Hiermee kunnen modellen gemakkelijker en sneller met observaties vergeleken worden. Tevens kunnen hiermee een aantal extra (niet-lineare) termen onderzocht worden. Dit zijn de niet-lineaire respons van de wind op SST anomalieen, de afhankelijkheid van atmosferische ruis van de achtergrondtemperatuur en de mate waarin deze ruis scheef is. De invloeden van de verschillende termen op ENSO kunnen apart van elkaar met een gereduceerd model bepaald worden.

Het gereduceerde model geeft relatief goed de ENSO karakteristieken uit observaties dan wel GCM's weer zonder extra aanpassingen te maken. Het model is echter nog niet uitontwikkeld. Extra termen kunnen relatief simpel worden toegevoegd zodat we ENSO beter leren begrijpen. Dit moet echter voorzichtig gedaan worden zodat alleen realistische aanpassingen gemaakt worden. Aan de hand van deze analyse kunnen modelleurs meer inzicht krijgen in de verschillen tussen hun model en observaties. We verwachten dat dit zal leiden tot betere modellen en daarmee tot betere seizoensverwachtingen en computerrealisaties voor een toekomstig klimaat.

DANKWOORD

CURRICULUM VITAE

Sjoukje Philip was born in Rotterdam, the Netherlands, on April 21st, 1981. She graduated at the Libanon Lyceum in Rotterdam in 1999. After that she moved to Utrecht where she started the study Geophysics at the Utrecht University. She received a Bachelor in Physics and graduated in 2004 in Geophysics. Her master graduation project was at the Seismology Department of the Royal Netherlands Meteorological Institute (KNMI).

In 2005 she started her PhD with subject 'El Niño in a changing climate'. This research has been carried out at the Oceanographic Research Department (later Global Climate Department) at KNMI, in collaboration with the Utrecht University. In 2009 she finished this research with six articles. The contents of five of these articles form the basis of this thesis.

In September 2009 she started a new job at Oranjewoud in the Climate and Energy division.